Spatio-temporal analysis of Ca^{2+}-dependent enzymatic activity in models of retinal degeneration

Dissertation

zur Erlangung des Grades eines

Doktors der Naturwissenschaften

der Mathematisch-Naturwissenschaftlichen Fakultät

und

der Medizinischen Fakultät

der Eberhard-Karls-Universität Tübingen

vorgelegt

von

Michael James Power
aus Waterford, Irland

April 2019

Tag der mündlichen Prüfung: 02/04/2019

Dekan der Math.-Nat. Fakultät: Prof. Dr. W. Rosenstiel

Dekan der Medizinischen Fakultät: Prof. Dr. I. B. Autenrieth

1. Berichterstatter: Prof. Dr. Francois Paquet-Durand

2. Berichterstatter: Prof. Dr. Thomas Euler

Prüfungskommission: Francois Paquet-Durand

Thomas Euler

Marlies Knipper

Frank Schaeffel

Erklärung / Declaration:

Ich erkläre, dass ich die zur Promotion eingereichte Arbeit mit dem Titel:

„Spatio-temporal analysis of Ca^{2+}-dependent enzymatic activity in models of retinal degeneration“

selbständig verfasst, nur die angegebenen Quellen und Hilfsmittel benutzt und wörtlich oder inhaltlich übernommene Stellen als solche gekennzeichnet habe. Ich versichere an Eides statt, dass diese Angaben wahr sind und dass ich nichts verschwiegen habe. Mir ist bekannt, dass die falsche Abgabe einer Versicherung an Eides statt mit Freiheitsstrafe bis zu drei Jahren oder mit Geldstrafe bestraft wird.

*I hereby declare that I have produced the work entitled "*Spatio-temporal analysis of Ca^{2+}-dependent enzymatic activity in models of retinal degeneration*", submitted for the award of a doctorate, on my own (without external help), have used only the sources and aids indicated and have marked passages included from other works, whether verbatim or in content, as such. I swear upon oath that these statements are true and that I have not concealed anything. I am aware that making a false declaration under oath is punishable by a term of imprisonment of up to three years or by a fine.*

Tübingen, den ....

Datum / Date Unterschrift /Signature

Table of contents Page

Table of Figures Page

Tables Page

Abbreviations

aa	Amino Acids
ACSF	Artificial cerebral spinal fluid
AIF	Apoptosis Inducing Factor
AMP	Amplitude
ANOVA	Analysis of variance
APAF-1	Apoptotic protease activating factor 1
ATP	Adenosine triphosphate
AUC	Area under the curve
Å	Angström
Bax	Bcl-2 associated X protein
BBB	Blood Brain Barrier
Bcl-2	B-cell Lymphoma 2
Bcl-xl	B-cell Lymphoma extra large
BP	Band pass
BSA	Bovine serum albumin

C	Cysteine
Ca^{2+}	Calcium ion
CAA	Calpain activity assay
$CaCl_2$	Calcium Chloride
cGMP	Cyclic guanosine monophosphate
CICR	Calcium induced calcium release
CNGA3	Cyclic nucleotide gated alpha 3
CNGB3	Cyclic nucleotide gated beta 3
CNGCs	Cyclic nucleotide gated channels
CO_2	Carbon Dioxide
Cones	Cone photoreceptors
cpfl1	Cone photoreceptor function loss 1
CRB	Calpain reaction buffer
CYPD	Cyclophilin D
D-cis	D-cis Diltiazem
Da	Dalton

ddH_2O	Double distilled water
DNA	Deoxyribonucleic acid
DTT	Dithiothreitol
ECFP	Enhanced cyan fluorescent protein
ER	Endoplasmic reticulum
ERG	Electroretinogram
EtOH	Ethanol
FRET transfer	Förster resonance energy
g	Gram
GCL	Ganglion cell layer
H	Histidine
HEPES	4-(2-hydroxyethyl)-1-piperazineethanesulfonic acid
HR2.1	Human red opsin promoter 2.1
IgM	Immunoglobulin M
IL-1β	Interleukin-1β
INL	Inner nuclear layer

IP3	Inositol 1,4,5-trisphosphate
IP3R	Inositol trisphosphate receptor
IPL	Inner plexiform layer
IS	Inner segment
K+	Potassium ion
KCL	Potassium Chloride
kDa	Kilodalton
kg	Kilogram
L-cis	L-cis Diltiazem
LDH	Lactate dehydrogenase
LED	Light-emitting diode
Mg^{2+}	Magnesium ion
$MgCl_2$	Magnesium Chloride
MIF	migration inhibitory factor
ml	Millilitre
MLKL	Mixed lineage kinase domain like pseudokinase
mM	Millimolar

µm	Micrometre
µM	Micromolar
MOMP	Mitochondrial outer membrane perturbations
N	Asparagine
N_2	Liquid Nitrogen
Na+	Sodium ion
NaCl	Sodium Chloride
NaH_2PO_4	Sodium dihydrogen phosphate
$NaHCO_3$	Sodium bicarbonate
NCKX	Sodium/Calcium, Potassium exchanger
O_2	Oxygen
ONL	Outer nuclear layer
OPL	Outer plexiform layer
OS	Outer segment
P	Postnatal day of age
$P*s^{-1}$	Photoisomerisation per second

PARP1	Poly [ADP-ribose] polymerase 1
PBS	Phosphate buffered saline
PDE	Phosphodiesterase
Pde6	Phosphodiesterase 6
PFA	Paraformaldehyde
PIP_2	Phosphatidylinositol 4,5-bisphosphate
PRs	Photoreceptors
RCD	Regulated cell death
RD	Retinal dystrophies
rd1 model	Retinal degeneration 1 mouse
rd10 model	Retinal degeneration 10 mouse
RIPK1	Receptor-interacting serine/threonine - protein kinase 1
RIPK3	Receptor-interacting serine/threonine - protein kinase 3

RNA	Ribonucleic acid
ROIs	Regions of interest
Rods	Rod photoreceptors
RP	Retinitis pigmentosa
RyR	Ryanodine receptors
SERCA	sarco/endoplasmic reticulum calcium-ATPase
SR101	Sulforhodamine 101
tBOC-Leu-Met-CMAC	*t* -BOC-L-leucyl-L-methionine amide 7-amino-4-chloromethylcoumarin
TnC	Troponin C
TN-XL	Troponin C extra large
TUNEL	Terminal deoxynucleotidyl transferase dUTP nick end labelling
UPR	Unfolded protein response
VGCCs	Voltage gated calcium channels
wt	Wild type

Abstract

Calcium (Ca^{2+}) levels in neurons are strictly regulated and Ca^{2+} dysregulation has previously been linked to neuronal cell death. In the mammalian retina, Ca^{2+} dysregulation may be connected to both cone and rod photoreceptor cell death (*e.g.* Arango-Gonzalez *et al*., 2014, Kulkarni et al., 2016). The interpretation of this research has, however, been hampered by spatial inhomogeneity of retinal degenerative events, depending on the model used.

Here we examined the spatio-temporal activation patterns of the Ca^{2+}-dependent cysteine protease calpain in comparison with cell death patterns across three different mutant mouse lines, and wildtype (wt) mice. We determined the spatial activation of calpain during disease progression in the primary cone degeneration model *cpfl1* and in the primary rod degeneration models *rd1* and *rd10*, relative to wt controls and showed an increase in calpain activity in the *rd1* and *rd10* models in a spatio-temporal pattern. We used the TUNEL assay to stain for dying cells and found the spatiotemporal cell death pattern corresponding to that of calpain activity. Similarly, we observed up-regulation of the calpain-2 isoform, whereas no up-regulation of calpain-1 was observed. In addition, we found an upregulation of apoptosis-inducing-factor (AIF) in the disease models compared to wt, while increases in caspase-3 activation were mainly found in cones late in the *rd1* degeneration. Together these results indicate that calpain activity plays a role in the non-apoptotic photoreceptor cell death seen during retinal degeneration.

To further link the effects of Ca^{2+} dynamics to photoreceptor degeneration, we used a transgenic mouse line that expresses the *HR2.1:TN-XL* (TN-XL) Ca^{2+} biosensor in cones. We used two-photon microscopy to study calcium levels and light-evoked responses in cone axon terminals in acute retinal slices (Kulkarni *et al.*, 2015) before and after the application of the Ca^{2+} channel blockers L-cis (blocker of outer segment CNG channels) and D-cis (blocker of synaptic voltage gated calcium channels) diltiazem. Our data suggest that both diltiazem enantiomers lower baseline Ca^{2+} levels in cone terminals, while light-induced responses were altered only by the L-cis enantiomer. To link Ca^{2+} dysregulation to calpain activation, we developed two-photon live imaging of calpain activity. With this approach, we disentangled part of the interaction between Ca^{2+}-mediated processes, calpain regulation, and photoreceptor cell death. Our data suggests a causal link between Ca^{2+} dysregulation and cell death, high-lighting a therapeutic target for future compound development.

Introduction

Retinal organisation in mammals

The retina is a highly specialised sensory tissue located in the back of the eye in mammals (Fig. 1) and is an outgrowth of the brain. Since sight is considered the primary sense in humans, one can say that the retina is the primary sensory tissue of the human body. The retina is composed of three cellular layers and two plexiform layers. Rod photoreceptors (rods) and cone photoreceptors (cones) in the outer nuclear layer (ONL) are responsible for the initiation of the phototransduction cascade within the retina. Photoreceptors (PRs) synapse onto bipolar cells in the inner nuclear layer (INL) which then relay the signal to the output neurons of the retina, the ganglion cells in the ganglion cell layer (GCL). This excitatory signal is modulated by two inhibitory interneuron classes: the horizontal cells in the outer plexiform layer (OPL) and by the amacrine cells in the inner plexiform layer (IPL) (Grossniklaus, Geisert, & Nickerson, 2015).

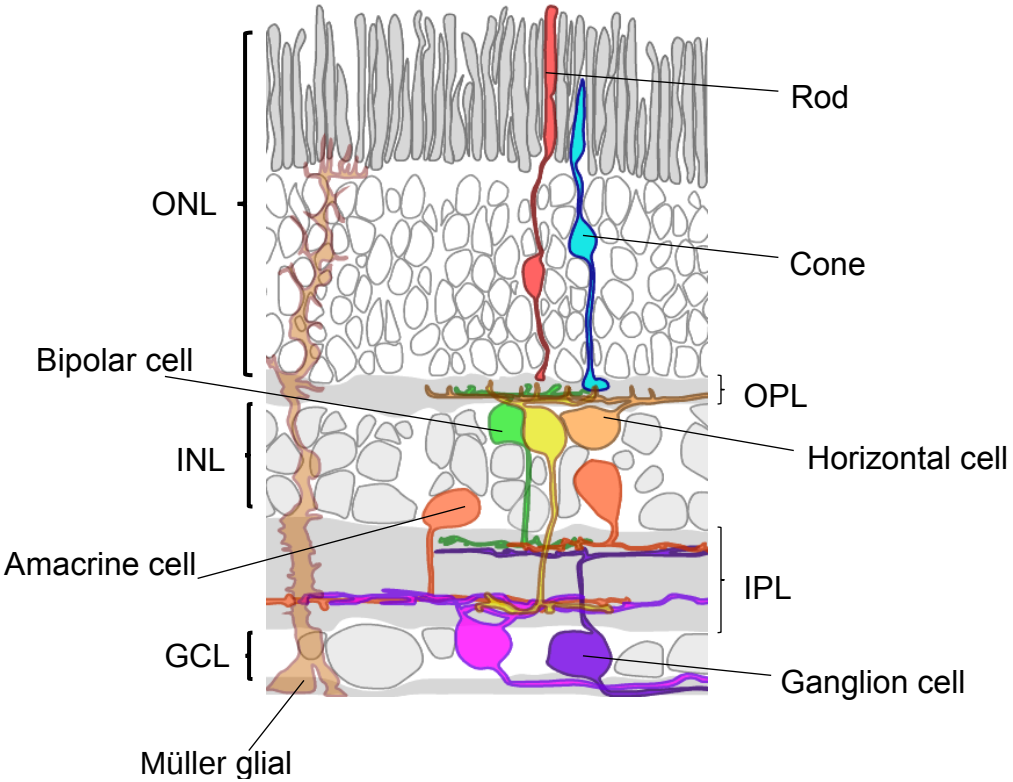

Fig.1 Scheme of a sagittal cross section of the mammalian retina. The retina is composed of two types of photoreceptors: rods and cones, which transmit signals to ganglion cells via bipolar cells. This signal is modulated by two inhibitory interneurons: the horizontal cells and amacrine cells. Müller cells are glial cells that support retinal physiological functions. Retinal neurons are organized into three different cellular layers: outer nuclear layer (ONL), inner nuclear layer (INL), and ganglion cell layer (GCL). These layers form two synaptic layers, one between the ONL and INL (outer plexiform layer; OPL), and one between the INL and GCL (inner plexiform layer; IPL). Modified from (Euler & Schubert, 2015).

Photoreceptor structure and function

Photoreceptor structure

Rods and cones are light sensing cells located in the outer nuclear layer of the retina, at the back of the eye. Both rods and cones are composed of four main cellular components: an outer segment, inner segment, cell body and the cell axon terminal (Fig. 2).

The outer segments (OSs) are composed of dense stacks of membrane disks equally spaced apart that contain the visual pigment necessary for cellular function (rhodopsin in the case of rods, and opsins with different spectral tuning in the case of cones). The structural support provided by the abundance of the visual pigment is essential as rhodopsin knockout mice fail to properly form OSs. The large quantity of visual pigment in the OS of PRs greatly increases the chances of photon capture by the cells.

The inner segment (IS) is a support structure for the OS in a number of ways. The IS not only physically supports the OS but also contains the Golgi apparatus and endoplasmic reticulum which are necessary to replace the huge protein turnover seen in the OS. The IS also contains many of the cells' mitochondria, providing the energy needed for phototransduction. All proteins needed for the normal function of the OS must travel from the IS to the OS through the narrow connecting cilium. The cell soma contains the cell's nucleus, responsible for DNA transcription before the RNA is transported to the endoplasmic reticulum in the IS. The synaptic terminal transmits

the light signal to the second order neurons of the retina, the horizontal and bipolar cells. In darkness, the cells maintain a steady stream of glutamate release controlled by calcium (Ca^{2+}), to the horizontal and bipolar cells while this transmission is terminated in light.

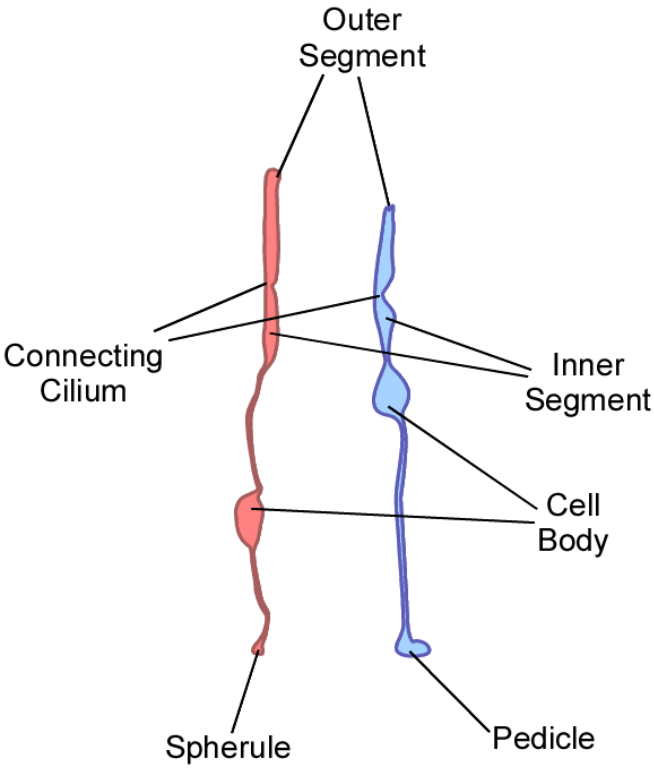

Fig 2. Anatomical structure of mammalian photoreceptors
Photoreceptors are composed of several distinct anatomical and functional compartments: the outer segment (OS) contains the visual pigment and cyclic nucleotide gated channels (CNGCs) and is responsible for phototransduction. The inner segment (IS) contains ribosomes and mitochondria to supply energy and proteins for the maintenance of the OS, the soma is responsible for gene expression and contains L-type Ca^{2+} channels. The axon terminals are responsible for glutamate release, controlled by L-type Ca^{2+} channels. Modified from (Euler & Schubert, 2015)**.**

At the plasma membrane, Ca^{2+} channels allow the entry of Ca^{2+} into the cell. Two types of Ca^{2+} channels are present at the plasma membranes of PRs. On the outer segments (OS) of PRs, cyclic nucleotide gated (CNG) channels are present (Butler et al., 2017) while voltage gated Ca^{2+} channels (VGCCs) are present on the cell body and cone pedicles (Morgans et al., 2005). Two different isoforms of VGCCs are expressed in PRs. Cone PRs contain α_{1D} VGCCs (Cav 1.3) on their cell bodies and terminals while rod PRs contain α_{1F} VGCCs (Cav 1.4) on their cell bodies and terminals (McRory et al., 2004, Morgans et al., 2005). Cone CNG channels are composed of two structurally related subunits, CNGA3 and CNGB3 (Kaupp & Seifert, 2002), while rod PRs are composed of three CNGA1 subunits and one CNGB1 subunit (Shuart, Haitin, Camp, Black, & Zagotta, 2011). While CNG channels are permeable to both sodium (Na^{+}) and Ca^{2+} (~80% Na^{+}, 15% Ca^{2+} and 5%Mg^{2+}) (Yau, 1994), CNG channels on the OS have increased Ca^{2+} permeability necessary for proper function with cone CNG channels showing higher Ca^{2+} affinity than those of rods (Hackos & Korenbrot, 1999).

Photoreceptor function

Within the rod OS, rhodopsin acts as a receptor to the photons. Upon photon absorption, the rhodopsin molecule becomes enzymatically active resulting in the catalysis and activation of the G protein transducin. Transducin then activates phosphodiesterase-6 (PDE6), hydrolysing the diffusible secondary messenger cGMP. The resulting decrease in cytoplasmic free cGMP concentration leads to the closure of the cGMP-gated channels on the plasma membrane. Rods respond to light with graded hyperpolarization whose amplitude increases incrementally as a function of flash intensity until saturation. Reproducibility of a single photon response in both amplitude and kinetics is a hallmark of rod phototransduction (reviewed in Fu & Yau, 2007). In cone PRs the phototransduction is essentially identical to that of rods; although differences do exist. Light activated spectrally tuned opsins, rather than rhodopsin, are sensitive to light within cones with transducin, and PDE is still responsible for continuing the cascade (Kefalov, 2010). While rods are sensitive to one photon of light (Hecht, Shlaer, & Pirenne, 1942) cones are 40-100 times less sensitive, requiring the simultaneous activation of tens to hundreds of visual pigment molecules to generate a detectable response (Kefalov, 2010).

The biosensor TN-XL

In 2005, the group of Oliver Griesback at the Max Planck Institute at Martinsried generated a FRET-based Ca^{2+} biosensor by utilising troponin C (TnC) as a Ca^{2+} binding moiety (Mank et al., 2006). They

generated a biosensor, dubbed TN-XL, by flanking the TnC moiety with a citrine and enhanced cyan fluorescent protein (ECFP) (Fig. 3). As this is a Förster resonance energy transfer (FRET)-based system, ratiometric analysis of the difference in levels of ECFP and citrine detected is utilised to determine the relative Ca^{2+} levels. When the cellular [Ca^{2+}] increases, TnC undergoes a conformational change bringing the ECFP and citrine closer together, allowing ECFP to donate energy required to excite citrine. However, when cellular [Ca^{2+}] is low, no conformational reconfiguration of the TnC peptide takes place and so excitation of the ECFP moiety results in measurement of the ECFP emission only. It was shown (Mank et al., 2006) that TnC is an ideal candidate for Ca^{2+} signalling as the binding of Ca^{2+} is fast and stable with significant changes in fluorescence change. Mank et al. also reported that the off rate of this biosensor is faster than the fastest single fluorophore to date reported, and is significantly faster than double chromophore biosensors. TN-XL has stable and reproducible fluorescence properties, is pH insensitive in the physiological range due to the combination ECFP/citrine, folds well at room temperature and at 37°C, and offers the benefits of ratiometric imaging.

The TN-XL biosensor was inserted into the cones in the mouse retina by Wei et al., (2012) through the use of a plasmid containing the human red opsin promoter (HR2.1) ensuring efficient transduction of cones. This stable incorporation of the TN-XL into the cones of the mouse retina allows for the measurement of Ca^{2+} dynamics within the cell upon the presentation of a light stimulus, as described in Kulkarni

et al., (2015). The incorporation of TN-XL into the cones allows indirect probing of the phototransduction cascade but does not affect the cellular morphology or electroretinogram (ERG) response. The fact that the TN-XL does not interfere with the light response of the cone may be due to the lack of the TN-XL in the OS. This lack of TN-XL in the OS of the cell may be due to a lack of transporter proteins for the TN-XL within the cell, preventing its transport through the connecting cilium between the OS and IS (Kennedy & Malicki, 2009). This lack of TN-XL in the OS restricts examination of the Ca^{2+} dynamics to the IS, cell body and cone terminals. Measurements of the Ca^{2+} dynamics in these structures are indirect measures, but the shared membrane potential of the cell allows us to partially infer the dynamics within the OS and the cell in general.

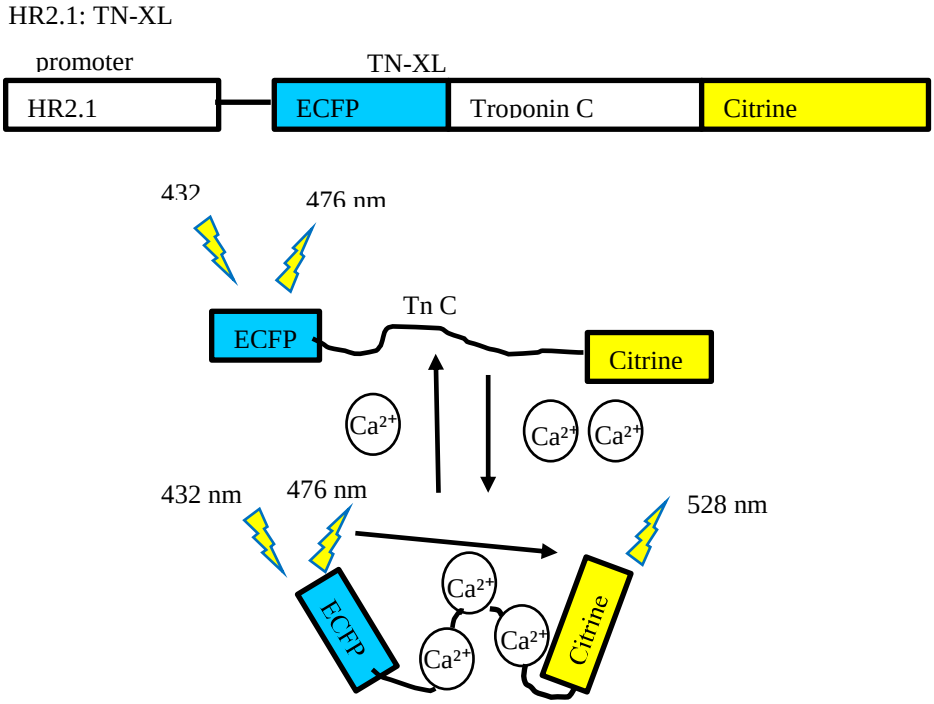

Fig 3. Schematic illustration of the TN-XL Ca^{2+} biosensor.

Illustration of the TN-XL biosensor developed by Mank et al., (2006) with the construct generated by Wei et al., (2012). The TN-XL biosensor is comprised of a Ca^{2+} sensitive Troponin C peptide (TnC) flanked by an enhanced cyan fluorescent protein (ECFP) and a citrine protein under the control of the human red opsin 2.1 promoter (HR.2.1). The construct is expressed only in cones. When Ca^{2+} levels in the cones are low, the stimulation of the ECFP results in the ECFP

fluorescing. However, when Ca^{2+} levels are high, the TnC undergoes a conformational change in which, after the ECFP is excited, it donates energy to the citrine protein, exciting it and causing it to fluoresce.

Retinal Dystrophies

To date, more than 250 genes have been implicated in human retinal dystrophies (Berger, Kloeckener-Gruissem, & Neidhardt, 2010) (Fig. 4). Due to their involvement in both the phototransduction cascade and Ca^{2+} homeostasis within the cell, we will focus here on diseases caused by mutations in *Pde6* genes. Mutations causing PDE6 enzyme dysfunction have been implicated in night blindness and retinitis pigmentosa (*Pde6a*, *Pde6b*, *Pde6g*), cone-rod dystrophies(*Pde6c*, *Pde6h*) and colour vision defects (*Pde6c*) (Berger et al., 2010). Retinitis pigmentosa (RP) is a family of inherited diseases which present with clinical and genetic heterogeneity causing retinal dysfunction that leads to PR cell death (Daiger, Sullivan, & Bowne, 2013; Farrar, Kenna, & Humphries, 2002; Sancho-Pelluz et al., 2008). RP presents clinically as autosomal dominant, autosomal recessive or X-linked (Hamel, 2006; Humphries, Farrar, Kenna, & McWilliam, 1990; Kaplan, Bonneau, Frézal, Munnich, & Dufier, 1990) with mutations in the *Pde6* gene encoding the beta subunit of the protein linked to autosomal recessive RP (DANCIGER et al., 1995; McLaughlin, Ehrhart, Berson, & Dryja, 1995; McLaughlin, Sandberg, Berson, & Dryja, 1993). RP affects more than one million individuals worldwide (Ammann, Klein, & Franceschetti, 1965;

Boughman, Conneally, & Nance, 1980; Jay, 1982) and autosomal recessive RP represents approximately 50-60% of those cases (Bunker, Berson, Bromley, Hayes, & Roderick, 1984; Grøndahl, 1987; Novak-Lauš, Kukulj, Zoric-Geber, & Bastaic, 2002). Interestingly, the most severe cases of RP are autosomal recessive forms that occur within the first decade of life, while autosomal dominant are comparatively mild forms of RP and develop later in life (as late as age 50) (Hamel, 2006). As PDE6 is an essential part of the phototransduction cascade due to it hydrolysing cGMP, closing Ca^{2+} channels in the cell (Debora B Farber, 1995), mutations in the PDE6B result in an accumulation of the cGMP in the PR (Bowes et al., 1990; D B Farber & Lolley, 1976; Debora B Farber & Lolley, 1974). This increase in levels of cGMP has also been shown to lead to PR cell death (Debora B Farber & Lolley, 1974; Lolley, Farber, Rayborn, & Hollyfield, 1977; Sancho-Pelluz et al., 2008)

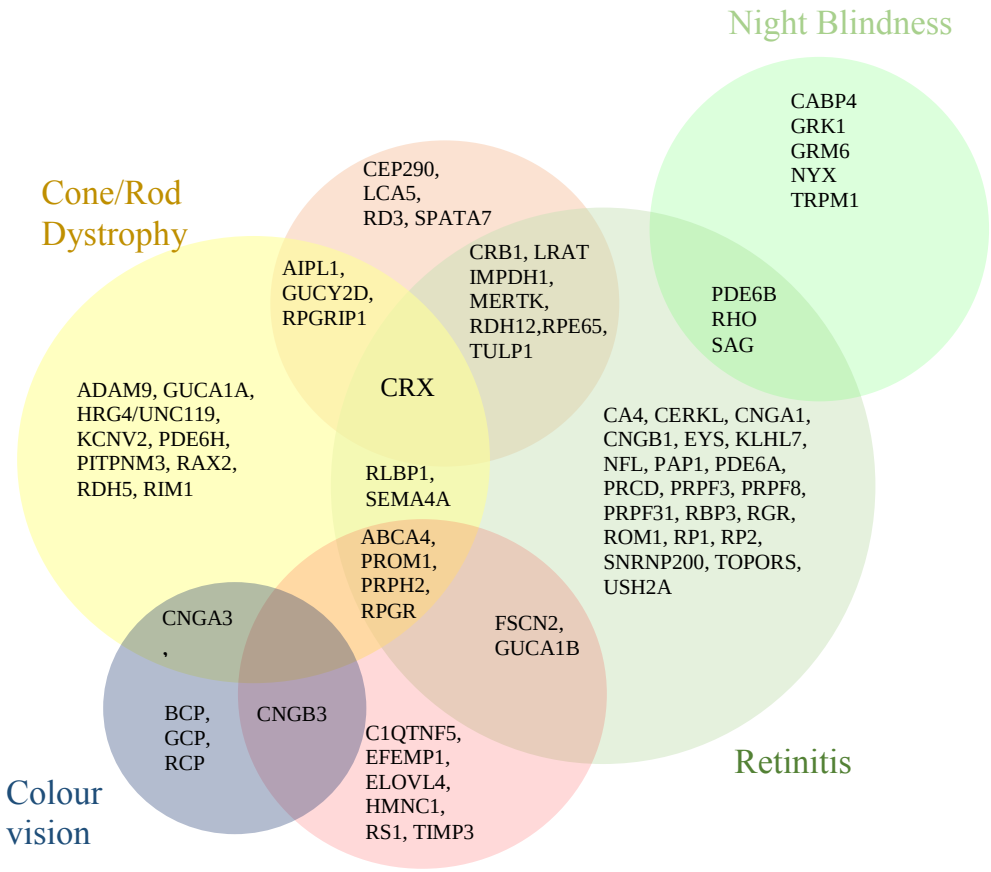

Fig. 4. Schematic illustration of some of the genes involved in various retinal dystrophies. Clinical diagnoses are indicated by coloured circles but only those involving mutations in PDE6 have been highlighted. Gene symbols in the overlapping areas show that

mutations in the same gene can lead to different phenotypes. Modified from Berger et al., 2010.

While the cellular mechanism leading to the cell death of the PRs has not been fully elucidated, the presentation of the disease in patients is better known. Initially patients complain of night blindness though this usually goes unnoticed until teenage years (Hamel, 2006). The disease then progresses to more complete loss of night time vision and a loss of peripheral vision during day: it is this stage that the disease is usually noticed by patients and diagnosed by clinicians (Hamel, 2006). The mid stages of the disease continue until the patients lose their ability to perform daily tasks and are considered legally blind. This continues to progress until finally the central field is lost, rendering them totally blind (Hamel, 2006).

Disease models

Retinal dystrophies are modelled in several animal models. In mice, mutations in the *Pde6b* located on chromosome five and causes the rod degeneration, such as in the *rd1* mouse model (Sidman & Green, 1965). The *rd1* mutation is shown to model the autosomal recessive form of RP, making it as aggressive in the mouse as it is in humans (McLaughlin et al., 1995). Another model for RP which carries a *Pde6b* mutation is the *rd10* mouse model. While a nonsense mutation in exon 7 of the *Pde6b* gene is the cause of the *rd1* degeneration (Dräger & Hubel, 1978), a missense mutation in exon 13 of the *Pde6b* gene is the cause of the *rd10* mouse's visual defect (Chang et al.,

2000). Due to the less aggressive nature of the *rd10* mouse, cells in the retina have matured further before the degeneration occurs, unlike in the *rd1* (Chang et al., 2007; Gargini, Terzibasi, Mazzoni, & Strettoi, 2007). The less aggressive nature of the phenotype is thought to be due to residual PDE6B in the *rd10* preventing a toxic build-up of cGMP delaying the onset of the PR death (McLaughlin et al., 1995).

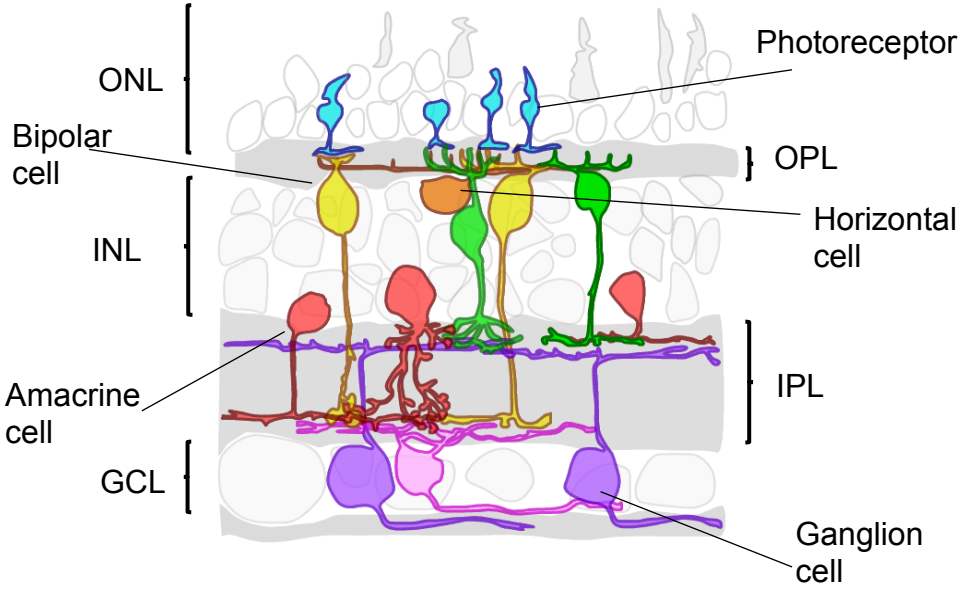

Fig.5 Scheme of a sagittal cross section through diseased mammalian retina.
In RP, mutations in *Pde6a* or *Pde6b* leads to the death of rods followed by a secondary death of cones. This results in the thinning

of the ONL as seen here, before the ONL disappears entirely. Initially little change is seen in the INL or GCL initially, but after a more prolonged period of time these layers also undergo remodelling: outer nuclear layer (ONL), inner nuclear layer (INL), ganglion cell layer (GCL), outer plexiform layer (OPL), inner plexiform layer (IPL). Modified from (Euler & Schubert, 2015).

For modelling achromatopsia in humans, the cone photoreceptor function loss 1 (*cpfl1*) mouse is used. Cone ERG recordings from the *cpfl1* mouse show no light induced responses and while the retinas show normal structural development cone cell numbers diminish with age (Chang et al., 2001). Autosomal recessive mutations in the *Pde6c* gene on chromosome 19 in mice is responsible for the phenotype, mimicking the mutation for congenital achromatopsia in human (Chang et al., 2001).

Calcium within the cells

Ca^{2+} is the most abundant cation in vertebrates (20-30g/kg body weight, in humans) (Bringhurst, 1995) and is a common secondary messenger in the cell with proposed regulatory functions in cellular functions such as cell growth, differentiation, motility, and death (Berridge, 2012; Clapham, 2007). Upon binding to effector proteins such as calmodulin and synaptotagmins, Ca^{2+} regulates cellular processes such as gene transcription, secretion, and muscle contraction (Berridge, 2012; Clapham, 2007). Ca^{2+} concentrations ($[Ca^{2+}]$) in the cell are tightly regulated with resting cytosolic $[Ca^{2+}]$

having a range of 50-300nM (Jacquemond, 1997; Maravall, Mainen, Sabatini, & Svoboda, 2000). Intracellular [Ca^{2+}] is dwarfed by the concentrations in the extracellular environment (~ 2mM) (Berridge, Lipp, & Bootman, 2000) and by the concentration seen in intracellular organelles.

Most intracellular organelles are known to act to some degree as Ca^{2+} stores. The endoplasmic reticulum (ER), Golgi apparatus, nucleus and mitochondria are all involved in the storage of Ca^{2+} within the cell (Bagur & Hajnóczky, 2017; Patel & Cai, 2015; Raffaello, Mammucari, Gherardi, & Rizzuto, 2016; Rizzuto, De Stefani, Raffaello, & Mammucari, 2012; Xu, Martinoia, & Szabo, 2015). The ER is the largest Ca^{2+} stores within the cell (Phillips & Voeltz, 2016) with Ca^{2+} concentrations in the ER estimated to be approximately 5,000 times higher than that of cytosolic [Ca^{2+}] (Berridge et al., 2000; Prakriya & Lewis, 2015). Sarcoendoplasmic reticulum Ca^{2+} transport ATPase (SERCA) pumps maintain inward flows of Ca^{2+} into the ER, while release of Ca^{2+} from the ER is enacted through inositol 1,4,5-trisphosphate receptors (IP3Rs) and ryanodine receptors (RyRs) that release Ca^{2+} into the cytosol upon stimulation (Prakriya & Lewis, 2015). Ca^{2+} within the ER can be rapidly mobilised into the cell although a single extracellular cue will only partially deplete this store (Berridge et al., 2000; Prakriya & Lewis, 2015). The ER is continuous with the nuclear envelope, with this membrane containing IP3R and RyR Ca^{2+} release channels in addition to SERCA pumps (Bootman, Fearnley, Smyrnias, MacDonald, & Roderick, 2009). IP3Rs, RyRs,

and SERCA are also expressed on the Golgi apparatus membranes (Pizzo, Lissandron, Capitanio, & Pozzan, 2011). The golgi apparatus hold unevenly distributed Ca^{2+} stores with trans-Golgi cisternae Ca^{2+} stores (~130µM) having lower concentrations than those of cis-Golgi cisterna (~250µM). Mitochondria are known to take Ca^{2+} into their matrix under high cytosolic [Ca^{2+}] acting as a Ca^{2+} sink for the cell. Ca^{2+} within smaller cellular organelles such as lysosomes has been reported (Christensen, Myers, & Swanson, 2002; Lloyd-Evans et al., 2008). It can be speculated that semi-continuous cellular organelles with a regular flow of Ca^{2+} may not occur in PRs. In PRs, mitochondria and ER are located in the inner segment, while the nucleus is spatially distant, located in the cell body. This distance would make it impossible for SERCA pumps to transport Ca^{2+} between the two organelles as their membranes are no longer continuous. Due to the more sequestered nature of the nucleus in PRs from the other Ca^{2+} stores within the cell, it is tempting to speculate that the dysregulation of Ca^{2+} would have to be severe to affect the nucleus and trigger cell death.

Various Ca^{2+} stores within the cells have different roles and as such, their relationship with extracellular and cytosolic Ca^{2+} are very diversified. These differences between various Ca^{2+} storage compartments are not solely based on their rate of exchange but pertain also to their function. In the mitochondria Ca^{2+} has been shown to have a regulatory role in metabolism (Denton & McCormack, 1990; McCormack & Denton, 1994; McCormack,

Halestrap, & Denton, 1990). ER Ca^{2+} stores act as a rapidly accessible and mobilisable store, while the trans-Golgi network store has critical function in regulated luminal content packaging leading to the processing of secretory granules (reviewed in Pozzan, Rizzuto, Volpe, & Meldolesi, 1994). While Ca^{2+} is a widely used secondary messenger within the cell due to the large number of immobile Ca^{2+} binding sites within the cell, its diffusion is very slow (Allbritton, Meyer, & Stryer, 1992). The various Ca^{2+} stores within the cell, widely distributed throughout the cell, aid in overcoming this slowness of Ca^{2+} mobility. The activity of more rapidly diffusing secondary messengers such as inositol 1,4,5-trisphosphate (IP3) or self-perpetuating cellular mechanisms such as Ca^{2+} induced Ca^{2+} release (CICR), help ensure a more regulated maintenance of Ca^{2+} within the cell (reviewed in Pozzan et al., 1994).

Ca^{2+} dysregulation

Dysregulation of [Ca^{2+}] has long been linked to cell death, but its exact role or underlying mechanism is still much debated (reviewed in Liu, Van Vleet, & Schnellmann, 2004; Rizzuto et al., 2003). The "high Ca^{2+}" hypothesis was put forward by (Fox, Poblenz, & He, 1999) who theorised that high intra-cellular [Ca^{2+}] leads to cell death. Some believe that Ca^{2+} dysregulation triggers apoptosis (Orrenius, Zhihotovsky, & Nicotera, 2003), while others refute this arguing that caspases, the proteases responsible for the activation and progression of apoptosis, are not upregulated in models of RP nor achromatopsia (Arango-Gonzalez et al., 2014; Doonan, Donovan, & Cotter, 2005).

Confusion may occur from apoptosis becoming a catch all term for any form of cell death seen, even when caspases are shown to not be activated (Donovan & Cotter, 2002; Doonan, Donovan, & Cotter, 2003). Hence, the exact mechanism driving PR cell death in these diseases is still unknown. Ca^{2+} dysregulation has been linked to mitochondrial damage leading to the release of pro-apoptotic proteins or pro-oncotic proteins from the organelle (Liu & Schnellmann, 2003; Orrenius et al., 2003; Pinton, Giorgi, Siviero, Zecchini, & Rizzuto, 2008). It has also been shown that an unregulated Ca^{2+} uptake leads to cell death through the unfolded protein response (UPR) in the endoplasmic reticulum. Cell death involving low [Ca^{2+}] is less well studied although as Ca^{2+} is necessary for so many cellular functions: the lack of Ca^{2+} would undoubtedly have disastrous effects.

The Calpain family

Calpains are a family of cytosolic cysteine proteases whose enzymatic activities are dependent on Ca^{2+}. To date, 15 calpain isoforms have been discovered in mammals. The calpain family can be subdivided into typical (calpain 1, 2, 3, 8, 9, 11 and 12) and atypical calpains (calpain 5, 6, 7, 8b, 10a and 15) (Huang & Wang, 2001; Sorimachi, Ishiura, & Suzuki, 1997). Each of these calpain isoforms are an 80kDa protein but only some of them (calpain 1, 2 and 9) interact with the regulatory 30kDa calpain-4 (Huang & Wang, 2001; Sorimachi et al., 1997). This interaction has caused some

nomenclature issues. When interacting with the small regulatory calpain-4, calpain-1 and calpain-2 are referred to as μ-calpain and m-calpain respectively. Calpains are constitutive enzymes but cannot be considered household proteins as the transcription of their genes is regulated (Cottin et al., 1994) by a promoter while most household proteins are constitutively transcribed. Both calpain-1 and -2 are expressed in every cell in the mammalian body (Huang & Wang, 2001; Sorimachi et al., 1997) while others calpain-3 and calpain 8, are expressed only in specific tissues (Suzuki, Hata, Kawabata, & Sorimachi, 2004). Calpains have been implicated in several cellular functions including signal transduction, cell proliferation, cell cycle progression, differentiation, apoptosis, membrane fusion and platelet activation (Carafori, 1998; Huang & Wang, 2001; Saido, Sorimachi, & Suzuki, 1994; Sorimachi et al., 1997). Here, we will focus on calpain-1 and calpain-2, two extensively studied isoforms of the calpain family, which are expressed in the retina.

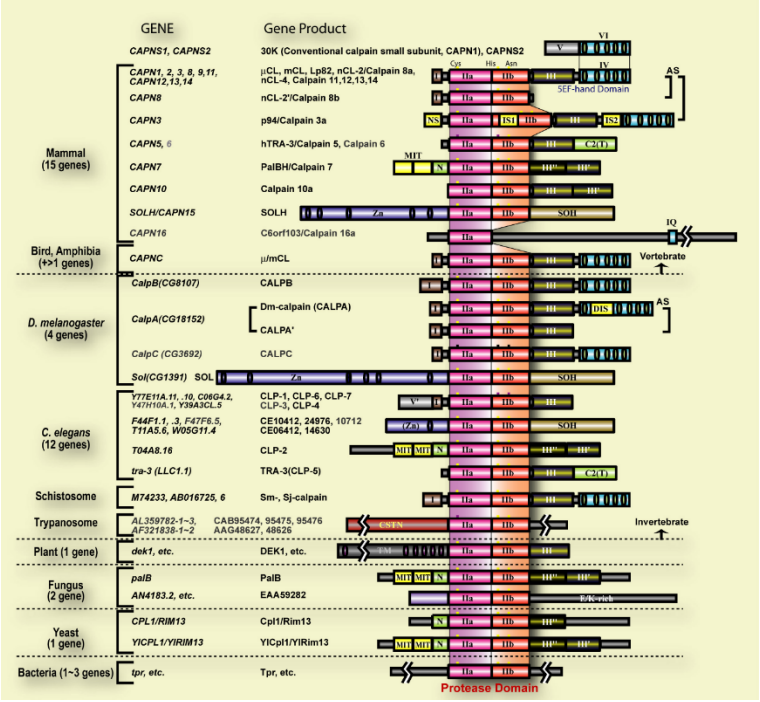

Fig. 6 Evolutionarily conserved calpain isoforms

Calpain proteases are ubiquitously expressed and have been identified in almost all cell types. The evolutionarily conserved protease domain has been maintained in almost all calpain isoforms in all forms of life except for the atypical mammalian calpain 16. This would also point to the ubiquitous use of Ca^{2+} in all cell types, as calpain are dependent on Ca^{2+} for activation. Figure taken from Calpain for Modulatory Proteolysis Database, http://www.calpain.org/overview.rb?cls=calpain taken 13/11/2018.

Calpain structure

Both calpain-1 and calpain-2 are composed of an 80kDa active subunit and the regulatory 30kDa subunit. The 80kDa subunit of calpain-1 is slightly larger than that of calpain-2 (81,889Da compared to 79,900 Da) (Aoki et al., 1986; Imajoh et al., 1988). Generation of two-knockout mice proved embryonically lethal, demonstrating that these proteases are essential for life

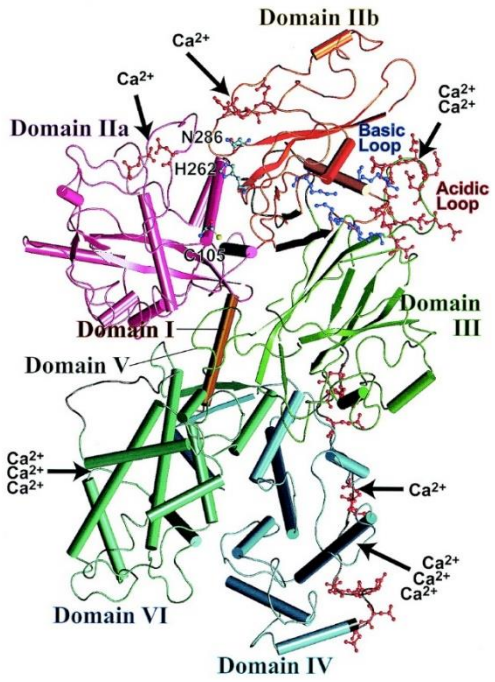

Fig.7 Crystallised structure of m-calpain without Ca^{2+}

Structure of m-calpain without Ca^{2+}. As can be seen domains I-IV of calpain-2 contain several Ca^{2+} binding sites as does the regulatory calpain-4 which forms domains V and VI. The catalytic triad of C105, H262 and N286 can be seen in domain IIa. Image from Suzuki et al., (2004).

however, mice with calpain-1 knockout survived showing that only calpain-2 is essential for normal embryonic development (Arthur, Elce, Hegadorn, Williams, & Greer, 2000; Azam et al., 2001). Calpain-1 and calpain-2 are both composed of four protein domains (Suzuki, 1990). The regulatory subunit calpain-4 contains two domains bringing the total number of subunits on m- and μ-calpain to six (Suzuki, 1990).

Calpain activation

While calpains are expressed in every cell, they are not constitutively active but rather are activated in a number of steps by Ca^{2+}. Calpain-2 has been discovered to have 11 Ca^{2+} binding sits across the six domains (two on domain II, two on domain III, four on domain IV, and three on domain VI) and due to the sequence homology the same can be assumed for calpain-1. Domain II forms the active site of calpain-1 and calpain-2 with the catalytic triad of amino acids (aa). The catalytic triad is composed of, a cysteine (aa 115 or 105 on

calpain-1 and calpain-2 respectively), a histidine (aa 272 or 262) and an asparagine (aa 296 or 286) (Moldoveanu et al., 2002).

Molecular mechanism of calpain activation

Calpain activation is controlled by Ca^{2+} and is aided by the autolysis of domain I. Autolysis occurs 40 Angström (Å) from the catalytic active site and so is not an intermolecular event (Suzuki, 1990). Autolysis of calpain-1 involves the removal of 14aa from the 80kDa subunit, forming a 78kDa intermediate before a further 12aa are removed to form the 76kDa autolytic fragment (Zimmerman & Schlaepfer, 1991). For calpain-2, nine n-terminal aa are removed before an additional 10 are cleaved off, producing a 78kDa fragment (Brown & Crawford, 1993). Binding of Ca^{2+} induces conformational changes by breaking salt bridges between a set of glutamine and asparagine residues and a set of lysine aa allowing domain IIb to move toward domain IIa (Strobl et al., 2000). This movement allows the formation of the catalytic triad by reducing the distance of the cysteine residue 10.5 Å to ~3.7 Å from the histidine and asparagine making the calpain catalytically active (Reverter, Sorimachi, & Bode, 2001).

$[Ca^{2+}]$ required for calpain activation

Investigation of calpain-1 and -2 in bovine skeletal muscle revealed the levels of Ca^{2+} required for half maximal activity of both calpains. Autolysis of calpain-1 lowers the $[Ca^{2+}]$ required for proteolytic

activity from a range of 3-50μM to 0.5-2μM (Cong, Goll, Peterson, & Kapprell, 1989; D E Goll, 1995). Autolysis of calpain-2 however lowers [Ca^{2+}] required for proteolytic activity from 400-800μM to 50-150μM (Cong et al., 1989; D E Goll, 1995). The concentration of Ca^{2+} for autolysis of calpain was shown to be lowered by the interaction with phospholipids (Coolican & Hathaway, 1984).

Lowering the threshold required for calpain activation

Phosphatidylinositol was shown to be the most effective at lowering the [Ca^{2+}] for calpain autolysis (from 50-150μM to 0.8-50μM from for calpain-1, 550-800μM to 90-400μM for calpain-2) (Cong et al., 1989). Other phospholipids such as phosphatidylinositol 4,5-bisphosphate (PIP_2) reduced the concentrations needed for autolysis by approximately six-fold (Cong et al., 1989; Saido, Mizuno, & Suzuki, 1991; Saido, Shibata, Takenawa, Murofushi, & Suzuki, 1992). Phospholipids are thought to bind to domain III of calpain which suggests phospholipids have an effect on the structure of other calpain domains as domain III does not seem to have any Ca^{2+} binding sites (Tompa, Emori, Sorimachi, Suzuki, & Friedrich, 2001). However, it was shown in *in vitro* assays that high molar ratios of 375-4,100 phospholipids to each calpain was needed to have an effect on the [Ca^{2+}] required for autolysis (Cong et al., 1989; D E Goll, 1995). Others report that calpains do not bind to the phospholipids but rather proteins on the plasma membranes (Inomata, Hayashi, Nakamura, Saito, & Kawashima, 1989; Inomata, Saito, Kon, & Kawashima, 1990; Kuboki, Ishii, & Kazama, 1990). Regardless of

whether calpain interacts with the phospholipids or proteins on the plasma membrane, one may speculate that this interaction locates the calpain closer to Ca^{2+} channels, helping to further activate the protease.

Functional roles for calpain

Calpain isoforms have been implicated in cellular functions such as signal transduction, cell cycle, proliferation, differentiation, migration, apoptosis, membrane function, formation of muscle fibres, dendritic spine formation and pruning, and many others. We will discuss some of these here (Darrel E Goll, Thompson, Li, Wei, & Cong, 2003; Kanamori et al., 2013; Smalheiser & Lugli, 2009; Sorimachi et al., 1997).

Calpain in fertilisation

Calpain proteases are vital for survival. Calpain-2 knockout mice are shown to be embryonically lethal (Dutt et al., 2006). This is probably due to the fact that an increase in intracellular $[Ca^{2+}]$ is the earliest event in the activation of fertilised egg induced by penetration of the sperm cell (D, 1992). Fertilisation of the egg is accompanied by the activation of calpain (Haim, Ben-Aharon, & Shalgi, 2006), as estimated by the cleavage of α-spectrin into calpain specific products (Haim et al., 2006).

Calpain in diabetes

Polymorphisms within intron 3 the calpain 10 gene (Baier et al., 2000) have been associated with increases in free fatty acids and insulin resistance (Orho-Melander et al., 2002). Mutations within the calpain 10 results in upregulation of protein kinase C (a calpain substrate) leading to hyperphosphorylation of the insulin receptors reducing the kinase activity of these insulin receptors, increasing insulin resistance (Griffin et al., 1999; Suzuki et al., 2004).

Calpain in oncosis/necrosis

Calpain has been implicated in a variety of the physiological changes seen during oncosis/necrosis. Cellular membrane permeability (a hallmark of oncosis) is thought to occur in three stages, with each stage increasing permeability from propidium iodide in stage one, to allowing the release of 130kDa Lactate dehydrogenase (LDH) in stage three (J Chen & Mandel, 1997; Jing Chen, Liu, Mandel, & Schnellmann, 2001). Increases in calpain proteolysis have been linked to the increased plasma membrane permeability. Hydrolysis of paxillin occurs at the same time as propidium iodide entry, while hydrolysis of cytoskeletal proteins talin and vinculin occurs concomitantly with LDH release (Liu & Schnellmann, 2003).

Calpain promotes disruption and hyperpermeability in the blood brain barrier (BBB) through disruption of the tight junctions *in vitro* (Alluri et al., 2016). It was shown that calpain mediated dysfunction of the

BBB was induced by interleukin-1β (IL-1β) and this disruption of the BBB was abolished with calpain inhibition (Alluri et al., 2016). IL-1β is a marker for inflammation in mammalian tissues and the involvement of calpain in an inflammatory response (also associated with oncosis) suggests links between calpain and oncosis.

Calpain in apoptosis

Apoptosis is a programmed form of regulated cell death carried out by the caspase family of proteins (discussed further below). The role of calpain in apoptosis is difficult to fully elucidate due to a combination of improper nomenclature and the use of calpain inhibitors which also inhibit other molecules more well established in the apoptosis pathway. Especially the interactions between caspases and calpains are complex to understand. It has been shown that calpains cleave caspase-7, -8 and -9 inactivating capase-7 and -8 (Chua, Guo, & Li, 2000). However, calpain-2 has been suggested to cleave procaspase-12, activating it and cleaving the Bcl-xl loop region and changing it from an anti-apoptotic molecule into a pro-apoptotic molecule (Nakagawa & Yuan, 2000).

Activation of calpain in apoptotic HL-60 cells by treating them with the topoisomerase I inhibitor 9-amino-20(s)-camptothecin, was shown to occur after the activation of the caspase molecules and at the same time as the cleavage of Bax (Wood & Newcomb, 1999). This activation of calpain was theorised to be mediated through caspase degradation of calpastatin but this apoptosis was not stopped

by calpain inhibition, indicating that calpain activation was a consequence of apoptosis, but not a driver of it.

The nature of the insult has been shown to have a role in the method of apoptosis. In human platelets, calpain-1 was shown to activate the apoptosis through caspase-9, caspase-3, apoptotic protease activating factor 1 (APAF-1) and, cytochrome-c and not by other caspases. Anti-IgM induced apoptosis in immature B-cells was blocked by overexpressing calpastatin but, actinomycin D induced apoptosis in the same cell line was not stopped by calpastatin overexpression.

Due to the different roles of calpain-1 and calpain-2 and their differential expression, the role of each calpain isoform in apoptosis may be difficult to fully elucidate by the use of different cell lines and cell types. Greater stringency in the cell lines used, and the conditions the cells are kept in, need to be asserted in order to properly determine the relationship between calpain and caspases in the execution of apoptosis.

Cell death mechanisms

Recently Galluzzi et al. published the findings of the nomenclature committee on cell death (Galluzzi et al., 2018) where the definition of several forms of cell death were updated. Some of these relevant to Ca^{2+} dysregulation in PRs, we will discuss here. Alongside these modes of cell death from Galluzzi et al. we will discuss two more which they did not examine.

Cell death is an essential part of life and is the irreversible degeneration of vital cellular functions (notably ATP production and preservation of redox homeostasis) culminating in the loss of cellular integrity (permanent plasma membrane permeabilization or cellular fragmentation) (Galluzzi et al., 2018). Cell death can be regulated (i.e. results from the activation of one or more signal transduction modules, and hence can be pharmacologically or genetically modulated) (Galluzzi et al., 2018) or unregulated. In the case of regulated cell death, some forms are programmed cell death which occur in strictly physiological scenarios, i.e., it does not relate to perturbations of homeostasis and hence does not occur in the context of failing adaptation to stress (Galluzzi et al., 2018).

Cell death mechanism	Markers	Reported in PRs	Linked to Ca^{2+} dysregulation	Regulated/ Unregulated
Anoikis	Loss of Integrin-dependent anchorage	-	Yes	Regulated
Mitochondrial permeability transition - driven necrosis	CYPD	-	Yes	Regulated

Parthanatos	PARP1, AIF, MIF	Yes	Yes	Regulated
Necroptosis	MLKL, RIPK3, RIPK1	Yes	Yes	Regulated

Table 1. List of diverse forms of cell death and their relationship to reported mechanisms of PR cell death and Ca^{2+} dysregulation.

Apart from these definitions we will also discuss apoptosis, oncosis, and necrosis though these are harder to succinctly define.

Intrinsic apoptosis is type of regulated cell death initiated by perturbations of the extracellular or intracellular microenvironment, demarcated by mitochondrial outer membrane perturbations (MOMP), and precipitated by executioner caspases, mainly caspase-3 (Galluzzi et al., 2018).

Oncosis/Necrosis

Oncosis is often used in place of necrosis in the literature, although Weerasinghe & Buja, (2012) described oncosis as a form of cell death opposite to apoptosis, marked by a drop in ATP and completed through a necrotic form of cell death, suggesting that all oncosis is necrotic but not all necrosis is oncotic. Oncosis is a more zonal form of tissue cell death than apoptosis which affects cells on a more singular basis (Majno & Joris, 1995). Oncosis often affects contiguous cell populations (Majno & Joris, 1995) resulting in cellular swelling, formation of cytoplasmic vacuoles, distended

endoplasmic reticulum, formation of cytoplasmic blebs, condensed, swollen or ruptured mitochondria, disaggregation and detachment of ribosomes, disrupted organelle membranes, swollen and ruptured lysosomes, and even disruption of the cell membrane (Kerr, Wyllie, & Currie, 1972; Majno & Joris, 1995; Trump, Berezesky, Chang, & Phelps, 1997). These structural changes in the cell are followed by plasma membrane breakdown, release of intracellular contents, and inflammation (Majno & Joris, 1995). Unlike apoptosis, oncosis is a passive process and so can take place regardless of the ATP concentration within the cell (Leist, Single, Castoldi, Kühnle, & Nicotera, 1997).

Necrosis was defined by Fink & Cookson, (2005) as "postmortem observation of dead cells that have come into equilibrium with their environment", while J.M. Cullen, (2010) defined necrosis as "cell death caused by loss of membrane integrity, intracellular organelle swelling and adenosine triphosphate (ATP) depletion leading to an influx of Ca^{2+}." Interestingly, J.M. Cullen, (2010) continued by suggesting that this influx of Ca^{2+} led to the disruption of the cellular cytoskeleton, leading to the destruction of cellular elements. Although never mentioned by Cullen, cytoskeleton proteins are targets of calpain and so this activity could be ascribed to calpain. Here we will discuss more deeply two types of cell death modes employed by the cell for a variety of insults and the role calpain is theorised to play in both.

Apoptosis

Apoptosis is an essential, genetically regulated and finely tuned process of cell elimination essential for tissue maintenance, embryogenesis and development (Kerr et al., 1972). Apoptosis is an essential part of normal development and has functions in organisms as diverse as nematodes, insects and humans (Twomey & McCarthy, 2005). Cell death by apoptosis is characterised by a series of events including cell collapse, formation of membrane blebs, chromatin condensation, and DNA degradation (Kerr et al., 1972). Due to the shrinkage of the cells, the cytoplasm appears denser and the organelles more tightly packed. The caspase family has been discovered to be central regulators of apoptosis with at least 14 members of the caspase family present in the cell as proenzymes before activation (Donovan & Cotter, 2002). Our understanding of the mechanisms involved in apoptosis in mammalian cells comes from the investigation of programmed cell death in the nematode *Caenorhabditis elegans* (Ellis & Horvitz, 1986). Apoptosis has been recognised as a distinctive and important form of "programmed cell death" which involves genetically timed removal of cells though several other forms of programmed cell death have been discovered (Debnath, Baehrecke, & Kroemer, 2005; Formigli et al., 2000; Howden et al., 2005; Sperandio, de Belle, & Bredesen, 2000). Extensive blebbing of the plasma membrane is followed by karyorrhexis and separation of cell fragments into apoptotic bodies during the "budding" process (Howden et al., 2005). Apoptosis is a process without inflammation or tissue swelling for three reasons: 1)

apoptotic cells do not release their cellular contents into the surrounding tissue, 2) they are quickly phagocytosed by surrounding cells, and 3) the engulfing cells do not produce anti-inflammatory cytokines (Kurosaka, Takahashi, Watanabe, & Kobayashi, 2003; Savill & Fadok, 2000).

Choosing the right for of cell death mechanism for the dying cell

As several forms of programmed cell death other than apoptosis have been discovered (Debnath et al., 2005; Formigli et al., 2000; Howden et al., 2005; Sperandio et al., 2000), the involvement of caspase proteases is the best indication that apoptosis is occurring and not another form of cell death. Necrosis is less easy to define by protein involvement although apoptosis inducing factor (AIF) has been implicated in the necrotic process within cells (Shang et al., 2014). Several factors may determine whether a cell uses necrosis or apoptosis to die. The availability of energy is a large determinant. As necrosis is a passive process, which does not require ATP, it has long been suspected that the levels of ATP in the cell are a determining factor for whether the cell chooses apoptosis or necrosis to complete cell death under stress (Criddle et al., 2007; Leist et al., 1997; Tsujimoto, 1997). If levels decreases in ATP drop to less than 80-85%, the cell will die by apoptosis or survive if mitochondrial function can be restored (Lieberthal, Menza, & Levine, 1998). If, however, ATP depletion is greater than 80-85%, necrosis will occur (Lieberthal et al., 1998). The type or degree of stimuli determines if

the cell die by apoptosis or necrosis. At low doses, stimuli such as, heat, radiation, hypoxia, and cytosolic anticancer drugs can induce apoptosis but these same stimuli result in necrosis at higher doses or prolonged exposure (Elmore, 2007).

Aims

While mutations in PDE6 have been known to result in dysregulation of Ca^{2+} within the cells, the exact effects of this are still much debated. Here, we aim to further elucidate the effects of this Ca^{2+} dysregulation, including the mechanism of cell death it leads to. Knowing the mechanism utilised by the cell machinery to kill the cell could allow for new therapeutic developments and eventually effective clinical interventions to treat retinal degeneration.

The aims of this study are:

1. Investigate the levels of calpain activity across the retina as a marker for Ca^{2+} dysregulation and examine whether and to what extent calpain-1 and -2 may be implicated with this activity.
2. Measure the levels of cell death in the retina using the TUNEL assay and further elucidate the cell death mechanisms using markers for different cell death pathways, t-AIF and cleaved caspase-3.
3. Investigate the temporal and spatial progression of the six markers (calpain activity, calpain-1, calpain-2, TUNEL, AIF and caspase-3) across wild-type and degenerating retina.
4. Measure light mediated Ca^{2+} responses in cones using two-photon microscopy and Ca^{2+} channel blockers to assess how blocking Ca^{2+} channels affect light responses and cellular Ca^{2+} concentration.

5. Develop a methodology for the simultaneous imaging of calpain activity and calcium levels in individual photoreceptors.

Materials and Methods

Animals for two-photon Ca^{2+} *imaging*: The transgenic mouse line *HR2.1:TN-XL* (C57BL/6J background) expresses the Ca^{2+} biosensor TN-XL (Mank et al., 2006) under the control of the human red opsin promoter (HR2.1) selectively in cone PRs (Wei et al., 2012). The TN-XL biosensor was crossbred with the C57BL/6J mouse to allow us to study Ca^{2+} dynamics within the cone terminals. Animals from these lines were used irrespective of gender. For measuring Ca^{2+} responses in *HR2.1:TN-XL* mice were used regardless of age ranging from P34-P181. For imaging calpain under the two-photon *HR2.1:TN-XL* x *rd1* mice aged between P11-P13 were used while wt mice were used regardless of age (P19-P249). In brief, for all imaging experiments, mice were dark adapted for two hours. They were deeply anesthetized with isoflurane (CP-Pharma, Germany) and then sacrificed by cervical dislocation.

Animals. To study primary and secondary cone degeneration, *rd1* (C57BL/6J x C3H background) and *cpfl1* (C57BL/6J) mutant mouse models were used. We used the more slowly degenerating *rd10* mice (C57Bl6/J) to assess primary rod degeneration at a longer timescale than *rd1* and because in *rd10*, developmental and degenerative cell death are temporally less overlapping. Animals from these lines were used irrespective of gender. Wild-type and mutant *rd1* and *cpfl1* mice were crossbred with the transgenic mouse line *HR2.1:TN-XL* (C57BL/6J background), which expresses the Ca^{2+} biosensor TN-XL (Mank et al., 2006) under the control of the human red opsin promoter

(HR2.1), selectively in cone PRs (Wei et al., 2012). The mouse lines thereby generated were the *HR2.1:TN-XL* x *cpfl1*and *HR2.1:TN-XL* x *rd1* lines; for simplicity, we refer to these biosensor lines in the following as wt, *cpfl1*, and *rd1*. In the context of the present study, these mouse lines allow for a direct identification of cone PRs. Animals above P12 were sacrificed by CO_2 asphyxiation followed by cervical dislocation. Mice below P12 were sacrificed by decapitation. All procedures were performed in accordance with the law on animal protection issued by the German Federal Government (Tierschutzgesetz) and approved by the institutional animal welfare board of the University of Tübingen.

Calpain activity assay. Following earlier work (Kulkarni, Trifunović, Schubert, Euler, & Paquet-Durand, 2016), calpain activity was initially analysed in mice at P14, 18, 24, 30, 60, 90 and 120 (Supplemental Table 1). In *rd1* and, for comparison, wt, we added P10 and 12, as degeneration peaks early in the *rd1* mutant. Eyes were marked on the nasal side prior to enucleation, flash-frozen in liquid N_2, embedded in Tissue-Tek OCT compound (Sakura Finetek Europe, Alphen aan Den Rijn, Netherlands), and stored at -20°C until cryo-sectioning into 16µm thick vertical sections. Sections were rehydrated in calpain reaction buffer (CRB) (5.96g HEPES, 4.85g KCl, 0.47g $MgCl_2$, 0.22g$CaCl_2$ in 100ml ddH_2O; pH 7.2) with 2mM dithiothreitol (DTT), and then incubated for 2h at 37°C in CRB containing 50µM of tBOC-Leu-Met-CMAC (Molecular Probes), a

calpain-specific substrate, whose fluorescence increases after cleavage by calpain (Francois Paquet-Durand et al., 2006).

Immunohistochemistry. For immunostainings, we analysed mice at P10, 12, 14, 18, 24, and 30 (Supplemental Table 1). Due to the lack of a discernible outer nuclear layer (ONL) in *rd1* and *rd10* post P30-animals, and the lack of significant difference in calpain activity in *cpfl1* and wt post P30-animals, we limited our examination to time points between P10 and P30. Eyes were fixed in 4% PFA in 0.1M phosphate buffer saline (PBS, pH 7.4; for 45mins) and cryo-protected in sucrose gradients in PBS at room temperature for 2hrs. Then, eyes were embedded in Tissue-Tek OCT cryomatrix (Sakura Finetek Europe, Alphen aan Den Rijn, Netherlands) and stored at -20°C until cryo-sectioning into 16µm thick vertical sections. Sections were rehydrated with PBS, permeabilized in 0.3% Tween in PBS containing blocking solution (10% goat serum, 1% BSA). As primary antibodies, we used rabbit anti-calpain-2 (ab39165; 1:300; Abcam, Cambridge, UK), rabbit anti-calpain-1 (ab39170; 1:100; Abcam, Cambridge, UK), rabbit anti-cleaved-caspase-3 (#9664; 1:300, Cell Signalling Technology, Frankfurt, Germany) and, rabbit anti-AIF (ab1998; 1:350; Abcam, Cambridge, UK). As secondary antibodies, we used Alexa Fluor 488 goat anti-rabbit (1:350; Molecular Probes, Eugene, USA).

Cell death detection: For the detection of cell death, we analysed mice

at P10, 12, 14, 18, 24, and 30 (Supplemental Table 1). The terminal deoxynucleotidyl transferase dUTP nick end labelling (TUNEL) assay was performed using the TMR red kit from Roche Diagnostics (Mannheim, Germany). Sections were incubated in blocking solution (1% BSA, 10% normal goat serum, 1% fish gelatine for 1hr after 5mins incubation with alcohol acetic acid mixture (62% EtOH, 11% Acetic Acid, 27% H_2O). Sections were then incubated with TMR red TUNEL kit as per manufacturer's instructions.

Microscopy and image processing. Z-stack images were captured on an Imager Z1 ApoTome microscope using a 20x air objective (0.8 NA; *cf.*), and Zen (v.2.3 Pro) software (Carl Zeiss Microscopy GmbH, Oberkochen, Germany). Zen Lite v.2.3 software was used to reconstruct images and ImageJ 1.52e (http://imagej.nih.gov/ij) was used to count positive markers in each image. Figures were generated in IGOR Pro (Wavemetrics, Lake Oswego, USA) and arranged in Canvas 11 (ACD Systems International Inc., Seattle, USA).

Analysis of marker data. Data was obtained from at least three different animals for each parameter examined. For each animal, vertical sections were quantified using collapsed Z-stacks of n=~16, 0.75µm-spaced images acquired at 20x magnification (Supplemental Table S1). For each section, five regions across the retina were imaged and analysed (Supplementary Fig. 1). Calpain-active, as well as calpain-2-, calpain-1-, caspase-3-, AIF-, and TUNEL-labelled cells

were counted and expressed as number of positive cells in the ONL per 1,000µm² in all mouse lines, at all time points. Statistical comparisons were made using the Kruskal–Wallis one-way analysis of variance test using GraphPad Prism 7 (La Jolla, USA). Dunn's posthoc test was performed after Kruskal-Wallis and measured variance between the groups at each time point but not between time points.

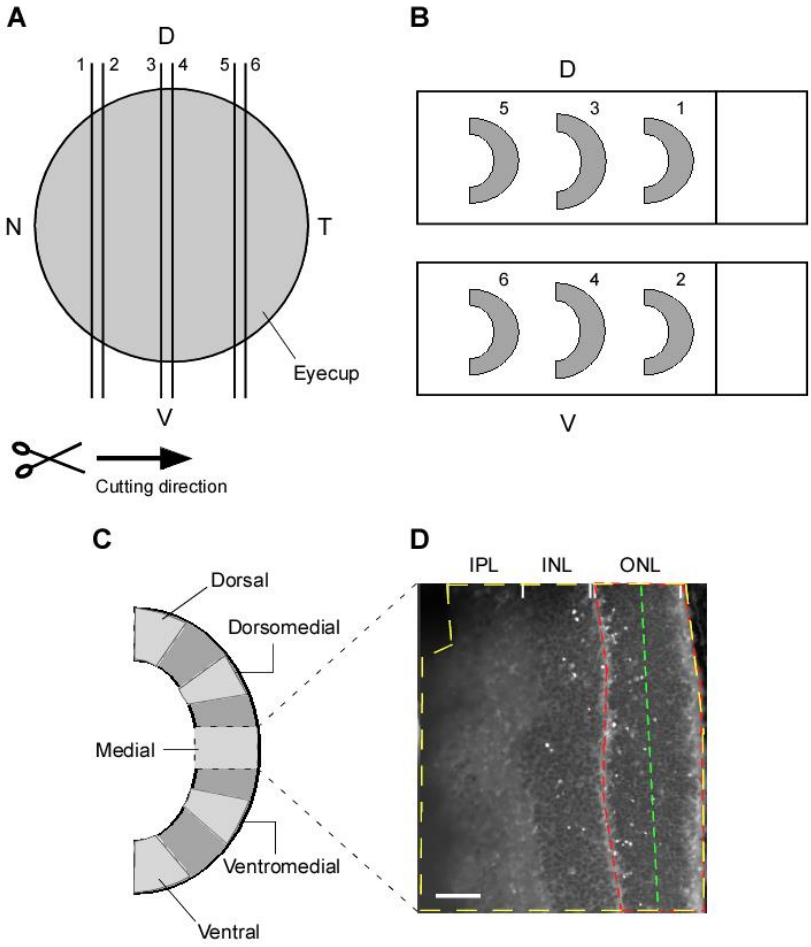

Figure 8. Illustration of the preparation protocol. Mouse eyes were marked nasally before being enucleated, dissected, fixed, and flash frozen in liquid nitrogen before sectioning. Eyes were sectioned from the nasal side towards the temporal side along the dorso-ventral axis (**A**). Consecutive sections were kept on consecutive slides (**B**). Sections were imaged along the dorso-ventral axis at five locations: Dorsal, Dorsomedial, Medial, Ventromedial and Ventral (**C**). Images

were then analysed (**D**) by measuring the whole retinal area imaged (yellow dashed line), the ONL area imaged (red dashed line) and, ONL length imaged (green dashed line) for each image. ONL width was calculated by dividing the area by the length for each image.

Gaussian process modelling. Gaussian process models were used to estimate the mean and standard deviation of the activity of each cell death marker for each mouse line at the observed time points. These models were used as they can accommodate the non-linear change in the level of each marker and provide a generative model for estimating properties of interest (in our case, the likely peaks for each marker). Modelling was performed in Python 3.5 using the GPy ("GPI A gaussian Process Framew. phython," 2012) library. All Gaussian Process (GP) (Williams & Rasmussen, 2006) models used radial basis function kernels and additive Gaussian likelihood noise, and were optimised using the L-BFGS-B maximum likelihood algorithm. Prior to model fitting, a square root transformation was applied to the data to accommodate the left-skew and zero-bound; the inverse transformation was applied for subsequent inference. A distribution over the maxima of each GP was inferred by drawing 1,000 samples from the posterior of each fitted model.

Generation of heat maps. During retinal sectioning, order and orientation of sections was maintained and the retinal location of each image determined using the section number and the distance from the

optic nerve head along the section, providing x- (nasal-temporal) and y-coordinates (dorsal-ventral), respectively. To visualise the spatio-temporal progression of the markers, the mean activity at each location along the dorsal-ventral axis was used (averaging over the nasal-temporal dimension) and plotted for against each time point. Heat-maps were generated in Python 3 using the matplotlib library.

Two-photon Ca^{2+} imaging. The preparation of retinal slices for Ca^{2+} imaging was performed as described previously (Kulkarni et al., 2015; Wei et al., 2012). All preparations were performed under red light, eyes were enucleated and dissected in carboxygenated (95% O_2, 5% CO_2) artificial cerebral spinal fluid (ACSF) solution, made with (in mM): 125 NaCl, 2.5 KCl, 2 $CaCl_2$, 1 $MgCl_2$, 1.25 NaH_2PO_4, 26 $NaHCO_3$, 0.5 L-glutamine, and 20 glucose (Sigma-Aldrich or Merck, Germany); maintained at pH 7.4 using carboxygen. Consecutive vertical slices (~200 μm thick) were cut using a tissue slicer (Werblin, 1978) and then transferred to the two-photon microscope recording chamber where they were constantly perfused with warmed (~37°C) ACSF. The microscope (Euler et al., 2009), consisted of a customized MOM (movable objective microscope; designed by W. Denk, MPI of Neurobiology, Martinsried; purchased from Science Products/Sutter Instruments, Novato, USA), equipped with a mode-locked Ti:Sapphire laser (MaiTai-HP DeepSee; Newport Spectra-Physics, Darmstadt, Germany) tuned to 860 nm, two fluorescence detection channels (483 band-pass (BP) 32; 535 BP 50; AHF, Tübingen, Germany), and a 20x water-immersion objective (XLUMPlanFL,

0.95 NA; Olympus, Hamburg, Germany). The system was controlled by the image acquisition software ScanM (by M. Müller, MPI of Neurobiology, Martinsried, Germany, and T.Euler) running under IGOR Pro 6.3. A custom-built dichromatic light stimulator (Baden et al., 2013), equipped with two band-pass filtered LEDs (UV filter: 360 BP 12; green: 578 BP 10) and mounted below the recording chamber, was used to present temporally-modulated, full-field light stimuli (approx. 2 mm in diameter) to the retinal slices. Ca^{2+} recordings were performed with a constant background illumination of 10^4 P^*s^{-1} (photo-isomerization rate) for at least 15 seconds. Light stimuli consisted of a series of 1-second bright flashes with 4-second intervals. Flashes evoked similar photo-isomerization rates in both medium and short wavelength cones. Flashes from the UV and Green LED had light intensity of $6.5 \cdot 10^3$ P^*s^{-1}/cone (Chapot et al., 2017). At these light levels, rods are expected to be saturated and therefore light-evoked responses should originate in cones and not in electrically coupled rods. To record Ca^{2+} levels and light-evoked Ca^{2+} responses in cone axon terminals, we captured image series (128 x 32 pixels at 15.625), aligned with the outer plexiform layer (OPL) and covering an area of ~75 x 20 µm on the slice. We recorded both fluorescence channels as TN-XL allows ratiometric measurements *via* FRET between its fluorophores enhanced cyan fluorescent protein (ECFP, donor) and citrine (acceptor).

Pharmacology and drug application. All drugs were prepared as stock solutions in distilled water and were stored at 4°C. Before each experiment, drugs were freshly diluted from stock solution in carboxygenated ACSF solution. For bath application, the tissue was perfused with the drug added to the bathing solution for at least 1 min before commencing the recording (perfusion rate of ~1.5 ml/min). Rate of drug entry into the chamber was measured using sulforhodamine 101 (SR101) diffusion rates.

Analysis of Ca^{2+} imaging data. All Ca^{2+} data was analyzed using custom scripts for IGOR Pro 6.3 (Wavemetrics). To extract cone Ca^{2+} signals, regions of interest (ROIs) were drawn manually around the cone terminals and the pixels within ROIs were averaged for each image frame. The relative Ca^{2+} level was then determined as the ratio between acceptor and donor fluorescence (*F*A/*F*D) signals after background subtraction. For each ROI, stimulus trials were averaged and the mean trace was filtered (box-car, 320 ms filter-width). Baseline Ca^{2+} level (Baseline) was defined as the mean prior to the light flash and we quantified the area between baseline and light response (area under the curve, AUC), and response amplitude (AMP). Previous studies showed that during retinal slicing, cells close to the surface might be mechanically damaged and show altered Ca^{2+} ratios (Wei et al., 2012). We tried to address this issue by recording from cones at least 20-50 µm into the slice and by excluding cones with unstable baseline and/or high noise level.

Calpain activity imaging using 2-photon microscopy. After slicing and mounting, retinal slices were incubated in a water bath @ 37°C for at least 2hrs in a modified calpain activity assay (CAA). Slices were incubated in calpain reaction buffer (CRB, as above) dissolved in ACSF. Since retinal slices were live tissue, non-denatured, no DTT was added to the solution. 50 µM Boc-Leu-Met-CMAC was added to the CRB-ACSF solution. After incubation, slices were moved to the imaging chamber of the two-photon setup where they were constantly perfused with the CAA buffer in ACSF with 20 µM Boc-Leu-Met-CMAC with both the solution and chamber maintained at 37°C. Sections were scanned @860nm with 535 BP 50; 435 BP 40 (AHF, Tübingen, Germany) detecting the citrine signal from the TN-XL cones (used to locate cones and the ONL within the slice) and 435 BP 40 (AHF, Tübingen, Germany) to detect the calpain signal. The 435 BP 40 allows measurement of the fluorescently tagged calpain proteins while excluding the ECFP signal from the cones. Initially z-stacks of the retinal tissue were recorded to determine the efficacy of the assay under the two-photon conditions. After initial imaging, one location was recorded over a more prolonged period. As the slicing may damage the tissue, all imaging was performed at a minimum depth of 20µm.

Linear and multivariate linear modelling. We used a multivariate linear model to estimate the effect of drug application at different concentrations in retinal slice data. We used three measures for the outcome variable: the amplitude (AMP), area under the curve (AUC),

and baseline, and used our linear model to predict the effect of the treatment with a drug (Drug.y) and the concentration of the drug (Conc.y).

$$\mathbf{y_{AUC}}\ ,\ \mathbf{y_{AMP}},\ \mathbf{y_{Baseline}} \sim \mathbf{f}\left(\mathbf{x_{Drug}},\mathbf{x_{Conc}}\right)$$

Separate linear models were fitted for each outcome variable. For each, a complete model including all fixed effects and interactions was fitted using maximum likelihood estimation (as implemented in R's lmer package (Bates, Mächler, Bolker, & Walker, 2014). The significance of each effect and interaction was then evaluated using ANOVA. Effects and interactions whose significance were greater than $p < 0.05$ were retained in the final model for each outcome variable. The final models were as follows:

$$\mathbf{y_{AUC\text{-}Drug}} \sim \mathbf{a_1}.\mathbf{x_{Drug}}+\mathbf{a_2}.\mathbf{x_{Conc}}+\mathbf{a_3}.\mathbf{x_{AUC\text{-}ctrl}}+\mathbf{a_4}.\mathbf{x_{AUC\text{-}ctrl+Drug}}$$

$$+\mathbf{a_5}.\mathbf{x_{AUC\text{-}ctrl+conc}}+\mathbf{a_6}.\mathbf{x_{AUC\text{-}ctrl+Drug+conc}}$$

$$\mathbf{y_{AMP\text{-}Drug}} \sim \mathbf{a_1}.\mathbf{x_{Drug}}+\mathbf{a_2}.\mathbf{x_{Conc}}+\mathbf{a_3}.\mathbf{x_{AMP\text{-}ctrl}}\mathbf{a_4}.\mathbf{x_{AMP\text{-}ctrl+Drug}}$$

$$+\mathbf{a_5}.\mathbf{x_{AMP\text{-}ctrl+conc}}+\mathbf{a_6}.\mathbf{x_{AMP\text{-}ctrl+Drug+conc}}$$

$$y_{\text{Baseline-Drug}} \sim a_1.x_{\text{Drug}} + a_2.x_{\text{Conc}} + a_3.x_{\text{Baseline-ctrl}} a_4.x_{\text{Baseline-ctrl+Drug}}$$

$$+ a_5.x_{\text{Baseline-ctrl+conc}} + a_6.x_{\text{Baseline-ctrl+Drug+conc}}$$

The model was used to test the effect of each parameter to the responses by seeing which combination of factors more accurately mimicked the live cell recording data.

Results

The *rd1* and *rd10* lines share mutations in the *Pde6b* gene, whereas the *cpfl1* line suffers from a mutation in the homologous, cone-specific *Pde6c* gene. To align our experiments with earlier studies of mouse PR degeneration, we first compared changes in ONL thickness over the first post-natal month between the three mutants and wt mice (Fig. 9). The ONL thickness dramatically decreases in post-P13 *rd1* and in *rd10* after P18, illustrating the difference in onset PR cell death seen between these mouse models (Arango-Gonzalez et al., 2014). The *rd10* degeneration is also somewhat less aggressive than *rd1* as it takes longer for complete ablation of the ONL in *rd10* than in *rd1*. In contrast, ONL thickness is not dramatically different between the cone degeneration mutant *cpfl1* and wt, likely because in mice, rods outnumber cones approximately 20:1, such that the loss of cones is hardly noticeable in terms of overall ONL thickness.

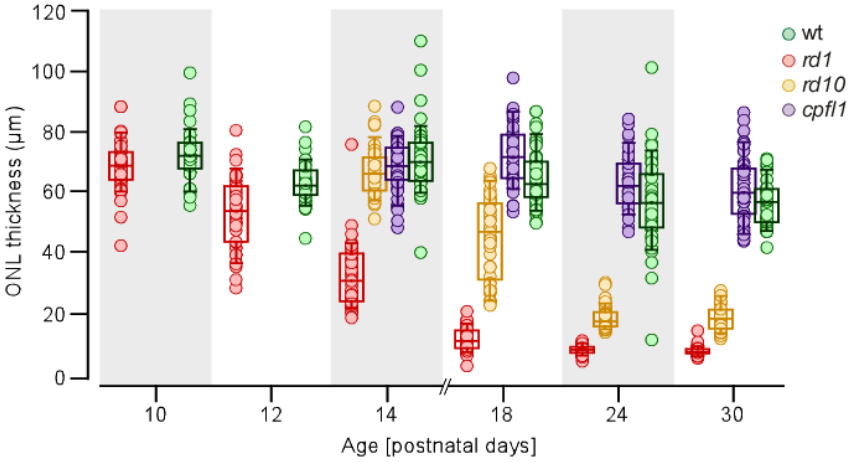

Figure 9. Photoreceptor degeneration-related cell loss in different mouse lines. Cell loss was measured using outer nuclear layer (ONL) thickness during the first post-natal month in *rd1* (cherry), *rd10* (amber), *cpfl1* (lilac), and wild-type (wt, emerald) mice (n=3 animals per mouse line and time-point).

Calpain activity increases in ONL of degenerating retina

Having set the timeframe and extent of cell loss in the mutant models, we next aimed at elucidating the role of Ca^{2+} dysregulation in PR cell death. To this end, we focussed first on the activity and regulation of the Ca^{2+}-dependent calpain-type proteases, among which are isoforms that are considered to be a suitable surrogate markers for Ca^{2+} dysregulation (Croall & Ersfeld, 2007; Darrel E Goll et al., 2003). Moreover, calpain activity can easily be assayed in unfixed

retinal sections (Francois Paquet-Durand et al., 2006). We examined calpain activity across the retina of RD mutant *vs.* wt retina (Fig. 10).

Figure 10. Temporal progression of calpain activity in different mouse lines. **A-C**, representative images of sections from *rd1* (A), *rd10* (B), and *cpfl1* (C) analysed with the calpain assay; each image of a mutant retina (right) is aged-matched with a wt control (left). **D**,

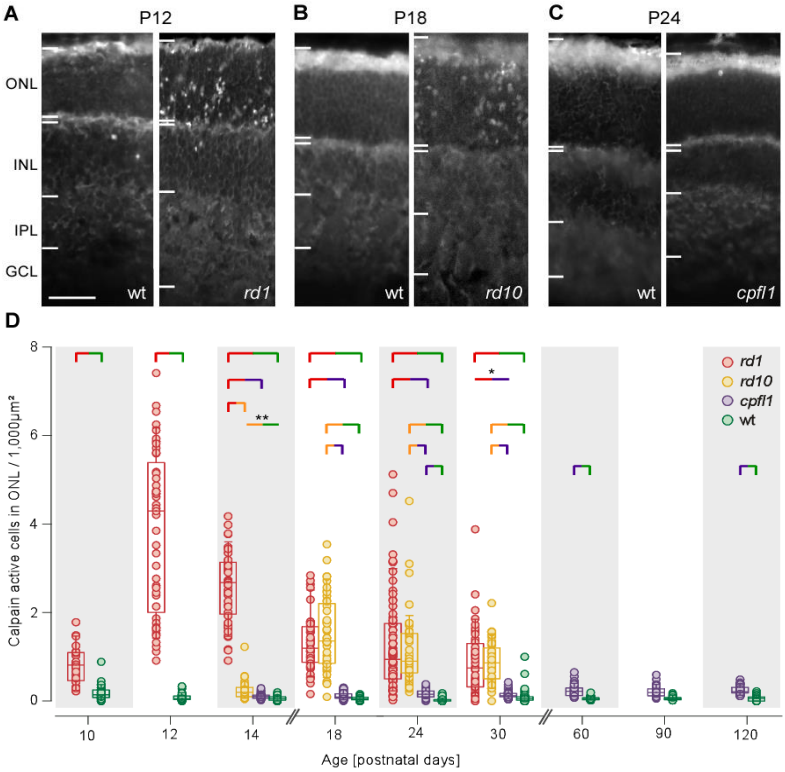

normalised number of fluorescent cells in the ONL (per 1,000 µm^2), indicative of calpain activity in PRs, as a function of age (n=45 observations obtained on 3 animals per mouse line and time-point). Statistical analysis was Kruskal–Wallis one-way analysis of variance,

statistical significance is *** ≤ 0.001 unless otherwise stated. Scale bar: A-C, 50 µm.

In *rd1* retina, the number of ONL cells showing increased calpain activity was significantly higher compared to wt and *cpfl1*, at all time-points, with a peak of activity at P12 (Fig. 10A, D; for detailed statistics of all comparisons, see Table 3). Calpain activity in *rd10* ONL was also significantly increased compared to wt and *cpfl1* (at P18, 24, and 30), peaking around P18 (Fig. 10B, D). Also, in c*pfl1*, calpain activity tended to be higher than in wt, although without a clear peak within the inspected time frame (Fig. 10C, D). Overall, *rd1* retina displayed the highest levels of calpain activity. These data are largely in line with (Arango-Gonzalez et al., 2014; Francois Paquet-Durand et al., 2006) who showed increases in calpain activity at specific time points in models of RP and achromatopsia (see Discussion).

Activation of calpain-2, but not calpain-1, increases during disease progression

We then investigated whether the high levels of calpain activity observed in the ONL could be attributed to specific calpain isoforms. While 15 different calpain isoforms have been identified (Nemova, Lysenko, & Kantserova, 2010), we focussed on calpain-1 and -2, which are reported to be ubiquitously expressed in all mammalian cells and have been generally reported to play opposite roles in neurodegeneration (L. Y. Chen, et al., 2007; Goñi-Oliver, et al., 2007). We hypothesized that calpain-2 may contribute to the observed

increased calpain activity as it requires high [Ca^{2+}] that are considered beyond the physiological range of PRs (D E Goll, 1995). Using antibodies recognizing the activated proteases, we found significantly increased numbers of calpain-2 positive cells in both *rd1* and *rd10* ONL, when compared to *cpfl1*, as well as to wt controls (Fig. 11A, B, D; for all statistics, see Table 3). The peaks appeared to coincide with those for the calpain assay, namely at P12 (*rd1*) and at P18 (*rd10*). In *cpfl1*, the number of calpain-2 positive cells was slightly increased over the wt level (Fig. 11C, D), although without a clear peak.

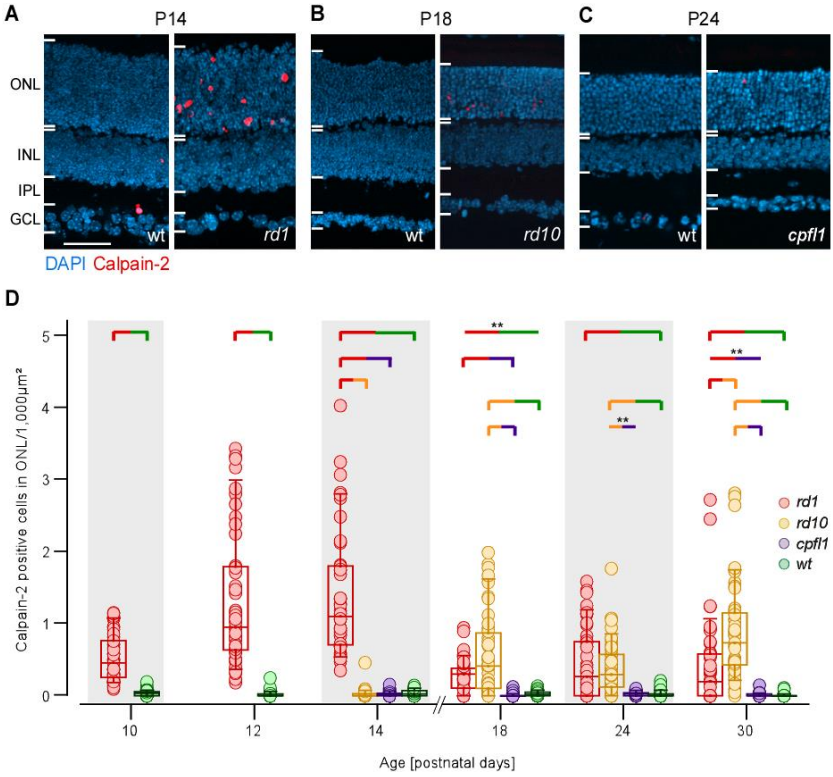

Figure 11. Calpain-2 becomes activated during photoreceptor degeneration. **A-C**, representative images of sections from *rd1* (A), *rd10* (B), and *cpfl1* (C) analysed for calpain-2 immunoreactivity; each image of a mutant retina (right) is aged-matched with a wt control (left). **D**, normalised number of fluorescent cells in the ONL (per 1,000 μm^2), indicative of calpain-2 immunoreactive PRs, as a function of age (n=45 observations obtained on 3 animals per mouse line and time-point). Statistical analysis was Kruskal–Wallis one-way analysis of variance, statistical significance is *** $\leq$ 0.001 unless otherwise stated. Scale bar: A-C, 50 µm

To our surprise, a significant increase in calpain-1 positive cell numbers from wt level was only observed in *rd10* (Fig. 12A-C). Calpain-1 labelling increased over background levels around P18 and was even more pronounced at the end of the observed time window (P30) (Fig. 12D). Next to *rd10*, only *rd1* showed a detectable (but much lower and not significant) increase in calpain-1 positive cell counts.

Taken together, we found a differential pattern of calpain isoform activation. While calpain-2 was strongly activated in *rd1* and *rd10* – and much less so in *cpfl1* – calpain-1 appeared more strongly activated in *rd10* compared to the other lines. In addition, the peaks of calpain-2 expression and of the calpain activity assay data coincide and precede that of calpain-1.

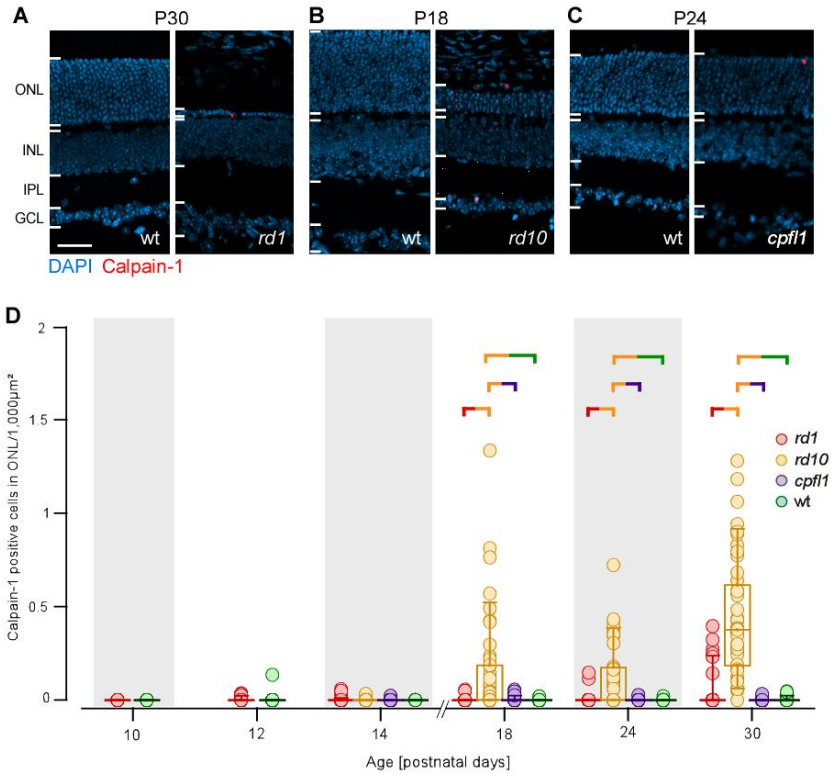

Figure 12. Calpain-1. **A-C**, representative images of sections from *rd1* (A), *rd10* (B), and *cpfl1* (C) analysed with the calpain-1 positivity; each image of a mutant retina (right) is aged-matched with a wt control (left). **D**, normalised number of fluorescent cells in the ONL (per 1,000 µm^2), indicative of calpain-1 immunoreactive PRs, as a function of age. Statistical analysis was performed using Kruskal–Wallis one-way analysis of variance, statistical significance is *** ≤ 0.001 unless otherwise stated. Scale bar: A-C, 50 µm

Cell death coincides with calpain activity

To quantify the levels of cell death and compare them to those of the activity and expression of calpain in the ONL, we used the TUNEL assay which labels dying cells. In agreement with earlier work (Arango-Gonzalez et al., 2014), we found significantly increased numbers of TUNEL positive cells in the ONL of the *rd1* and *rd10* mice (Fig. 13A, B, D: for all statistics, see Table 3). An increase in TUNEL-positive cell number was also seen in the *cpfl1* mouse (Fig. 13C, D) albeit at a much lower level and with no discernible peak. The peaks in TUNEL-positive ONL cell numbers of *rd1* (P12) and *rd10* (P24) coincided temporally with those of calpain activity and calpain-2 labelling in the respective lines. TUNEL labels nick-ends in a cell's DNA and while this makes it an excellent marker for cell death, it is non-specific to the actual cell death mechanism (Kraupp et al., 1995) .

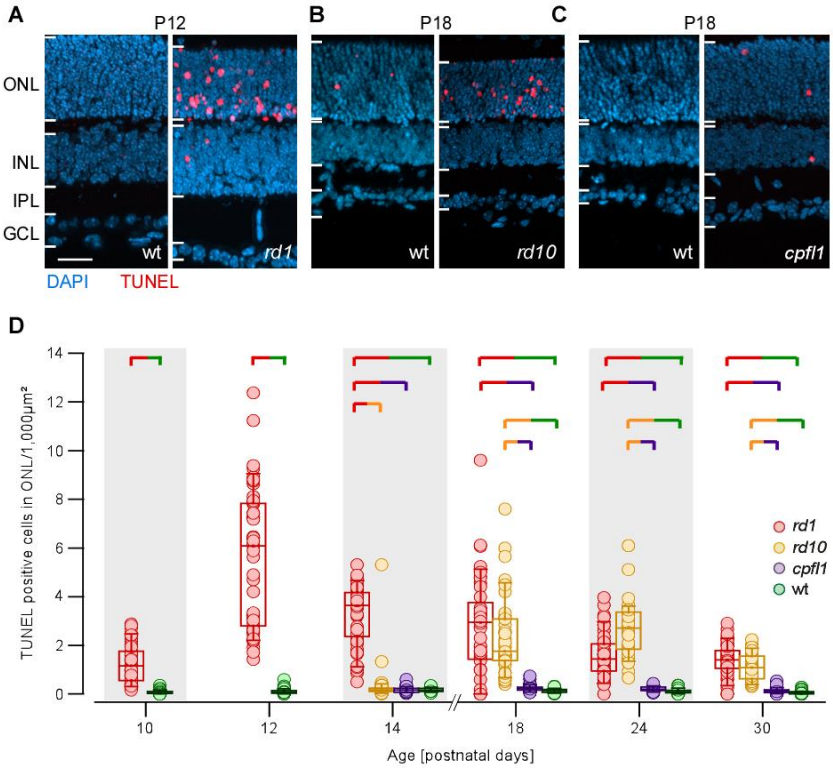

Figure 13. Temporal progression of cell death. **A-C**, representative images of sections from *rd1* (A), *rd10* (B), and *cpfl1* (C) analysed with the TUNEL assay; each image of a mutant retina (right) is aged-matched with a wt control (left). **D**, normalised number of fluorescent cells in the ONL (per 1,000 µm^2), indicative of TUNEL positivity in PRs, as a function of age (n=45 observations obtained on 3 animals per mouse line and time-point). Statistical analysis was Kruskal–Wallis one-way analysis of variance, statistical significance is *** ≤ 0.001 unless otherwise stated. Scale bar: A-C, 50 µm.

AIF and caspase-3 levels argue against classical apoptosis in degenerating rods

How high intracellular [Ca^{2+}] due to Ca^{2+} dysregulation is linked to PR cell death is still unclear. Prominent candidates for Ca^{2+}-dependent downstream pathways are apoptotic cell death through caspase effectors (Orrenius et al., 2003) and non-apoptotic cell death involving calpain activation (Arango-Gonzalez et al., 2014; Doonan et al., 2005; reviewed in Liu et al., 2004). To distinguish between these two proposed pathways, we used antibodies for cleaved caspase-3, a marker for apoptosis, and truncated AIF, seen as a marker for programmed necrosis (Arango-Gonzalez et al., 2014; S. Wang et al., 2018).

AIF-positive cells were observed in the ONL of all disease models (Fig. 14A-D). Significant increases in AIF-positive cell numbers in *rd10* occurred at the same time point (P18; for all statistics, see Table 3) as those of TUNEL and calpain activity. This was not the case for *rd1*, where a significant increase in AIF-positive cell numbers was not seen until late in the investigated time window (P30). In addition, a small, non-significant increase in AIF-positive cells number was seen in *cpfl1* retina.

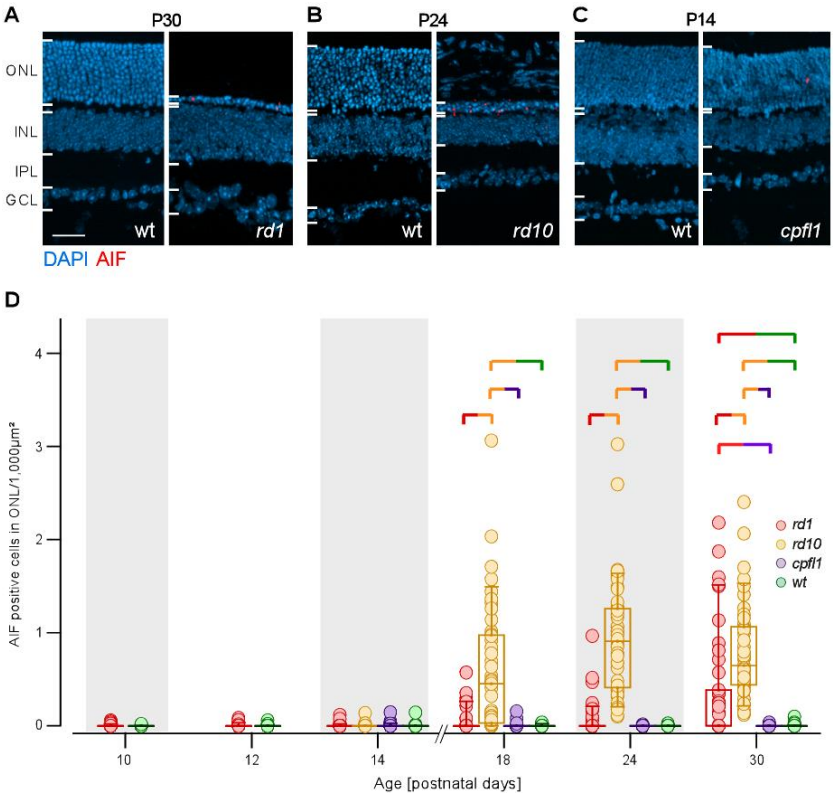

Figure 14. AIF. **A-C**, representative images of sections from *rd1* (A), *rd10* (B), and *cpfl1* (C) analysed with the AIF immunofluorescence; each image of a mutant retina (right) is aged-matched with a wt control (left). **D**, normalised number of fluorescent cells in the ONL (per 1,000 µm^2), indicative of AIF immunoreactive PRs, as a function of age (n=45 observations obtained on 3 animals per mouse line and time-point). Statistical analysis was Kruskal–Wallis one-way analysis of variance, statistical significance is *** ≤ 0.001 unless otherwise stated. Scale bar: A-C, 50 µm.

Increases in the numbers of cells showing caspase-3 activation were observed in all mouse lines (Fig. 15A-C) although to a low level (Fig.

15 D) and not at all time points (for all statistics, see Table 3). Significantly higher numbers of caspase-3 positive cells were seen in *rd1* retina from P18 on, peaking at P24. The increases in the levels of caspase-3 positive cells were not seen to the same extent in the *rd10* as in the *rd1*. Modest increases were seen in the *rd10* (for all statistics, see Table 3) comparable to those of *cpfl1*.

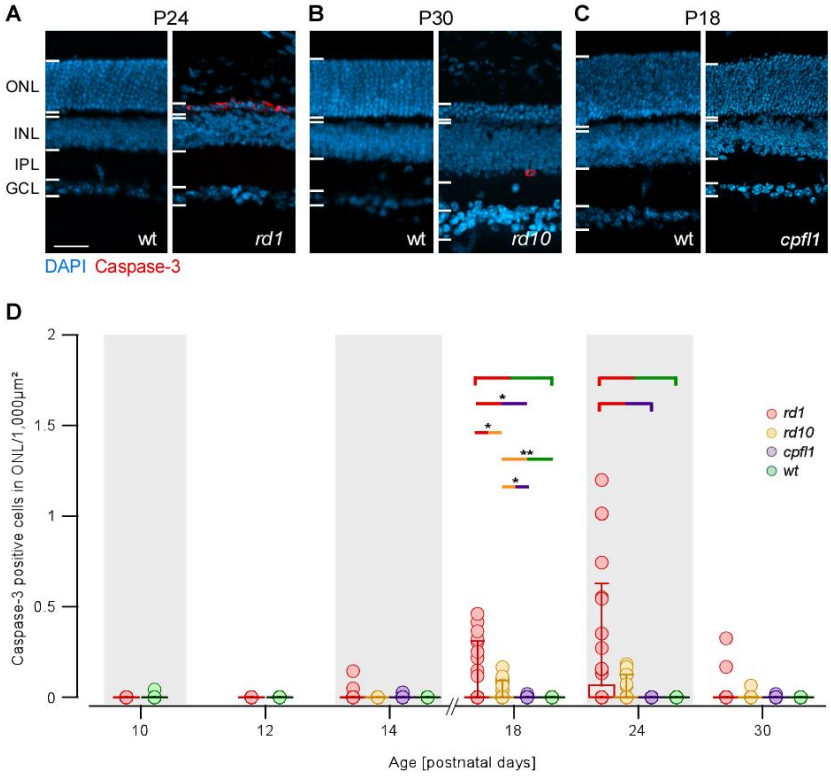

Figure 15. Activated caspase-3. **A-C**, representative images of sections from *rd1* (A), *rd10* (B), and *cpfl1* (C) stained with an antibody against activated caspase-3; each image of a mutant retina (right) is aged-matched with a wt control (left). **D**, normalised number of fluorescent cells in the ONL (per 1,000 μm^2), indicative of PRs with activated caspase-3, as a function of age (n=45 observations obtained on 3 animals per mouse line and time-point). Statistical analysis was Kruskal–Wallis one-way analysis of variance, statistical significance is *** ≤ 0.001 unless otherwise stated. Scale bar: A-C, 50 µm.

Upon further inspection, we noticed that in the *rd1* retina, caspase-3 positive cells were often overlapping with cones, as marked by the TN-XL biosensor. When we then analysed for *rd1* cones expressing caspase-3, we found that at P24 a substantial number of cones were positive for activated caspase-3 (Fig. 16A-D).

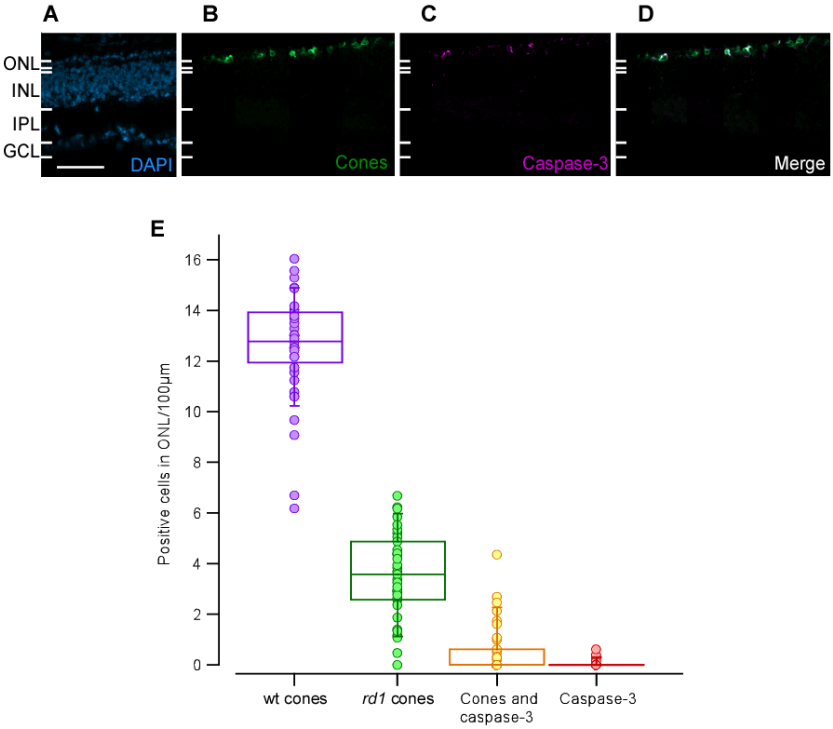

Figure 16. Activated caspase-3 in cones. **A-D**, representative images of sections from *rd1* P24 showing DAPI (A), cones (B), caspase-3 (C) and a merged imaged of caspase-3 and cones (D). **E**, normalised number of fluorescent cells in the ONL (per 100 µm), indicative of cones in the wt retina (violet), cones not showing caspase-3 activation in *rd1* (green), cones with activated caspase-3 (yellow) and caspase-3 positive cells that were not cones (red; n=45 observations obtained on 3 animals per mouse line and time-point). 778 cones that remained in the 45 images, 111 of them (14%) were also positive for caspase-3. Scale bar: A-D, 50 µm.

Gaussian process models infer probabilistic sequences of marker

In the experiments so far, we noticed that the distribution of data points for a certain time point was often quite broad and featured multiple peaks (e.g. Fig. 10D, *rd1* at P12; Fig. 11D, *rd10* at P24). Possible explanations for this are variability between individual mice and variability of degeneration state across the retina. We tested the latter by resolving the distributions of the markers along the retinas' dorso-ventral axis for all time points and mouse lines (Fig. 17). To this end, we collapsed data points along the naso-temporal axis, thus calculating the mean distribution along the dorso-ventral for each time point and visualized the whole time series as "spatio-temporal" heat maps (for original maps, see Figs. 18-23).

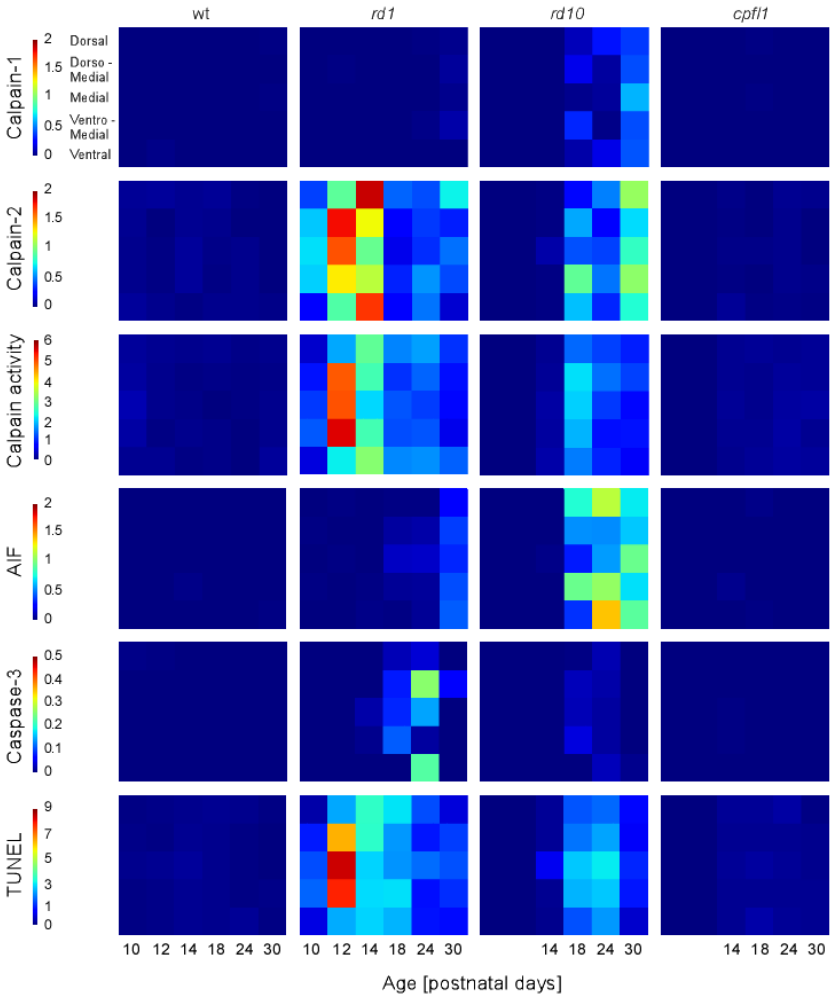

Figure 17. Summary heat maps illustrating the spatio-temporal progression of cell death markers, with image position along the y-axis (dorso-ventral) and time along x-axis (see Methods for details and Supplemental Figures 3-8 for individual maps). Each element in the heat map is the mean value averaged over the naso-temporal axis.

Colours represent number of fluorescent cells in the ONL (per 1,000 μm^2) of calpain-1, calpain-2, calpain activity, AIF, caspase-3, and TUNEL. Note the scaling may be different for different markers.

The spatial analysis revealed that degeneration did not occur uniformly across the retina of a given time point. For instance, in *rd1* animals, the peak in calpain activity at P12 first occurs in the central retina, and then at P14 in the peripheral retina (Fig. 18, 2nd row). This sequence is also visible in the spatio-temporal maps of *rd1* for calpain activity, TUNEL, and calpain-2 (Fig. 17, 2nd column). A similar trend, though somewhat less clear, was observed in *rd10* retina (Fig. 17, 3rd column; Figs. 18-23, 3rd row). Therefore, this spatial inhomogeneity of cell death markers for a given time point at least partially explains the aforementioned broad distribution of the data points (*cf*. Figs. 10-15).

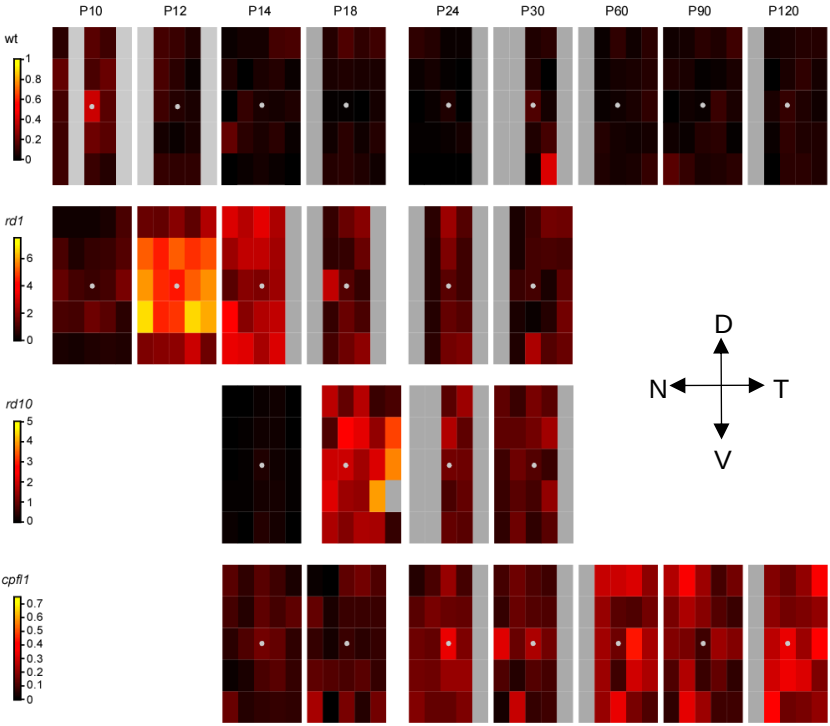

Figure 18. Heat maps for the spatio-temporal progression of calpain activity across the retina and for different mouse lines. Each map represents a time point, the grey disk the position of the optic nerve head (map origin). Each box in a map measures 1,000 µm by 400 µm, with the colour encoding the average number of fluorescent cells in the ONL (per 1,000 μm^2). Grey areas denote areas that were not examined.

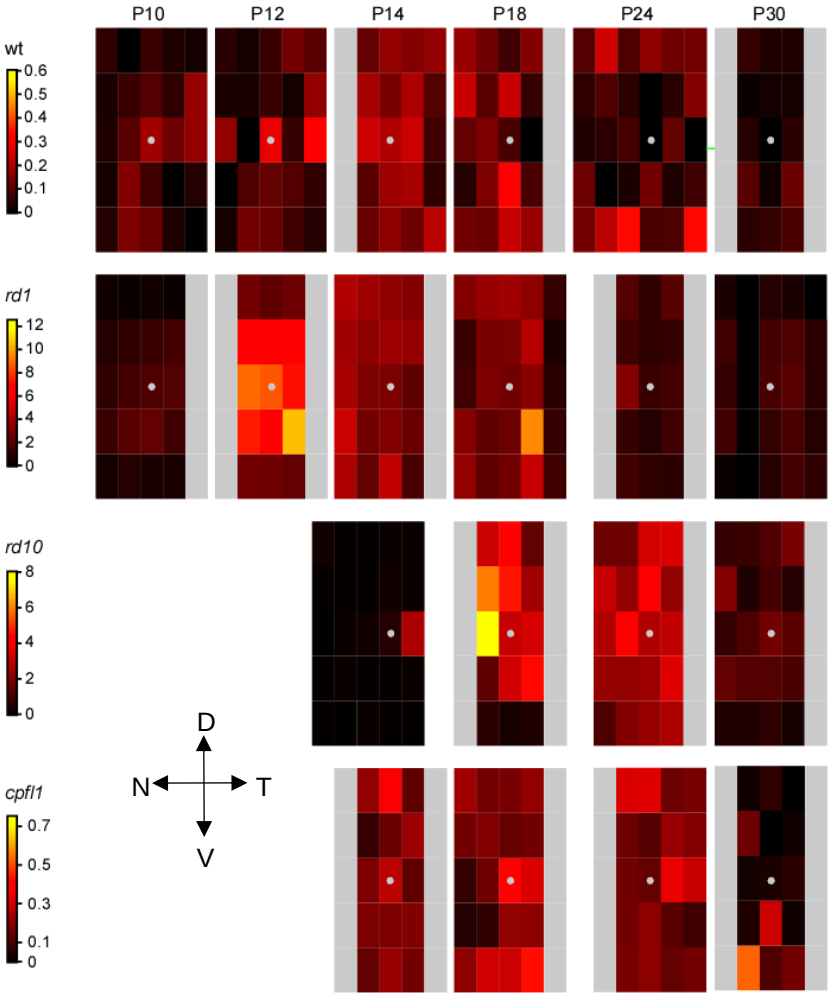

Figure 19. Heat maps for the spatio-temporal progression of cell death (TUNEL) across the retina and for different mouse lines. Each map represents a time point, the grey disk the position of the optic

nerve head (map origin). Each box in a map measures 1,000 µm by 400 µm, with the colour encoding the average number of TUNEL positive cells in the ONL (per 1,000 µm^2). Grey areas denote areas that were not examined.

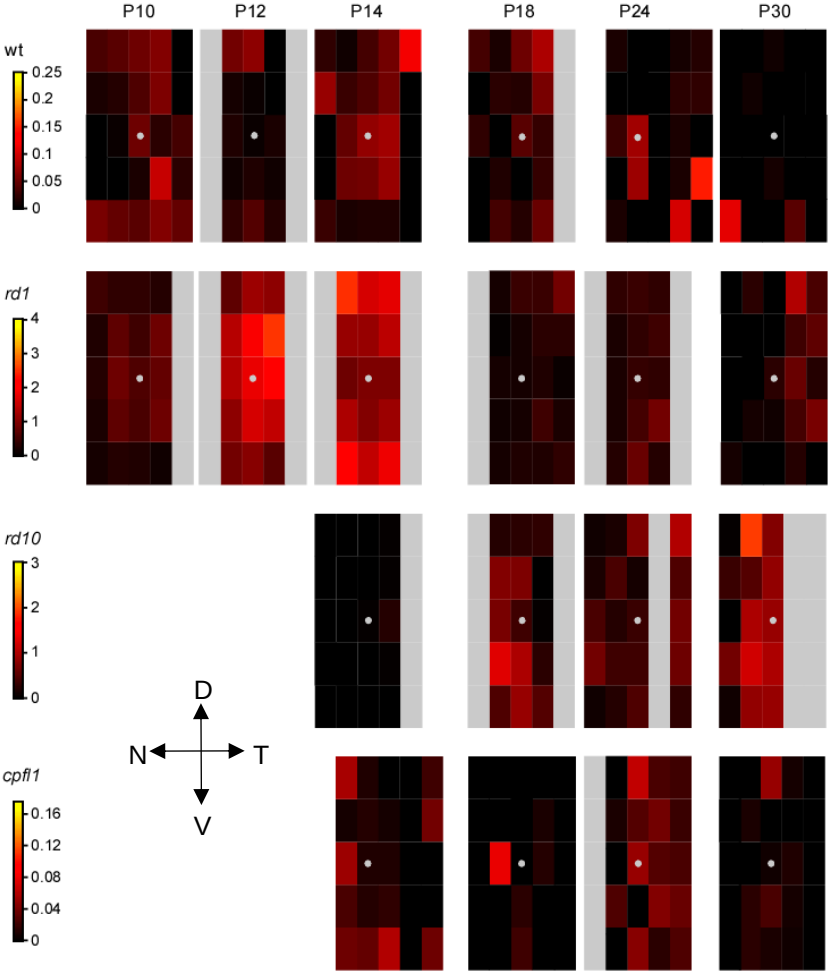

Figure 20. Heat maps for the spatio-temporal progression of calpain-2 activity across the retina and for different mouse lines. Each map represents a time point, the grey disk the position of the optic nerve head (map origin). Each box in a map measures 1,000 µm by 400 µm, with the colour encoding the average number of fluorescent cells in the ONL (per 1,000 μm^2). Grey areas denote areas that were not examined.

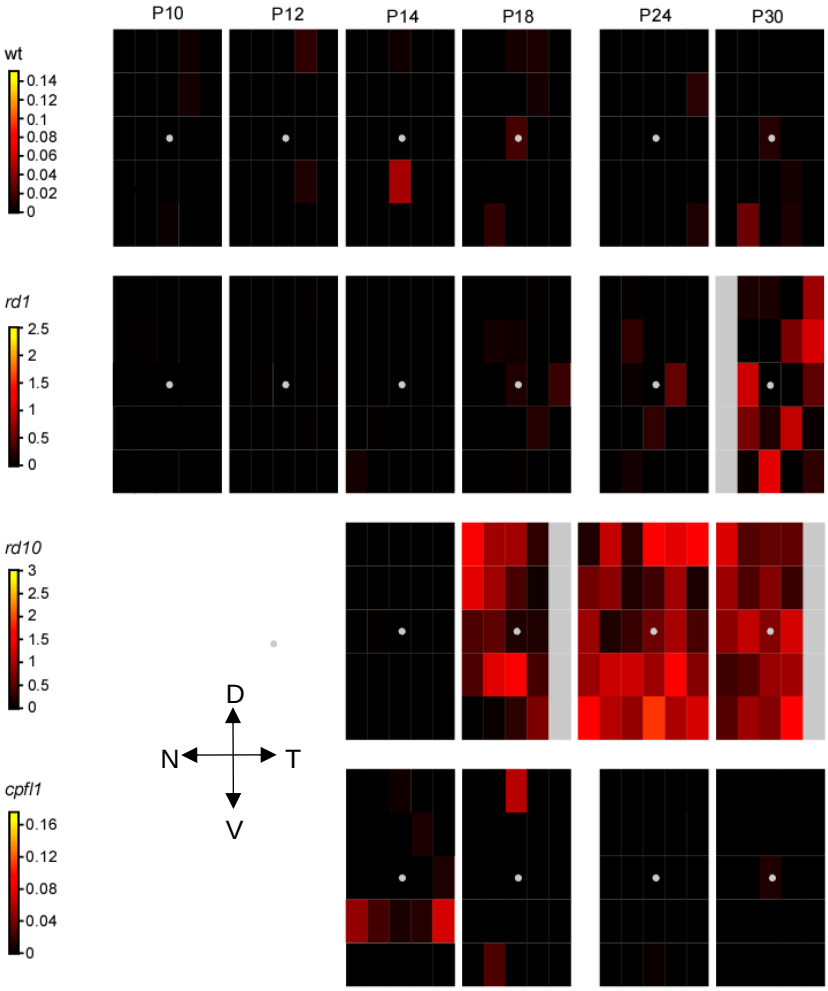

Figure 21. Heat maps for the spatio-temporal progression of AIF activity across the retina and for different mouse lines. Each map represents a time point, the grey disk the position of the optic nerve head (map origin). Each box in a map measures 1,000 µm by 400 µm, with the colour encoding the average number of fluorescent cells in

the ONL (per 1,000 µm^2). Grey areas denote areas that were not examined.

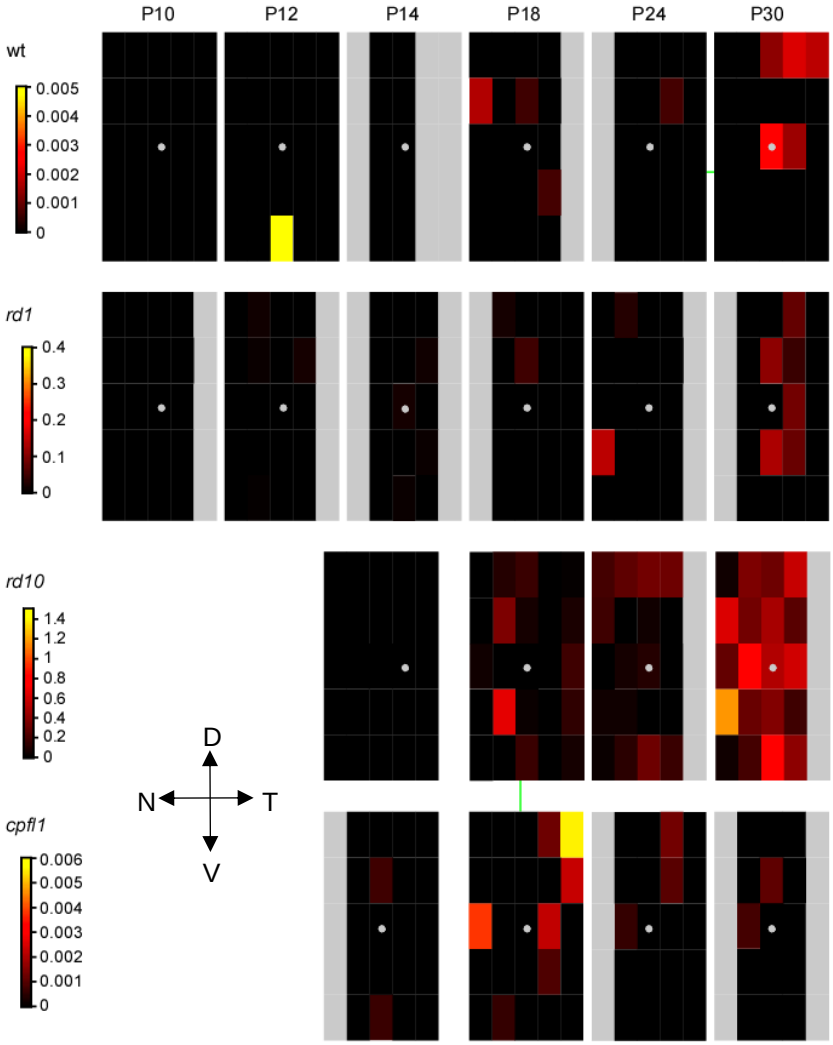

Figure 22. Heat maps for the spatio-temporal progression of calpain-1 across the retina and for different mouse lines. Each map represents a time point, the grey disk the position of the optic nerve head (map origin). Each box in a map measures 1,000 µm by 400 µm, with the colour encoding the average number of fluorescent cells in the ONL (per 1,000 μm^2). Grey areas denote areas that were not examined.

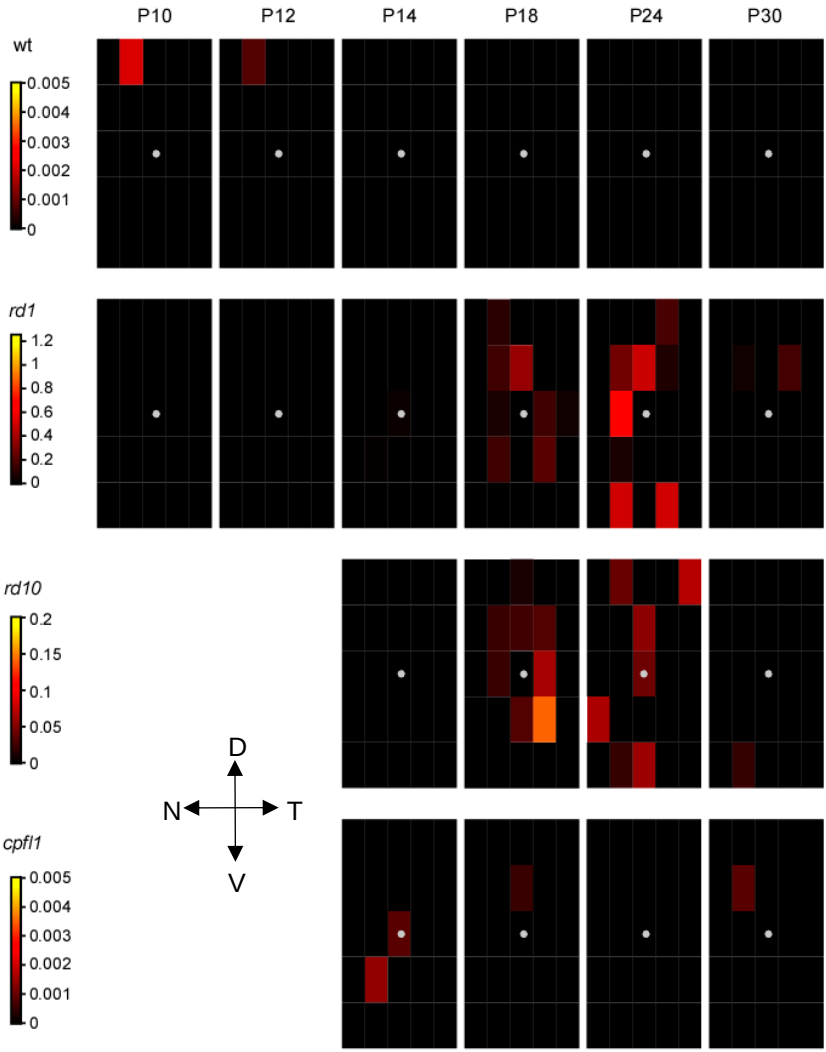

Figure 23. Heat maps for the spatio-temporal progression of caspase-3 activity across the retina and for different mouse lines. Each map

represents a time point, the grey disk the position of the optic nerve head (map origin). Each box in a map measures 1,000 µm by 400 µm, with the colour encoding the average number of fluorescent cells in the ONL (per 1,000 μm^2). Grey areas denote areas that were not examined.

When comparing the spatio-temporal heat maps for different markers, we noticed that markers within the same retinal region appear in a certain temporal sequence that differs and/or is delayed between mouse lines. For example, in *rd1* central retina, the peaks of calpain-2, calpain activity, and TUNEL appear to coincide (~P12), followed by smaller peaks of caspase-3 (P24) and AIF (P30 or later). In *rd10*, the broader "peaks" of calpain-2, calpain activity, and TUNEL also coincide, yet are more spread out (from P18 to P30) and – different to *rd1* – are associated with minor elevations of AIF- and calpain-1, but less caspase-3.

To more quantitatively identify the time points at which each cell death marker peaked in each mouse line, we fitted a set of Gaussian process models (Fig. 24; for details, see Methods). These models infer the mean and standard deviation of the number of labelled ONL cells over time. To estimate the time at which each marker peaked, we drew 10,000 samples from the posterior of each fitted Gaussian process model and identified the maxima in each sample.

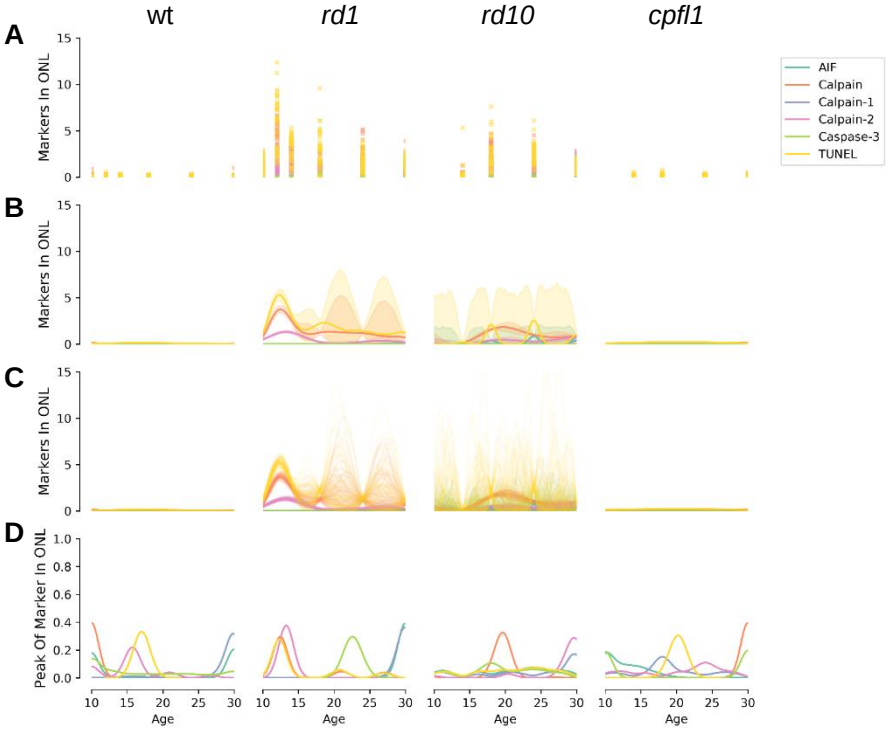

Figure 24. Gaussian process model for the kinetics of in cell death related processes. **A**, Parameters associated with photoreceptor cell

death as measured in the ONL (per 1,000 μm^2). **B**, Gaussian Process (GP) models with radial basis function kernel and additive Gaussian noise, fitted to observations to each cross of marker and mouse line. Observations are square root transformed prior to fitting, and after fitting are squared to return the model to its original state. 5% and 95% confidence intervals are estimated using a bootstrap of 1k posterior samples, excluding the additive likelihood noise. **C,** 100 of the 1k posterior samples from the GPs. **D,** Density of the maxima of the GP posterior samples for each marker.

The distribution of these maxima indicated the likely peak of each marker (Fig. 25). From these distributions, we identified the sequences of molecular markers which occurred in at least 5% of samples (Fig. 25).

wt	Probability						
	0.1478	AIF	Calpain	Caspase-3	Calpain-2	TUNEL	Calpain-1
	0.1101	AIF	Calpain	Calpain-2	TUNEL	Caspase-3	Calpain-1
	0.1071	Calpain	Caspase-3	Calpain-2	TUNEL	AIF	Calpain-1
	0.0853	Calpain	Calpain-2	TUNEL	Caspase-3	AIF	Calpain-1
	0.0625	AIF	Calpain	Calpain-2	Caspase-3	TUNEL	Calpain-1
	0.0563	Calpain	Caspase-3	Calpain-2	TUNEL	Calpain-1	AIF
rd1							
	0.264	TUNEL	Calpain	Calpain-2	Caspase-3	AIF	Calpain-1
	0.1489	Calpain	TUNEL	Calpain-2	Caspase-3	AIF	Calpain-1
	0.0935	Calpain	Calpain-2	TUNEL	Caspase-3	AIF	Calpain-1
	0.0856	TUNEL	Calpain	Calpain-2	Caspase-3	Calpain-1	AIF
	0.0705	Calpain	Calpain-2	Caspase-3	TUNEL	AIF	Calpain-1
	0.0695	TUNEL	Calpain-2	Calpain	Caspase-3	AIF	Calpain-1
	0.0511	Calpain	Calpain-2	Caspase-3	Calpain	AIF	Calpain-1
cpfl1							
	0.1701	AIF	Calpain-1	TUNEL	Calpain-2	Calpain	Caspase-3
	0.1032	Caspase-3	AIF	Calpain-1	TUNEL	Calpain-2	Calpain
	0.0718	AIF	Caspase-3	Calpain-1	TUNEL	Calpain-2	Calpain
	0.0518	AIF	Calpain-2	Calpain-1	TUNEL	Calpain	Caspase-3

Figure 25. Estimation of marker sequences, using probabilistic Gaussian Process bootstrap. Marker sequences from probabilistic Gaussian Process bootstrap where the probability of observing the sequence was estimated to be greater than 0.05. Probabilities estimated from 1,000 samples for each marker, in each mouse line.

In *rd1*, increased calpain activity, calpain-2, and TUNEL-positive cells tended to occur first in the sequence, while AIF and calpain-1 were predicted to always be the last two markers (Fig. 25). In *rd10* no sequence had a probability greater than 0.05 (Fig. 26). In wt mice, calpain activity preceded calpain-2 followed by TUNEL and calpain-1, while in *cpfl1*, AIF was predicted to precede calpain-1 before TUNEL, calpain-2, and calpain activity. The overall levels of all markers were low for data obtained from wt and *cpfl1*animals, causing a relatively low level of confidence in the model predictions.

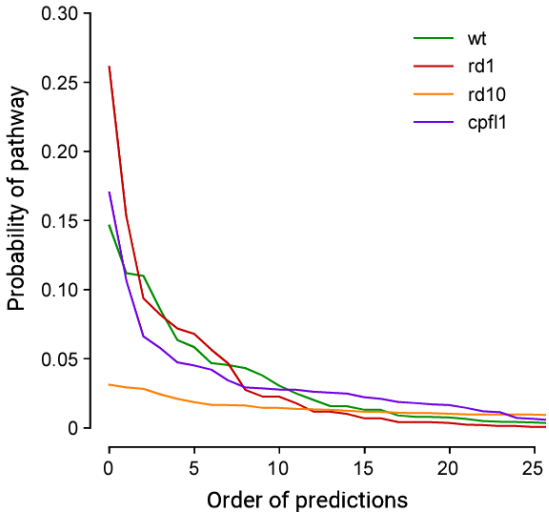

Figure 26. Probability of each prediction. Sequence is defined to be the expected order of the peaks for each marker from probabilistic Gaussian Process bootstrap. The probability of each prediction for the order of markers is shown for each mouse line.

Differential effects of diltiazem enantiomers on cone baseline Ca^{2+}

Having investigated the activity and expression of calpain throughout the cell, we next set out to elucidate Ca^{2+} dynamics within the cell. As noted above, Ca^{2+} is responsible for the activation of calpain and so dysregulation of Ca^{2+} leads to increases in calpain activation. $[Ca^{2+}]$ within the cell are maintained by Ca^{2+} channels on the plasma membrane, allowing extracellular Ca^{2+} into the cell in a regulated manner. As mutations in *Pde6* lead to CNGCs being kept open, Ca^{2+} channel blockers that could rebalance $[Ca^{2+}]$ are an attractive target for slowing or possibly ceasing the progression of the degeneration. While CNGCs are the channels affected by the *Pde6* mutations they are not the only Ca^{2+} channels in the PRs, as VGCCs are located on several cellular compartments (see Introduction). To selectively block VGCCs, we used D-cis diltiazem (D-cis, selectively targets VGCCs; Glossmann et al., 1987) while an enantiomer L-cis diltiazem was used to target CNGCs (L-cis; Koch & Kaupp, 1985). We first measured Ca^{2+} dynamics in wild type cones expressing the TN-XL biosensor. Once these dynamics were established, we then treated the cells with D-cis or L-cis to explore how selective inhibition of cellular Ca^{2+} entry affected the Ca^{2+} responses to light. As CNGCs are located on the outer segment, and VGCCs are located on the cell bodies and cone terminals, this strategy would tell us what effect, if any, handicapping the initiation, or completion of the phototransduction signal would have. To analyse the Ca^{2+} response, we examined three separate parts of it: the baseline (the starting level of Ca^{2+} within the cell before presentation with light), the amplitude (AMP, the maximum drop in

cellular [Ca^{2+}] achieved by the cell from the baseline after being presented with light), and area under the curve (AUC, the area under the curve created by the exit of Ca^{2+} from the cell upon presentation with light, before the Ca^{2+} levels return to baseline levels), all with and without drug treatment.

We saw that L-cis treatment showed a marked decrease in both the AMP and the AUC at 100 µM (Fig 27A, B). The effect of the L-cis on both AUC and AMP was concentration dependent as reductions were seen at 25 and 50 µM with the reduction becoming more pronounced with increases in concentration (Fig. 27A, B). No decrease was seen in either the AMP or the AUC upon treatment with D-cis with any concentration. Decreases in the baseline were seen with both the L-cis and D-cis treated cells while L-cis had a slight concentration dependent decrease that was not seen in the D-cis group (Fig. 27D). These decreases in baseline Ca^{2+} we similar to those seen between two control recordings (Fig. 27C) implying that the decreases may be more due to the recording conditions than the drug application.

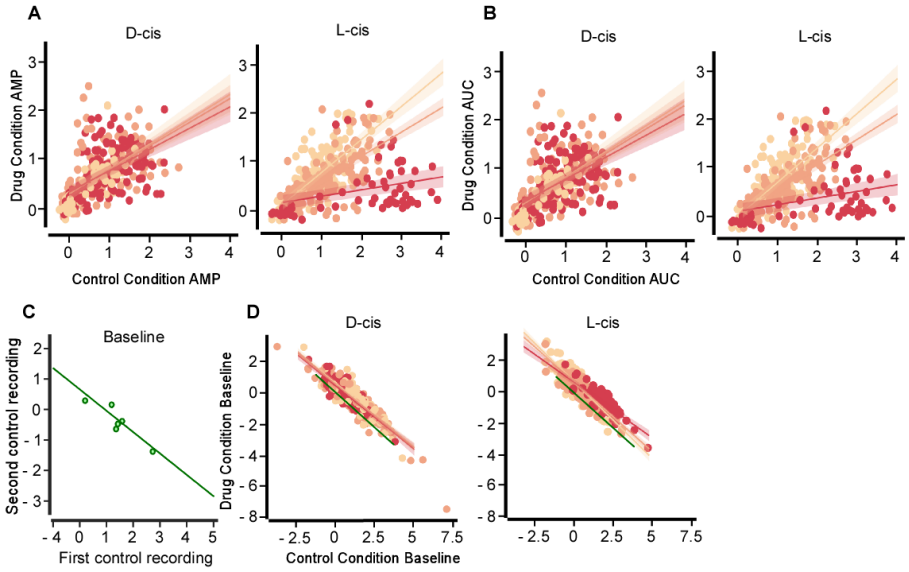

E

	Probability		Probability		Probability
AMP	< 2.2e-16 ***	AUC	< 2.2e-16 ***	Baseline	< 2.2e-16 ***
Drug	0.0152413 *	Drug	0.015616 *	Drug	0.8851976
Conc	0.2584328	Conc	0.676313	Conc	0.0702355
AMP + Drug	0.0001034 ***	AUC + Drug	0.000439 ***	Baseline + Conc	0.0002425 ***
AMP + Conc	0.2918698	AUC + Conc	0.354746	Baseline + Drug	0.9092923
AMP + Drug + Conc	8.635e-09 ***	AUC + Drug + Conc	7.18e-08 ***	Baseline + Drug + Conc	0.0005201 ***

Figure 27. Effect of drug on cone Ca^{2+} response. Scatter plot with predictions from a mixed model, showing mean predictions and standard errors for both L- cis- and D- cis- diltiazem at 25 (peach), 50 (orange) and 100 µM (scarlet) for the amplitude (AMP, **A**), and area under the curve (AUC, **B**). Scatter plot for the drop in baseline Ca^{2+} levels between two control recordings (**C**). Scatter plot with predictions from a mixed model, showing mean predictions and standard errors for both L- cis- and D- cis- diltiazem at 25 (peach), 50 (orange) and 100 µM (scarlet) baseline (**D**) with the drop in baseline Ca^{2+} seen in **C** overlaid. Multivariate linear model (**E**) predicting the explanatory power to the degree in which it improved model performance and importance of each factor and slope of the intercept of the mean response seen in **A, B** and **D.** Each parameter is combined with each other parameter to investigate which factor or group of factors is best at modelling the values seen in **A, B** and **D.** Statistical analysis is calculated using ANOVA with a numerical limiter below which values cannot drop * ≤ 0.05, *** ≤ 0.001.

The effects of each factor were then evaluated in a multivariate linear model (Fig. 27D). This suggested that the state of the cell under control conditions (Baseline.x, AUC.x, and AMP.x) is highly significant for determining the state of the cell after treatment. This modelling also suggested that the state of the cell pre-treatment (*i.e.* whether it is responsive or not) in combination with the drug used (which enantiomer was applied) was also highly significant. This can be seen in Fig 27A and B, as in order for the drug to have an effect the cell must first be responsive. We then must know which enantiomer was applied as, L-cis caused a reduction in the light induced Ca^{2+} response, while D-cis did not. The third most significant factor when modelling the response was the pre-treatment state of the cell with the drug used and the concentration of drug used. Again, this

can be seen from Fig. 27A and B where L-cis reduced the Ca^{2+} response in a concentration dependent manner while D-cis did not. As seen in Fig 27, and confirmed by modelling, the particular drug used is also a significant indicator of the effect on the AMP and AUC, though not on baseline.

Taken together, our data and modelling suggest that L-cis diltiazem impacts phototransduction more strongly than D-cis diltiazem, as measured by the AMP and AUC. Drops in the baseline $[Ca^{2+}]$ seen upon application of both enantiomers is similar to that with no drug applied. Modelling suggests that to recreate the data the initial responsiveness of the cell is of vital importance, followed in importance by the combination of the responsiveness, drug used, and concentration of the drug. Initial responsiveness and drug used were also found to be significant for all three criteria tests, while knowing the drug that was used was significant for AMP and AUC. Having seen the effect of these drugs on the Ca^{2+} dynamics within the cell, we next moved to see how treatment with these drugs effected the activity of calpain within PRs.

Different diltiazem enantiomers have opposite effects on calpain activity

Previous work from our lab has shown that treatment of retinal cultures with L-cis or D-cis diltiazem has a variety of effects on the levels of cell death seen in the ONL (Soumyaparna Das,

unpublished). Treatment with 100 µM L-cis diltiazem showed a decrease in the level of cell death in the *rd1* mutant model but an increase in the level of cell death in the wt control. Conversely, 100 µM D-cis diltiazem treatment resulted in an increase in the level of cell death in the mutant mouse but a decrease in the levels of cell death in the wt (Das, unpublished).

To investigate how diltiazem treatment effected calpain activity, we used cultured *rd1* or wt explants and applied either 100 µM of L-cis or D-cis diltiazem and compared with a non-treated control for each. Treatment with L-cis resulted in a dramatic reduction in calpain activity in the cultured *rd1* retinas but a noticeable increase in the activity of calpain in the wt compared to untreated condition (Fig. 28). Treatment of cultures with D-cis showed a reduction in the calpain activity of *rd1* treated mice compared to untreated controls and a marked reduction in the calpain activity in the wt treated retinas compared to untreated controls (Fig 28). These results largely agreed with data previously produced in our lab by Soumyaparna Das examining the effect of diltiazem on cell death (unpublished). The difference between these two studies is the increase in cell death seen in *rd1* treated with D-cis compared to a decrease in calpain activity seen under these same conditions. To allow us to investigate real time Ca^{2+} imaging with its effect on cellular protein, we next moved to develop a method to image calpain activity under two-photon conditions.

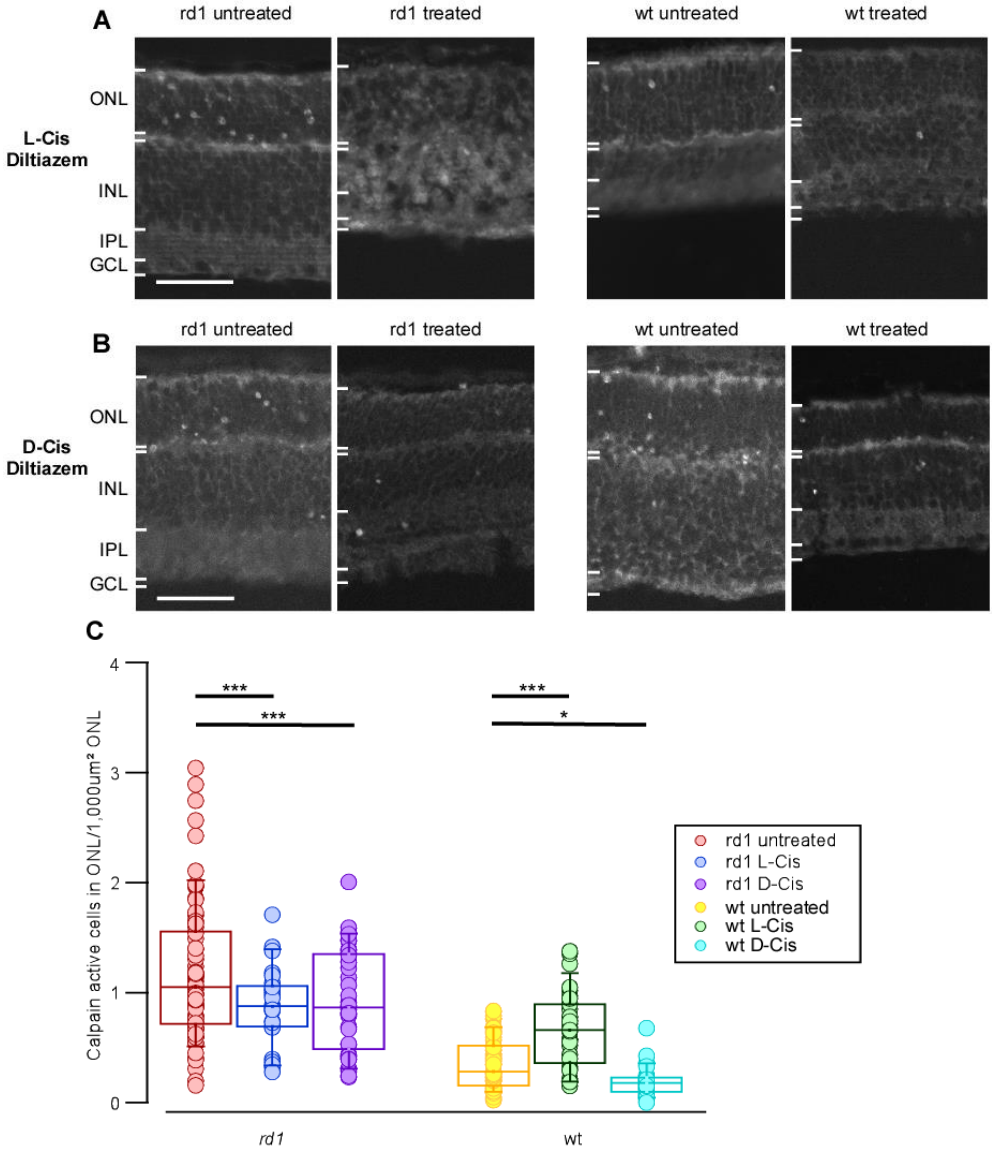
A
rd1 untreated
rd1 treated
wt untreated
wt treated
L-Cis Diltiazem
ONL
INL
IPL
GCL
B
rd1 untreated
rd1 treated
wt untreated
wt treated
D-Cis Diltiazem
ONL
INL
IPL
GCL
C
Calpain active cells in ONL/1,000um² ONL
0
1
2
3
4
***
***
***
*
rd1 untreated
rd1 L-Cis
rd1 D-Cis
wt untreated
wt L-Cis
wt D-Cis
rd1
wt

Figure 28. Diltiazem treatment on calpain activity. **A, B**, representative images of sections from *rd1* and wt treated and untreated with L-cis diltiazem (A) or D-cis diltiazem (B) analysed with the calpain assay; each image of an untreated control retina (left) is matched with a treated retina (right). **C**, normalised number of fluorescent cells in the ONL (per 1,000 μm^2), indicative of calpain activity in photoreceptors, as a function of treatment. Statistical analysis was two-way ANOVA with Bonferroni posthoc statistical significance: *** ≥ 0.001; * ≥ 0.05 unless otherwise stated. Scale bar: A, B is 50 µm

Imaging of calpain activity using two-photon microscopy

We adapted the protocol originally used to detect calpain activity *ex vivo*, using unfixed tissue sections and widefield fluorescence microscopy (Paquet-Durand et al., 2006), to be used *in vitro*, on live retina slices under a two-photon microscope. Using this new protocol, we readily detected calpain activity in the plasma membrane of both wt and *rd1* PRs (Fig. 29), in agreement with the membranous localization of different calpain isoforms described previously (Paquet-Durand et al. 2006). In the ONL of the *rd1* retina there were occasional cells that appeared to show higher calpain activity, however, their number was relatively low when compared to the number of calpain positive PRs seen in *ex vivo* preparations. Calpain activity was also seen in the INL and in retinal ganglion cells, in agreement with a similar increase observed in cultured retinas (François Paquet-Durand, Johnson, & Ekström, 2007). This increase

in calpain activity in ganglion cells is probably triggered by severing of the optic nerve, which is common to both preparations.

Under the *in vitro* imaging conditions described above, however, the calpain activity signal, in particular, the numbers of calpain activity positive cells, turned out to be rather low when compared to *ex vivo* preparations. To increase the cellular calpain activity signal, we then proceeded with incubating the retinal slices with the CAA and the Ca^{2+} ionophore ionomycin. While the addition of ionomycin did increase calpain activity in PRs, the *in vitro* staining was still weaker when compared to the *ex vivo* situation. With the addition of ionomycin the detection rate of calpain positive cells using the two-photon microscope was approximately 12% of what was seen in the ONL of *ex vivo* preparations (Fig 30).

Taken together, while calpain activity could be measured in living retina using two-photon microscopy, and while the results agree with previous findings on high calpain activity in the *rd1* ONL, the sensitivity of detection under two-photon *in vitro* imaging was lower than that under *ex vivo* assay conditions. This reduction in signal to noise ratio is likely due to the osmolarity of the solution used to incubate the tissue, making it difficult to discern calpain positive cells from the background noise especially when compared to *ex vivo* imaging (see Discussion).

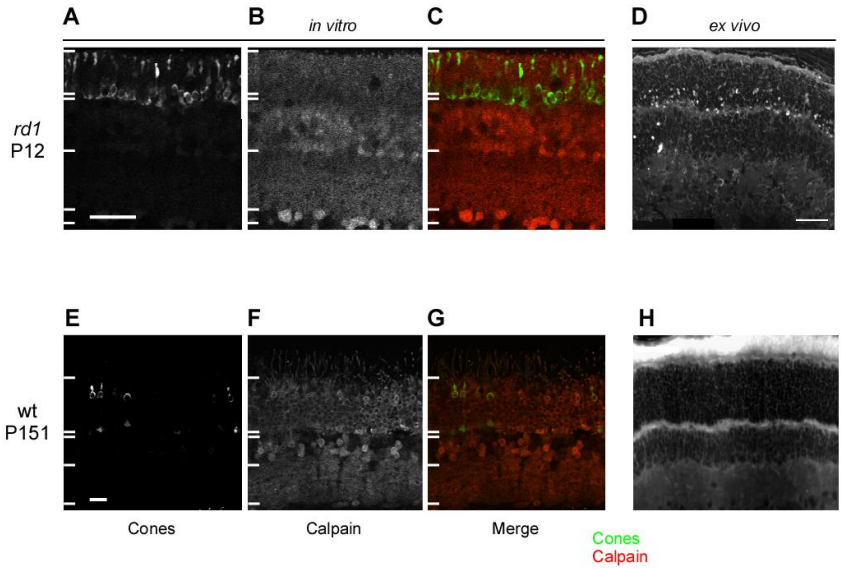

Figure 29. Two-photon imaging of calpain activity in wt and *rd1* retina. The TN-XL biosensor labels cones within the outer nuclear layer (ONL) in *rd1* (**A**) and wt (**E**) retina. Calpain activity imaged in *rd1* (**B**) and wt (**F**) retina. Merged images displaying cones (in green, **C**) and calpain activity (red, **G**). Note that that calpain activity was also observed in the inner retina, especially in the ganglion cell layer (GCL). Retinal calpain activity detected with the *ex vivo* assay is shown for *rd1* (**D**) and wt (**H**), for comparison. Scale bar = 50 µm. INL, inner nuclear layer; IPL, inner plexiform layer.

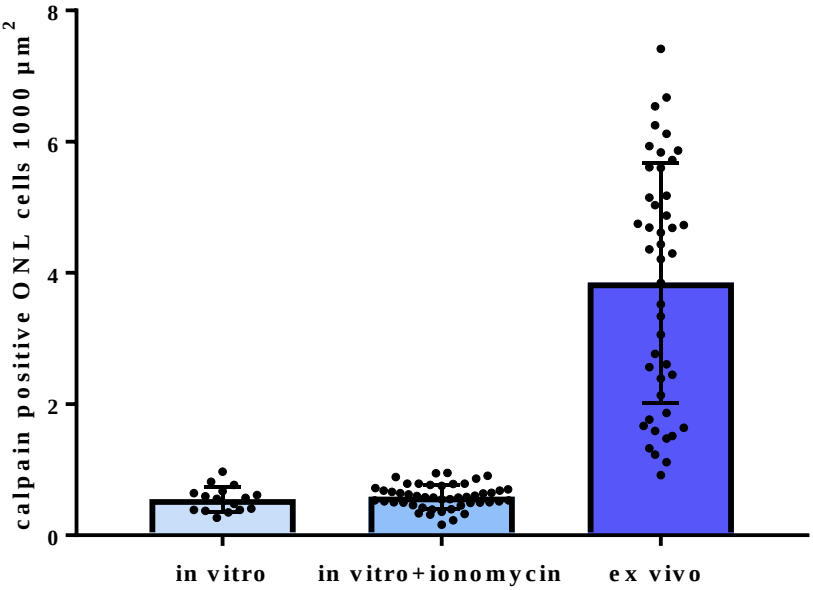

Figure 30. Quantification of calpain activity positive cells. Within the ONL, cells positive for calpain activity were counted. The *in vitro* 2-photon live imaging (n= 1 mouse, 16 images) situation was compared to *in vitro* imaging with the addition of ionomycin (n= 2 mice, 50 images) as well as with the *ex vivo* situation ((n= 3 mice, 45 images) using unfixed retinal sections.

Calpain activity								
	Wild type		*rd1*		*rd10*		*cpfl1*	
	Mice	Images	Mice	Images	Mice	Images	Mice	Images
P10	3	45	3	45	-	-	-	-
P12	3	44	3	45	-	-	-	-
P14	3	44	3	50	5	75	3	55
P18	3	45	3	41	4	74	3	54
P24	3	39	6	76	3	50	3	45
P30	3	45	3	40	3	45	3	45
P60	3	44	-	-	-	-	3	43
P90	3	32	-	-	-	-	3	45
P120	3	45	-	-	-	-	3	45
Calpain-2								
P10	3	45	3	45	-	-	-	-
P12	3	45	3	45	-	-	-	-
P14	3	45	3	44	3	45	3	45
P18	3	45	3	45	3	44	3	45
P24	3	45	3	45	3	45	3	45
P30	3	45	3	45	3	45	3	45
TUNEL								
P10	3	45	3	45	-	-	-	-
P12	3	45	3	45	-	-	-	-
P14	3	45	3	45	3	45	3	45
P18	3	45	3	45	3	45	3	45
P24	3	45	3	45	3	45	3	45
P30	3	45	3	45	3	45	3	45
AIF								
P10	3	45	3	45	-	-	-	-
P12	3	45	3	45	-	-	-	-
P14	3	44	3	40	3	45	3	45
P18	3	45	3	45	3	45	3	44
P24	3	45	3	45	3	45	3	45
P30	3	45	3	45	3	45	3	45

Caspase-3								
P10	3	45	3	45	-	-	-	-
P12	3	45	3	45	-	-	-	-
P14	3	44	3	40	3	45	3	45
P18	2	30	3	45	3	45	3	45
P24	3	45	3	45	3	45	3	45
P30	3	45	3	45	3	45	3	45
Calpain-1								
P10	3	32	3	45	-	-	-	-
P12	3	39	3	44	-	-	-	-
P14	1	12	3	44	3	45	3	45
P18	3	45	3	45	3	45	3	45
P24	3	45	3	45	3	45	3	45
P30	3	45	3	45	3	45	3	45

Table 2. Number of mice used for each genotype, post-natal time-point and marker as well as numbers of images recorded.

Calpain Activity				
	Wild type	*rd1*	*rd10*	*cpfl1*
P10	0.14±0.023	0.78±0.068	-	-
P12	0.055±0.012	4.3±0.27	-	-
P14	0.053±0.0074	2.69±0.11	0.11±0.019	0.09±0.008
P18	0.051±0.0057	1.19±0.13	1.36±0.145	0.08±0.01
P24	0.0255±0.006	1.001±0.13	0.878±0.122	0.15±0.01
P30	0.06±0.02	0.74±0.12	0.82±0.068	0.12±0.01
P60	0.044±0.005	-	-	0.22±0.02
P90	0.054±0.007	-	-	0.176±0.02
P120	0.058±0.008	-	-	0.21±0.016
TUNEL				
P10	0.046±0.01	1.15±0.116	-	-
P12	0.078±0.016	6.1±0.42	-	-
P14	0.156±0.011	3.63±0.18	0.17±0.12	0.16±0.017
P18	0.14±0.011	2.94±0.3	1.76±0.23	0.21±0.019
P24	0.086±0.013	1.44±0.14	2.7±0.16	0.19±0.01
P30	0.03±0.0088	1.40±0.101	1.08±0.08	0.1±0.02
Calpain-2				
P10	0.034±0.006	0.46±0.05	-	-
P12	0±0.006	0.95±0.14	-	-
P14	0.026±0.006	1.10±0.13	0±0.01	0.016±0.0049
P18	0.019±0.005	0.3±0.033	0.41±0.09	0±0.003
P24	0±0.007	0.26±0.07	0.29±0.05	0.024±0.0038
P30	0±0.003	0.19±0.088	0.73±0.1	0±0.004
Calpain-1				
P10	0±0	0±0	-	-

P12	0±0.0035	0±0.0015	-	-
P14	0±0	0±0.002	0±0.002	0±0.0007
P18	0±0.0007	0±0.0016	0±0.04	0±0.002
P24	0±0.0004	0±0.004	0±0.025	0±0.0009
P30	0±0.002	0±0.014	0.38±0.05	0±0.0009
Caspase-3				
P10	0±0.00095	0±0	-	-
P12	0±0.00057	0±0	-	-
P14	0±0	0±0.004	0±0	0±0.0009
P18	0±0	0±0.019	0±0.006	0±0.0004
P24	0±0	0±0.045	0±0.007	0±0
P30	0±0	0±0.008	0±0.001	0±0.0004
AIF				
P10	0±0.0006	0±0.002	-	-
P12	0±0.001	0±0.0025	-	-
P14	0±0.003	0±0.0035	0±0.003	0±0.004
P18	0±0.001	0±0.018	0.45±0.1	0±0.004
P24	0±0.0007	0±0.027	0.91±0.091	0±0.0003
P30	0±0.0023	0±0.085	0.65±0.08	0±0.0008

Table 3: Median values plus/minus the standard error of the mean recorded from each mouse model at each time point and for each marker.

Discussion

Here, we provide several lines of evidence on the role of calpain activity as a driver of PR degeneration and show that calpain-2, but not calpain-1, is likely implicated in PR cell death. AIF appears to be contributing to the primary rod PR death while caspase-3 does not. However, caspase-3 may be involved in secondary cone degeneration. These trends coincide temporally with peaks occurring at approximately the same time, but they also correlate with each other spatially, typically starting in the centre of the retina before spreading to the periphery. We also provide evidence that application of a CNGC blocker ablates light induced Ca^{2+} responses when blocking VGCCs does not.

To discuss the role of calpain activity, we will consider the effects of energy metabolism; the interactions between calpain and caspase and suggestions for how to elucidate their interactions; the secondary cone death; the spatial occurrences of markers and progression of cell death; how calpain as a viable marker for Ca^{2+} based cellular distress; and lastly, the effect of Diltiazem on the retina. We will discuss the statistical and analytical approaches to time point selection, including calpain imaging under two-photon conditions before considering the impact of this research, its limitations and directions for the future.

Effects of energy metabolism on Ca^{2+} dysregulation and cell death

Ca^{2+} dysregulation occurs in PRs with *PDE6* gene mutations, typically resulting in higher Ca^{2+} concentrations (Kulkarni et al.,

2016). This rise in Ca^{2+} would lead to increased activity of the plasma membrane NCKX, an antiporter responsible for maintaining appropriate Ca^{2+} levels in PR outer segments (Jensen, Buckby, & Empson, 2004). NCKX is driven by a K^{+} gradient, which in turn is maintained by K^{+}-ATPases. Elsewhere in the cell, low intracellular Ca^{2+} levels are ensured by specific Ca^{2+}-ATPases that have the highest ATP affinity of all ATPases. This may explain why low Ca^{2+} can be maintained even when general cellular [ATP] is very low (Bruce, 2017).

As necrosis is a passive process that does not require ATP, it has long been suspected that the levels of ATP in the cell are a determining factor for whether, under stress, the cell chooses apoptosis or necrosis to complete cell death (Criddle et al., 2007; Leist et al., 1997; Tsujimoto, 1997). It was theorised by Liu et al., (2004) that cells that have been cultured prefer apoptosis as a method of cell death, due to the availability of glucose in the media allowing for a ready production of ATP in the cell. This steady state of ATP production by cells being cultured would drive an injured cell towards apoptosis, something that should be considered were culturing necessary to fully elucidate any caspase and calpain activation in damaged cells. In our dataset, we saw high levels of calpain activity, especially high levels of calpain-2 activation. The high affinity of Ca^{2+}-ATPases for ATP, combined with the high levels of Ca^{2+} required for the activation of calpain-2, would indicate that in dying PRs any remaining ATP had already been used up.

Thus, a cell death pathway not dependent on ATP (such as necrosis, although not necessarily necrosis) would seem to be the preferred pathway for the PRs to avail of, as seen by the increase in AIF staining in the ONL. This energy requirement would also explain why caspase-3 activation is only seen in later time points examined and predominantly in cone PRs. We do however, provide evidence that calpain activity is an early event and peaks with cell death in both *rd1* and *rd10* models, but that levels of activity and regulation of harmful calpain isoforms (calpain-2) are low prior to the increase in cell death and rise in tandem with it. This rise in calpain activity and calpain-2 activation would suggest that calpain, were it involved in cell death, would be part of a passive, ATP independent cell death mechanism.

Calpain and caspase

It is worth noting that there is a complex set of interactions between calpain and caspase. For instance, calpastatin, the natural inhibitor of calpains, is cleaved by caspase isoforms (Pörn-Ares, Samali, & Orrenius, 1998; K. K. W. Wang et al., 1998) suggesting a role for caspase in the activation of calpains. Calpain isoforms, however, also have a role in the inactivation of caspase molecules. It was shown in cultured monkey RPE cells that under hypoxic conditions, procaspase-3 was cleaved into inactive forms (Emi Nakajima et al., 2017) by calpain, likely calpain-1 based on their western blotting results. These fragment sizes were shown to be unique to calpain cleavage by E Nakajima et al., (2014). These contradictions lead to more questions about the interaction between caspase and calpain

isoforms. It is possible that some caspase isoforms activate calpain-2 through the cleavage of calpastatin. These caspase isoforms however, cannot execute the apoptosis pathway through the activation of executor caspases, as these have already been cleaved inactive by calpain-1. It is also possible that caspase isoforms are in fact activated by the dysregulation of Ca^{2+} through disruptions of the mitochondrial membrane, and are then cleaved by calpain-1, temporarily saving the cell until the persistent Ca^{2+} dysregulation leads to the activation of the calpain-2 and therefore the process of cell death continues, albeit through a different mechanism.

Very fine temporal analysis and rigorous experimental conditions are needed to full elucidate these pathways as we will discuss here. As mentioned above, the energy state of the cell can be a large determining factor for which cell death pathway is utilised. A possible experiment to determine caspase-calpain interactions under various energy conditions would be to first tag the different caspase and calpain isoforms being investigated (here calpain-1, calpain-2 and caspase-3) with FRET based molecules, a donor FRET to caspase and an acceptor FRET moiety to the calpains. If the caspase-3 were to donate energy to the calpain-2 isoform before the calpain-1 isoform, one could tell by the colour of the tags being detected. It would also be possible to do this semi-continuously in a cell culture where the levels of the insult and glucose (as two possible parameters) could be tightly regulated probing the exact conditions each interaction took place under. As this would initially be done in cell culture the FRET linked proteins transfected into the cells and then moved to mouse

lines using transgenic mice. Highly regulated cell culture, or an inducible model of cell death within the retina, would be the preferred methods of elucidating these interactions as experimenters would have greater control over the timing of the intracellular events and not be constrained by heterogeneous cell death patterns.

Regardless of the form of cell death taken by PRs with *Pde6* mutations, we are confident that the dysregulation of Ca^{2+} precipitates cell death. As the other PRs in the retina are unaffected by this mutation (rods in *cpfl1* and cones in *rd1* and *rd10*) it is unlikely that they would die from the same mechanism as that of the diseased PRs (as discussed below). It is therefore imperative that methods be developed that can rebalance Ca^{2+} regulation within injured PRs, be it through pharmacological interventions to target the channels, or pumps, or a gene therapy that would replace the non-functional mutated genes.

It is notable that levels of calpain-1 appear abruptly in the *rd10* but not in other mouse models. This may be a mechanism employed by the remaining PRs to try and survive. Calpain-1 has been implicated in more neuroprotective mechanisms, (discussed in Baudry & Bi, 2016) and the different mutations between *rd1* and *rd10* and the somewhat slower progression of the *rd10* degeneration may give the cells more time to activate such calpain-1 dependent neuroprotective processes.

Secondary cone death driven by apoptosis in rd1

While the majority of *rd1* rod PRs die between P12-P14, some cells (mostly cones) remain beyond P18. Interestingly, we did find that a substantial cohort of the remaining cones were positive for caspase-3 in the *rd1* mouse at P24. This would suggest that while the primary rod degeneration is non-apoptotic, secondary cone degeneration might well be an apoptotic process. Since apoptosis is a "clean" form of cell death for the tissue at large that does not cause inflammation or otherwise detrimental tissue reactions, it is often employed to remove stressed cells. The exact reason for this cell death (*e.g.* starvation, physical pressure by the RPE as the rods no longer provide structural support) is not clear from our data set, however.

Another unknown is the stress that affects the cones causing them to enter the apoptotic cycle. The stress on the cones may be due to metabolic dysregulation or physical stress, or both at the same time. We see that the morphology of cones is affected by the degeneration (Fig. 16B) while detachment of the retina from the RPE, which is part of a delicate metabolic ecosystem along with the PRs and Mueller glial cells (Kanow et al., 2017) has also been observed in clinics (Ishida et al., 2013). At any rate, the more distal causes for the secondary degeneration are beyond the scope of our present investigation.

Spatial occurrences of markers, and progression of cell death

Within the *rd1* mouse retina a clear centre to periphery trend can be seen for calpain activity, calpain-2 up-regulation, and TUNEL. This suggests that the activity of calpain (likely calpain-2) drives the progression of cell death across the retina. The centre to periphery wave of cell death is well established and is theorised to follow cell maturation patterns in the *rd1* mouse (Noell, 1958). Cell death patterns seen in the *rd10* are less well known. In our examination, a centre to periphery gradient was seen for calpain activity, calpain-2 and TUNEL in the *rd10* mouse, although this gradient was not as distinct as that in the *rd1* mouse. This could be due to time point selection or to the fact that the degeneration seen in the *rd10* mouse is less homogeneous than that in the *rd1* mouse. No pattern of marker up-regulation or activation was detectable in the *cpfl1* mouse model as seen in the individual heat maps (Fig. 18-23). This is probably due to the low number of cones in the mouse retina and the stochastic nature of the cell death seen in all mouse models of retinal dystrophies.

While some studies have investigated the expression patterns and cell death patterns across the retina (Schaefer et al., 2017), most studies focus their investigations on the area of the retina around the optic nerve. Our study builds on these and expands, showing that previous links between Ca^{2+}, calpain, and cell death are not only present in populations of cells around the optic nerve, but throughout the retina. This shared link and the temporal order of the progression of the

disease is important to know as were the initial stages of the disease diagnosed, populations of cells, in the periphery in case of the mouse and in the fovea in the case of humans, could be saved through intervention. While the finding that rods throughout the *rd1* and *rd10* retinas degenerate through similar pathways may seem obvious, it would have been just as easy to assume that cones in these retinas die through the same pathways as rods, which, we have evidence to suggest is not the case. Our study is also limited somewhat: we rigorously sampled values along the dorsal – ventral axis, often at the expense of the temporal – nasal axis, and we can only speculate whether there would be a differential pattern between the two axes had they been measured equally. Examining the markers across the whole eye in the nasal – temporal axis in the same manner might, for example, show a possible difference based on cone cell type, based on opsin expression (Baden et al., 2013) in the dorsal – ventral direction, which is not present on the nasal-temporal axis. This particular criterion would provide differences in examining the two axes, but as the mouse retina is so rod dominated, these differences would be slight and need untangling using cone specific markers.

Different cell death mechanisms in Pde6b mutants?

The differences seen between *rd1* and *rd10* may provide interesting insights into the causative degeneration mechanisms. While both models show high levels of calpain activity, calpain-2, and TUNEL, at ages corresponding to their respective peaks of degeneration (P12 and P18, respectively), there may be differences in the mode of cell

death utilised by the PRs. AIF and calpain-1 activation are seen more in the ONL of the *rd10* mouse while *rd1* retina did not show these markers until relatively late (P24), at which point they may be located predominately to cones. This leads us to ask whether different mutations within the two models might cause different pathways of cell death. The fact that we saw a peak of TUNEL staining in *rd1* several days before we saw AIF or caspase-3 up-regulation indicates that neither can be responsible for the DNA cleavage, pointing towards other proteins.

Calpain as a viable marker for Ca^{2+} based cellular distress

Calpain is a well-documented Ca^{2+} activated cysteine protease. It has been long implicated in both necrotic and apoptotic events within the cell, as well as a variety of physiological functions. Calpains are a very interesting family of cellular proteases as, unlike other families (caspases), the different isoforms often have opposing functions (discussed in Baudry & Bi, 2016). Calpain's dependence on Ca^{2+}, along with its implicated role in cell death makes it an ideal candidate for our investigation, as it may well act as a stepping stone between Ca^{2+} dysregulation, especially in the case of calpain-2 and cell death. Calpain is a plasma membrane associated protein, meaning cellular damage does not need to occur in order for calpain to act on cellular structures. Within the relevant literature, the Ca^{2+} dysregulation linked to cell death is often mediated through damage to the mitochondrial membrane, thus releasing apoptotic molecules such as

Bcl-2, Bax, and Bac. Due to the variety of calpain functions, it is possible that by the time the mitochondria are damaged, due to possible overfilling with Ca^{2+} ions, calpain isoforms have already been autolysed, activated and have acted on a variety of substrates already eliciting detrimental effects on cell survival. It has been estimated that a Ca^{2+} ion migrates no further than 0.5µm and lasts no more than 50µs, before encountering a binding protein, based on the assumption an on equilibrium (k_{on} of 10^8 $M^{-1}s^{-1}$ and a 300µM binding protein concentration) (Allbritton et al., 1992). The diffusion of Ca^{2+} is also a variable condition, dependant on the saturation of buffering stores and proteins. It is a non-uniform system, with buffering entities distributed in a function based, rather than a uniform, manner (Allbritton et al., 1992). This restriction of Ca^{2+} diffusion would again indicate that calpain activation, as well as the binding of Ca^{2+} to all other membrane or cytosolic Ca^{2+} binding proteins, would precede mitochondrial saturation and damage, key requirements for the apoptotic cascade.

The effect of Diltiazem on the retina

The use of the Ca^{2+} channel blocker Diltiazem has been utilised by retinal researchers since 1999, when, Frasson et al. found it to delay *rd1* mouse PR degeneration. However, follow up studies aiming to reproduce this finding to rescue PRs had mixed results. Several studies (Bush, Kononen, Machida, & Sieving, 2000; Pawlyk, Li, Scimeca, Sandberg, & Berson, 2002; Pearce-Kelling et al., 2001) have shown that use of the D-cis enantiomer had little effect on the

progression of disease in PRs with mutations resulting in RD. Other groups (Paquet-Durand et al., 2010) however have shown that the CNGCs (which can be targeted by the L-cis enantiomer of diltiazem) did show some improvement in degenerating retinas suggesting that this enantiomer may in fact be beneficial to PR survival.

Our data suggests that calpain activity is decreased in ONL sections treated with D-cis diltiazem in both *rd1* and wt mice. The treatment of ONL sections with L-cis results in a decrease of calpain activity in the ONL of *rd1* mice but an increase in the levels of calpain activity in the ONL of wt mice. This data is conflicting for several reasons. The entry of Ca^{2+} into the outer segment of PRs is not only tightly regulated, but very strictly buffered (discussed in Krizaj & Copenhagen, 2002). The connecting cilium is thought to be a very efficient physical barrier of Ca^{2+} between the inner and outer segments, not allowing the movement of any remaining free Ca^{2+} between the two (Krizaj & Copenhagen, 1998). This buffering and segmentation of the PRs makes the interpretation of the L-cis treated sections difficult to interpret. As the decrease in Ca^{2+} cannot lead to an even distribution of lowered Ca^{2+} across the cell due to the buffering of the cell and stores, and the lowering of Ca^{2+} can only occur within the OS due to the distribution of CNG channels that L-cis targets, the reduction in the activation of calpain needs to be further examined. Data produced in our lab (by Soumyaparna Das and Maria Pia Polito) shows that rod CNG channels are present in the truncated OSs of rods at P11 in both wt and *rd1*. At P11, mouse PRs are not yet fully matured and so the barrier function of the cilium may

not yet be fully functional. This would allow for a drop in the Ca^{2+} levels in the OS to affect the overall cellular [Ca^{2+}], resulting in a drop in calpain activity. We see from our timelines that the level of calpain activity in the *rd1* mouse is already significantly higher at P10, indicating that the dysregulation of these few CNG channels is already in progress. Determination of the buffering capacity of the cilium could be determined by immunohistochemistry examination if not direct examination with a Ca^{2+} sensor (Fura-2 or Oregon green BAPTA-1). The cilium is filled with Ca^{2+} binding proteins such as centrin, calmodulin kinesin II, and myosin VII (Marszalek et al., 2000) and so antibodies for these proteins could be utilised to determine how developed the buffering capacity of the cilium is at various time points in both diseased and wt PRs.

We see that L-cis, but not D-cis, diltiazem reduces the light induced Ca^{2+} response in cones under the two-photon microscope. The effect of L-cis diltiazem on the light induced Ca^{2+} response would suggest that when the CNGCs are blocked, hyperpolarisation is not achieved. Therefore, the light induced response is not propagated. The blockage of the VGCCs by the D-cis isoform did not seem to inhibit phototransduction as the light induced Ca^{2+} response was unaffected. As the treatment of retinal explant cultures with diltiazem does produce an effect both on calpain activity and cell death (Das, unpublished), we propose that D-cis diltiazem does have an effect on rods but perhaps not on cones. This differential effect may be due to the different VGCC isoforms on the two PR types (Cav 1.3 on cones and Cav 1.4 on rods; Morgans et al., 2005) and the difference in

subtypes in the CNGCs. Little has been written about how diltiazem achieves its blockage of Ca^{2+} channels on the cells, or indeed the affinity of the channels for the particular isoform.

It was noted by Lee & Tsien, (1983) that the number of channels left unblocked increases in tandem with increases in the extracellular [Ca^{2+}]. Yet, the fact that D-cis diltiazem has a pronounced effect on calpain activity in sectioned retinal explant cultures suggests that D-cis affects rods, even if no effect on cones has been seen here. There may also be a timing and access issue: L-cis may be better at binding to the channel or may be given better access to the channels on the OSs as the OSs are solution facing in both protocols. The D-cis by comparison has further to travel through the tissue and in culture conditions has more time to reach the channels. We checked how fast the perfusion chamber filled with a drug solution by substituting ACSF for sulforhodamine and measuring how long it took to saturate the chamber. During the experiments both diltiazem enantiomers were given the same amount of time to affect the Ca^{2+} response. D-cis may need more time than this to be effective however, and so more chronic recordings (one-minute recording followed by a minute to allow the cell recovery time repeated n number of times) would allow us to disentangle this somewhat.

An issue with the interpretation of the diltiazem treated cultures data is the spatial element. Due to the increased difficulty in maintaining spatial orientation during the mounting of the retina to the membrane, in combination with the loss of large portions of the tissue during

slicing, we can ascertain that the tissue stained and imaged was from the medial portion of both *rd1* and wt. We see from our heat maps that the levels of calpain activity in both *rd1* and wt are increased in the very medial portions of the retina before the increase is seen in the periphery. This unknown spatial distribution of the cultured retinal sections imaged could be the reason an increase in calpain activity is seen in the wt after the treatment with L-cis diltiazem. As we see from the heat maps, a difference of 400µm could give higher or lower values. The difference between the treated and untreated wt sections treated with L-cis is ~0.25 active cells in the ONL per 1,000µm^2. As we do not know where in the retina these sections were taken from, a slight shift in the location imaged between the two drug treatments could account for the variation.

Statistical and analysis approaches to time point selection

We extensively investigated several time points in mouse models of RD. Some of these time points, such as P10 and P12, fill in previously underexplored time points, while others, such as P18 and P30, were well examined time points in previous studies (Arango-Gonzalez et al., 2014). Our data indicates that some of these time points may have been over sampled. Some instances, such as the values at P12 in the calpain-2, calpain activity and TUNEL timelines are hard to justify using fewer animals. The variability in the values seen in the above data sets was only explained by further analysis into the spatial distribution without which the distribution of the data would have been treated sceptically. This in itself points to an important issue in

our investigation. We added to previous work (Arango-Gonzalez et al., 2014) by adopting an experimental strategy that emphasised the use of large numbers of samples at a small number of predetermined time points (Kulkarni et al., 2016). Although this approach was useful for inferring the state of the system at particular stages of disease progression, the rigidity of the sampling came at the cost of lower temporal resolution.

For future work, where the temporal precision is critical, it would be preferable to adopt an adaptive strategy, using the GP models to select the optimal time points for particular hypotheses (Chaloner & Verdinelli, 1995; Lindley, 1956). This should make it possible to infer more accurately the non-linear progression of each marker over time, with fewer samples than would be needed in a predetermined or purely random approach. Follow-up studies would benefit from an adaptive strategy, using the GP models to identify time points of interest as data is acquired. This might also include testing the expression of further degeneration markers throughout the eye.

Calpain imaging under two-photon conditions

By adapting the previously established assay for calpain activity, we were able to image calpain activity in the retina under a two-photon (2P) microscope. As the calpain assay under apotome investigation is in unfixed tissue, this would point to possibilities of performing other enzymatic reactions under the 2P. The performance of these live cell assays would allow for interaction studies between the causative and reaction molecules such as calpain and Ca^{2+} used here. However,

further development and optimisation of the described system above is needed. While we have shown that the calpain activity assay under the 2P is viable in principle further optimisation of assay conditions is needed. The most obvious optimisation is the use of tighter light filters with narrow band pass ranges. This would prevent any bleed through of the calpain fluorescence into the ECFP channel ensuring that Ca^{2+} dynamics within the cell, alongside calpain activity, could be measured accurately. The osmolarity of the combined HEPES buffer with the ACSF is far too saline. The levels of potassium in particular are approximately 30 times higher than in ACSF alone. This is obviously an issue as the continuation of photo transduction requires strict ionic balance within the cell. The high level of potassium, is likely to affect the activity of NCKX in OS, possibly causing an artifactual reduction of OS Ca^{2+} levels. It is worth testing then, if an ACSF based solution with lower potassium levels would allow the detection of calpain activity in the *ex vivo* condition. This might require the addition of HEPES for further pH buffering.

The current system has two main limiting factors, the amount of calpain substrate needed per experiment, and the time it takes for a cell to die. The amount of the calpain substrate that needs to be used is prohibitively high and approximately two experiments can be performed per unit. Assuming good TN-XL expression in the cones, careful preparation and properly calibrated stimulations, this can still provide a wealth of data especially as a proof of concept for other live cell assays. Another limiting factor is the incubation time and tissue viability period. Currently the incubation of two hours in the water

bath accounts for a full one-third of the total tissue viability time. For the examination of cell death within the cell and the Ca^{2+} to calpain to cell death link, this time-window may be far too narrow. Ideally, one would treat the tissue within the imaging chamber with the calpain activity assay as soon as the slice was mounted, but this would dramatically increase the levels of substrate needed to maintain assay substrate concentration at the necessary levels.

As said above, the imaging of calpain under 2P conditions has its own value and is the first small step towards possible future clinical tests that could be performed by injecting a substrate into a patient and safely noting its fluorescence in the eye. As patients generally present to clinics after the onset of degeneration and as it is difficult to diagnose diseases before the onset of the degeneration, markers which allow for earlier diagnosis are in demand. For our study of cell death derived from Ca^{2+} dysfunction however, it is of limited use. This is again due to the tissue viability time frame of approximately six hours, while the time from the initiation of cell death to the execution of the cell is many multiples of this. The heterogenic nature of the PR cell death in RP and achromatopsia contributes to this limitation, especially in the *cpfl1* mouse model. The fact that in the *cpfl1* mouse only cones are degenerating implies that the chance of finding a stressed cone in the correct time window is 20-times when compared to rod degeneration. This fact alone complicates studies into cone Ca^{2+} dynamics and calpain activity. A fluorescent rod mouse model would provide its own challenges and the overlap of cells within the retina would cause an overlap of signal which would be a substantial

hurdle to overcome. A stimulation protocol that could elicit the closure of the Ca^{2+} channels within rods would also have to be devised. There is, however, a method to overcome the heterogenic nature of the PR cell death and to allow a more thorough investigation of Ca^{2+}, calpain, and cell death interaction. The lab of Dr. Enrica Strettoi in Pisa, Italy has *Tvrm4* mice, developed by Budzynski et al., (2010) at the Jackson Laboratories, whose retinal degeneration can be induced using high light levels in a protocol well established by (Budzynski et al., 2010), and further optimized to mimic RP by the Strettoi lab (Gargini, Novelli, Piano, Biagioni, & Strettoi, 2017). A *Tvrm4xHR2.1:TN-XL* mouse would allow the investigator to control the time of the onset of degeneration and to image Ca^{2+} dynamics within cones in this period. A pattern of cell death has been established by Antonia Stefanov, a PhD student in Dr Strettoi's group, which allows the investigator to examine certain areas in the retina with very precise knowledge of the stage of progression of the degeneration. As this *Tvrm4* mouse is a rhodopsin mutant model, and not a PDE6 mutant model the role of Ca^{2+} would be diminished as the mutation would not be directly linked to Ca^{2+} regulation, but this does point to a possible way to overcome the heterogeneous cell death pattern seen in RP and achromatopsia retinas. A model of *Pde6c* mutation in which the degeneration could be induced by the investigator, resulting in rapid uniform death in cones would overcome all the above obstacles, albeit highly labour intensive. Inducing the degeneration is key: there is no known reason why cells degenerate when they do, though many think it is in the same order at

which they form and mature (Noell, 1958). This leads to the inhomogeneous nature of the cell death patterns incorporating events such as order of birth, and light levels seen by each mouse while in the animal house. Control over inducing the degeneration allows the experimenter to induce the degeneration in any number of mice simultaneously or separately and record a detailed account of protein up-regulation, down-regulation, activation or suppression. This can then be combined with RNAseq analysis or any other molecular examination into the internal cellular environment, which can be as granular or fine as the experimenter would like.

Future Directions

Continuation of this study, aside from the thoughts on calpain imaging under the 2P above, centre around the further elucidation of calpain's functionality. An investigation into an increase in other calpain isoforms would be useful to ensure it is indeed calpain-2 which is the harmful isoform. More stringent investigations into the functionality of calpain-2 would also be useful. Of the four peptides stained for with antibodies, only calpain-2 was upregulated in the *rd1* before P24. The lack of caspase-3 or AIF suggests the mode of cell death is driven by neither of these and is unlikely to be apoptotic. Where the calpain-2 is acting as an activator protein, previous work demonstrates a preferred cleavage sequence of the active site, which would allow for bioinformatics investigations of known pro-enzymes within the cell to yield a list of suspects to act as mediators between calpain-2 and cell death. Modelling here presented has provided the

greatest indication of marker activity provided so far by the field at large. The use of a model with a synchronized onset of retinal degeneration would allow for greater understanding of the sequence of marker activity we measured here.

Concluding remarks

Here, we show that Ca^{2+} dysregulation resulting from *Pde6* mutations results in increased calpain activity and increased activation of calpain-2. Due to the high [Ca^{2+}] needed for calpain-2 activation we can surmise that this dysregulation results in increases [Ca^{2+}] in the diseased PRs. Our data suggests that primary rod cell death is non-apoptotic but secondary cone cell death is apoptotic. AIF truncation and activation levels between *rd1* and *rd10* in our data sets suggest different cell death mechanism in these models. We show that markers for [Ca^{2+}] dysregulation overlap with those for cell death spatially and temporally in the *rd1* and *rd10* mouse models. Our data indicates that L-cis diltiazem alters the cones response to light more effectively than the D-cis enantiomer. Our modelling suggests possible order of marker involvement in the PR degeneration in *rd1, cpfl1,* and wt but not to strongly in *rd10.* We also provide a proof of concept that calpain activity can be imaged under a 2P microscope though optimisation is needed.

Moving forward this work points to Ca^{2+} and calpain-2 as two targets for pharmacological intervention for people with RDs caused by

PDE6 mutations. We point to caspase inhibitors as potential therapies for the survival of cones in patients with RP. We propose that blocking VGCCS and not CNGCS decreases calpain activity in the PRs and does not diminish cone responsiveness. Finally, we propose that live imaging of protein activity can be achieved in retinal slices under the 2P microscope.

Acknowledgements

I would first like to thank Prof. Thomas Euler and Prof. François Paquet-Durand for welcoming me into their groups and for all their advice, guidance and support given throughout this project. I would like to thank them for sharing their expertise and insight and for introducing me to the scientific community at large by sending me to several conferences.

I would like to thank Timm Schubert for simplifying the animal use in the Euler lab and for his feedback on figures and papers, making both clearer and better.

I thank Norman Rieger for his maintenance of the animals in the Paquet-Durand lab and for making sure this project went as smoothly as possible. I would also like to thank him for the feedback he gave on figures and on presentations.

I thank Gordon Eske for tirelessly making sure the Euler lab ran smoothly be it through, animals, reagents or coffee. He was also instrumental in keeping the mood and morale in the lab high and having a greater role in helping this project progress then he realises.

I would like to thank Luke Rogerson for all his input on the statistical analysis of the timelines, the generation of the graphics and analysis of the Ca^{2+} imaging and his contribution of the modelling. I would also like to thank him for making this process far more fun and enjoyable then it would have been otherwise

I thank Camille Chapot for her coding help in generating the timeline graphics

I thank Tom Baden for his pre-processing scripts making analysing the Ca^{2+} data much easier.

I thank all members of the Euler and Paquet-Durand groups (past and present) for their insight, feedback and time given throughout this process, for making me feel welcome and for making the whole experience infinitely better.

I would like to thank Marius Ueffing, Eberhart Zrenner and the entire Tuebingen Institute for Ophthalmic Research for being open and welcoming and giving feedback to help guide the project.

Lastly I would like to thank my family and especially my parents for their ceaseless support, love and encouragement without which this project would have been a failure and it is to them that I dedicate this thesis.

Funding support

This work was funded by grants from the DFG (EU42/8-1 and PA1751/7-1).

References

Allbritton, N. L., Meyer, T., & Stryer, L. (1992). Range of messenger action of calcium ion and inositol 1, 4, 5-trisphosphate. *Science*, *258*(5089), 1812–1815.

Alluri, H., Grimsley, M., Shaji, C. A., Varghese, K. P., Zhang, S. L., Peddaboina, C., … Tharakan, B. (2016). Attenuation of blood-brain barrier breakdown and Hyperpermeability by Calpain inhibition. *Journal of Biological Chemistry*, jbc-M116.

Ammann, F., Klein, D., & Franceschetti, A. (1965). Genetic and epidemiological investigations on pigmentary degeneration of the retina and allied disorders in Switzerland. *Journal of the Neurological Sciences*, *2*(2), 183–196.

Aoki, K., Imajoh, S., Ohno, S., Emori, Y., Koike, M., Kosaki, G., & Suzuki, K. (1986). Complete amino acid sequence of the large subunit of the low-Ca2+-requiring form of human Ca2+-activated neutral protease (μCANP) deduced from its cDNA sequence. *FEBS Letters*, *205*(2), 313–317.

Arango-Gonzalez, B., Trifunović, D., Sahaboglu, A., Kranz, K., Michalakis, S., Farinelli, P., … Janssen-Bienhold, U. (2014). Identification of a common non-apoptotic cell death mechanism in hereditary retinal degeneration. *PloS One*, *9*(11), e112142.

Arthur, J. S. C., Elce, J. S., Hegadorn, C., Williams, K., & Greer, P.

A. (2000). Disruption of the murine calpain small subunit gene, Capn4: calpain is essential for embryonic development but not for cell growth and division. *Molecular and Cellular Biology*, *20*(12), 4474–4481.

Azam, M., Andrabi, S. S., Sahr, K. E., Kamath, L., Kuliopulos, A., & Chishti, A. H. (2001). Disruption of the mouse μ-calpain gene reveals an essential role in platelet function. *Molecular and Cellular Biology*, *21*(6), 2213–2220.

Baden, T., Schubert, T., Chang, L., Wei, T., Zaichuk, M., Wissinger, B., & Euler, T. (2013). A tale of two retinal domains: near-optimal sampling of achromatic contrasts in natural scenes through asymmetric photoreceptor distribution. *Neuron*, *80*(5), 1206–1217.

Bagur, R., & Hajnóczky, G. (2017). Intracellular Ca2+ sensing: its role in calcium homeostasis and signaling. *Molecular Cell*, *66*(6), 780–788.

Baier, L. J., Permana, P. A., Yang, X., Pratley, R. E., Hanson, R. L., Shen, G.-Q., … Horikawa, Y. (2000). A calpain-10 gene polymorphism is associated with reduced muscle mRNA levels and insulin resistance. *The Journal of Clinical Investigation*, *106*(7), R69–R73.

Bates, D., Mächler, M., Bolker, B., & Walker, S. (2014). Fitting linear mixed-effects models using lme4. *ArXiv Preprint ArXiv:1406.5823*.

Baudry, M., & Bi, X. (2016). Calpain-1 and calpain-2: the yin and yang of synaptic plasticity and neurodegeneration. *Trends in Neurosciences*, *39*(4), 235–245.

Berger, W., Kloeckener-Gruissem, B., & Neidhardt, J. (2010). The molecular basis of human retinal and vitreoretinal diseases. *Progress in Retinal and Eye Research*, *29*(5), 335–375.

Berridge, M. J. (2012). Calcium signalling remodelling and disease. Portland Press Limited.

Berridge, M. J., Lipp, P., & Bootman, M. D. (2000). The versatility and universality of calcium signalling. *Nature Reviews Molecular Cell Biology*, *1*(1), 11.

Bootman, M. D., Fearnley, C., Smyrnias, I., MacDonald, F., & Roderick, H. L. (2009). An update on nuclear calcium signalling. *J Cell Sci*, *122*(14), 2337–2350.

Boughman, J. A., Conneally, P. M., & Nance, W. E. (1980). Population genetic studies of retinitis pigmentosa. *American Journal of Human Genetics*, *32*(2), 223.

Bowes, C., Li, T., Danciger, M., Baxter, L. C., Applebury, M. L., & Farber, D. B. (1990). Retinal degeneration in the rd mouse is caused by a defect in the β subunit of rod cGMP-phosphodiesterase. *Nature*, *347*(6294), 677.

Bringhurst, F. R. (1995). Calcium and phosphate distribution, turnover, and metabolic actions. *Endocrinology*, 1015–1043.

Brown, N., & Crawford, C. (1993). Structural modifications associated with the change in Ca2+ sensitivity on activation of m-calpain. *FEBS Letters*, *322*(1), 65–68.

Bruce, J. I. E. (2017). Metabolic regulation of the PMCA: role in cell death and survival. *Cell Calcium*.

Budzynski, E., Gross, A. K., McAlear, S. D., Peachey, N. S., Shukla, M., He, F., … Wensel, T. G. (2010). Mutations of the opsin gene (Y102H and I307N) lead to light induced degeneration of photoreceptors and constitutive activation of phototransduction in mice. *Journal of Biological Chemistry*, jbc-M110.

Bunker, C. H., Berson, E. L., Bromley, W. C., Hayes, R. P., & Roderick, T. H. (1984). Prevalence of retinitis pigmentosa in Maine. *American Journal of Ophthalmology*, *97*(3), 357–365.

Bush, R. A., Kononen, L., Machida, S., & Sieving, P. A. (2000). The effect of calcium channel blocker diltiazem on photoreceptor degeneration in the rhodopsin Pro23His rat. *Investigative Ophthalmology & Visual Science*, *41*(9), 2697–2701.

Butler, M. R., Ma, H., Yang, F., Belcher, J., Le, Y.-Z., Mikoshiba, K., … Krizaj, D. (2017). Endoplasmic reticulum (ER) Ca2+-channel activity contributes to ER stress and cone death in cyclic nucleotide-gated channel deficiency. *Journal of Biological Chemistry*, jbc-M117.

Carafori, E. (1998). Calpain: a protease in search of a function? *Biochem Biophys Res Commun*, *247*, 193–203.

Chaloner, K., & Verdinelli, I. (1995). Bayesian experimental design: A review. *Statistical Science*, 273–304.

Chang, B., Hawes, N. L., Hurd, R. E., Davisson, M. T., Nusinowitz, S., & Heckenlively, J. R. (2000). A new mouse retinal degeneration (rd10) caused by a missense mutation in exon 13 of the beta-subunit of rod phosphodiesterase gene. In *INVESTIGATIVE OPHTHALMOLOGY & VISUAL SCIENCE* (Vol. 41, pp. S533–S533). ASSOC RESEARCH VISION OPHTHALMOLOGY INC 9650 ROCKVILLE PIKE, BETHESDA, MD 20814-3998 USA.

Chang, B., Hawes, N. L., Hurd, R. E., Davisson, M. T., Nusinowitz, S., & Heckenlively, J. R. (2001). A new mouse model of cone photoreceptor function loss (cpfl1). In *Investigative Ophthalmology & Visual Science* (Vol. 42, pp. S527–S527). ASSOC RESEARCH VISION OPHTHALMOLOGY INC 9650 ROCKVILLE PIKE, BETHESDA, MD 20814-3998 USA.

Chang, B., Hawes, N. L., Pardue, M. T., German, A. M., Hurd, R. E., Davisson, M. T., … Sidney, S. S. (2007). Two mouse retinal degenerations caused by missense mutations in the β-subunit of rod cGMP phosphodiesterase gene. *Vision Research*, *47*(5), 624–633.

Chapot, C. A., Behrens, C., Rogerson, L. E., Baden, T., Pop, S., Berens, P., … Schubert, T. (2017). Local signals in mouse horizontal cell dendrites. *Current Biology*, *27*(23), 3603–3615.

Chen, J., Liu, X., Mandel, L. J., & Schnellmann, R. G. (2001). Progressive disruption of the plasma membrane during renal proximal tubule cellular injury. *Toxicology and Applied Pharmacology*, *171*(1), 1–11.

Chen, J., & Mandel, L. J. (1997). Reversibility/irreversibility of anoxia-induced plasma membrane permeabilization. In *JOURNAL OF THE AMERICAN SOCIETY OF NEPHROLOGY* (Vol. 8, pp. A2723–A2723). AMER SOC NEPHROLOGY 1725 I ST, NW STE 510, WASHINGTON, DC 20006 USA.

Chen, L. Y., Rex, C. S., Casale, M. S., Gall, C. M., & Lynch, G. (2007). Changes in synaptic morphology accompany actin signaling during LTP. *Journal of Neuroscience*, *27*(20), 5363–5372.

Christensen, K. A., Myers, J. T., & Swanson, J. A. (2002). pH-dependent regulation of lysosomal calcium in macrophages. *Journal of Cell Science*, *115*(3), 599–607.

Chua, B. T., Guo, K., & Li, P. (2000). Direct cleavage by the calcium-activated protease calpain can lead to inactivation of caspases. *Journal of Biological Chemistry*, *275*(7), 5131–5135.

Clapham, D. E. (2007). Calcium signaling. *Cell*, *131*(6), 1047–1058.

Cong, J., Goll, D. E., Peterson, A. M., & Kapprell, H. P. (1989). The role of autolysis in activity of the Ca2+-dependent proteinases (mu-calpain and m-calpain). *Journal of Biological Chemistry*, *264*(17), 10096–10103.

Coolican, S. A., & Hathaway, D. R. (1984). Effect of L-alpha-phosphatidylinositol on a vascular smooth muscle Ca2+-dependent protease. Reduction of the Ca2+ requirement for autolysis. *Journal of Biological Chemistry*, *259*(19), 11627–11630.

Cottin, P., Brustis, J. J., Poussard, S., Elamrani, N., Broncard, S., & Ducastaing, A. (1994). Ca2+-dependent proteinases (calpains) and muscle cell differentiation. *Biochimica et Biophysica Acta (BBA)-Molecular Cell Research*, *1223*(2), 170–178.

Criddle, D. N., Gerasimenko, J. V., Baumgartner, H. K., Jaffar, M., Voronina, S., Sutton, R., … Gerasimenko, O. V. (2007). Calcium signalling and pancreatic cell death: apoptosis or necrosis? *Cell Death and Differentiation*, *14*(7), 1285.

Croall, D. E., & Ersfeld, K. (2007). The calpains: modular designs and functional diversity. *Genome Biology*, *8*(6), 218.

D, E. (1992). Development Inititation during Fertilization. *Ontogenez*, *220*, 507–512.

Daiger, S. P., Sullivan, L. S., & Bowne, S. J. (2013). Genes and

mutations causing retinitis pigmentosa. *Clinical Genetics*, *84*(2), 132–141.

DANCIGER, M., BLANEY, J., GAO, Y. Q., ZHAO, D. Y., HECKENLIVELY, J. R., JACOBSON, S. G., & FARBER, D. B. (1995). Mutations in the PDE6B Gene in Autosomal Recessive Retinitis Pigmentosa. *Genomics*, *30*(1), 1–7. https://doi.org/https://doi.org/10.1006/geno.1995.0001

Debnath, J., Baehrecke, E. H., & Kroemer, G. (2005). Does autophagy contribute to cell death? *Autophagy*, *1*(2), 66–74.

Denton, R. M., & McCormack, J. G. (1990). Ca2+ as a second messenger within mitochondria of the heart and other tissues. *Annual Review of Physiology*, *52*(1), 451–466.

Donovan, M., & Cotter, T. G. (2002). Caspase-independent photoreceptor apoptosis in vivo and differential expression of apoptotic protease activating factor-1 and caspase-3 during retinal development. *Cell Death and Differentiation*, *9*(11), 1220.

Doonan, F., Donovan, M., & Cotter, T. G. (2003). Caspase-independent photoreceptor apoptosis in mouse models of retinal degeneration. *Journal of Neuroscience*, *23*(13), 5723–5731.

Doonan, F., Donovan, M., & Cotter, T. G. (2005). Activation of multiple pathways during photoreceptor apoptosis in the rd

mouse. *Investigative Ophthalmology & Visual Science*, *46*(10), 3530–3538.

Dräger, U. C., & Hubel, D. H. (1978). Studies of visual function and its decay in mice with hereditary retinal degeneration. *Journal of Comparative Neurology*, *180*(1), 85–114.

Dutt, P., Croall, D. E., Arthur, J. S. C., De Veyra, T., Williams, K., Elce, J. S., & Greer, P. A. (2006). m-Calpain is required for preimplantation embryonic development in mice. *BMC Developmental Biology*, *6*(1), 3.

Ellis, H. M., & Horvitz, H. R. (1986). Genetic control of programmed cell death in the nematode C. elegans. *Cell*, *44*(6), 817–829.

Elmore, S. (2007). Apoptosis: a review of programmed cell death. *Toxicologic Pathology*, *35*(4), 495–516.

Euler, T., Hausselt, S. E., Margolis, D. J., Breuninger, T., Castell, X., Detwiler, P. B., & Denk, W. (2009). Eyecup scope—optical recordings of light stimulus-evoked fluorescence signals in the retina. *Pflügers Archiv-European Journal of Physiology*, *457*(6), 1393–1414.

Euler, T., & Schubert, T. (2015). Multiple Independent Oscillatory Networks in the Degenerating Retina. *Frontiers in Cellular Neuroscience*, *9*, 444. https://doi.org/10.3389/fncel.2015.00444

Farber, D. B. (1995). From mice to men: the cyclic GMP phosphodiesterase gene in vision and disease. The Proctor Lecture. *Investigative Ophthalmology & Visual Science*, *36*(2), 263–275.

Farber, D. B., & Lolley, R. N. (1974). Cyclic guanosine monophosphate: elevation in degenerating photoreceptor cells of the C3H mouse retina. *Science*, *186*(4162), 449–451.

Farber, D. B., & Lolley, R. N. (1976). Enzymic basis for cyclic GMP accumulation in degenerative photoreceptor cells of mouse retina. *Journal of Cyclic Nucleotide Research*, *2*(3), 139–148.

Farrar, G. J., Kenna, P. F., & Humphries, P. (2002). On the genetics of retinitis pigmentosa and on mutation-independent approaches to therapeutic intervention. *EMBO Journal*, *21*(5), 857–864. https://doi.org/10.1093/emboj/21.5.857

Fink, S. L., & Cookson, B. T. (2005). Apoptosis, pyroptosis, and necrosis: mechanistic description of dead and dying eukaryotic cells. *Infection and Immunity*, *73*(4), 1907–1916.

Formigli, L., Papucci, L., Tani, A., Schiavone, N., Tempestini, A., Orlandini, G. E., … Zecchi Orlandini, S. (2000). Aponecrosis: morphological and biochemical exploration of a syncretic process of cell death sharing apoptosis and necrosis. *Journal of Cellular Physiology*, *182*(1), 41–49.

FOX, D. A., POBLENZ, A. N. N. T., & HE, L. (1999). Calcium Overload Triggers Rod Photoreceptor Apoptotic Cell Death in Chemical-Induced and Inherited Retinal Degenerations. *Annals of the New York Academy of Sciences*, *893*(1), 282–285. https://doi.org/10.1111/j.1749-6632.1999.tb07837.x

Fu, Y., & Yau, K.-W. (2007). Phototransduction in mouse rods and cones. *Pflügers Archiv - European Journal of Physiology*, *454*(5), 805–819. https://doi.org/10.1007/s00424-006-0194-y

Galluzzi, L., Vitale, I., Aaronson, S. A., Abrams, J. M., Adam, D., Agostinis, P., … Kroemer, G. (2018). Molecular mechanisms of cell death: recommendations of the Nomenclature Committee on Cell Death 2018. *Cell Death & Differentiation*, *25*(3), 486–541. https://doi.org/10.1038/s41418-017-0012-4

Gargini, C., Novelli, E., Piano, I., Biagioni, M., & Strettoi, E. (2017). Pattern of retinal morphological and functional decay in a light-inducible, rhodopsin mutant mouse. *Scientific Reports*, *7*(1), 5730.

Gargini, C., Terzibasi, E., Mazzoni, F., & Strettoi, E. (2007). Retinal organization in the retinal degeneration 10 (rd10) mutant mouse: a morphological and ERG study. *Journal of Comparative Neurology*, *500*(2), 222–238.

Glossmann, H., Striessnig, J., Ferry, D. R., Goll, A., Moosburger, K., & Schirmer, M. (1987). Interaction between calcium channel ligands and calcium channels. *Circulation Research*,

61(4 Pt 2), I30-6.

Goll, D. E. (1995). Properties and biological regulation of the calpain system. *Expression of Tissue Proteinases and Regulation of Protein Degradation as Related to Meat Quality*, 47–68.

Goll, D. E., Thompson, V. F., Li, H., Wei, W. E. I., & Cong, J. (2003). The calpain system. *Physiological Reviews*, *83*(3), 731–801.

Goñi-Oliver, P., Lucas, J. J., Avila, J., & Hernández, F. (2007). N-terminal Cleavage of GSK-3 by Calpain a new form of GSK-3 regulation. *Journal of Biological Chemistry*, *282*(31), 22406–22413.

GPI: A gaussian process framework in phython. (2012).

Griffin, M. E., Marcucci, M. J., Cline, G. W., Bell, K., Barucci, N., Lee, D., … Shulman, G. I. (1999). Free fatty acid-induced insulin resistance is associated with activation of protein kinase C theta and alterations in the insulin signaling cascade. *Diabetes*, *48*(6), 1270–1274.

Grøndahl, J. (1987). Estimation of prognosis and prevalence of retinitis pigmentosa and Usher syndrome in Norway. *Clinical Genetics*, *31*(4), 255–264.

Grossniklaus, H. E., Geisert, E. E., & Nickerson, J. M. (2015). Introduction to the retina. In *Progress in molecular biology*

and translational science (Vol. 134, pp. 383–396). Elsevier.

Hackos, D. H., & Korenbrot, J. I. (1999). Divalent cation selectivity is a function of gating in native and recombinant cyclic nucleotide–gated ion channels from retinal photoreceptors. *The Journal of General Physiology*, *113*(6), 799–818.

Haim, K., Ben-Aharon, I., & Shalgi, R. (2006). Expression and immunolocalization of the calpain–calpastatin system during parthenogenetic activation and fertilization in the rat egg. *Reproduction*, *131*(1), 35–43.

Hamel, C. (2006). Retinitis pigmentosa. *Orphanet Journal of Rare Diseases*, *1*(1), 40.

Hecht, S., Shlaer, S., & Pirenne, M. H. (1942). Energy, quanta, and vision. *The Journal of General Physiology*, *25*(6), 819–840.

Howden, R., Hanlon, P. R., Petranka, J. G., Kleeberger, S., Bucher, J., Dunnick, J., … Murphy, E. (2005). Ephedrine plus caffeine causes age-dependent cardiovascular responses in Fischer 344 rats. *American Journal of Physiology-Heart and Circulatory Physiology*, *288*(5), H2219–H2224.

Huang, Y., & Wang, K. K. W. (2001). The calpain family and human disease. *Trends in Molecular Medicine*, *7*(8), 355–362.

Humphries, P., Farrar, G. J., Kenna, P., & McWilliam, P. (1990). Retinitis pigmentosa: genetic mapping in X-linked and autosomal forms of the disease. *Clinical Genetics*, *38*(1), 1–

13.

Imajoh, S., Aoki, K., Ohno, S., Emori, Y., Kawasaki, H., Sugihara, H., & Suzuki, K. (1988). Molecular cloning of the cDNA for the large subunit of the high-calcium-requiring form of human calcium-activated neutral protease. *Biochemistry*, *27*(21), 8122–8128.

Inomata, M., Hayashi, M., Nakamura, M., Saito, Y., & Kawashima, S. (1989). Properties of erythrocyte membrane binding and autolytic activation of calcium-activated neutral protease. *Journal of Biological Chemistry*, *264*(31), 18838–18843.

Inomata, M., Saito, Y., Kon, K., & Kawashima, S. (1990). Binding sites for calcium-activated neutral protease on erythrocyte membranes are not membrane phospholipids. *Biochemical and Biophysical Research Communications*, *171*(2), 625–632.

Ishida, T., Moriyama, M., Morohoshi, K., Furuse, Y., Fukuda, T., & Ohno-Matsui, K. (2013). Polypoidal choroidal vasculopathy in a case with retinitis pigmentosa. *International Ophthalmology*, *33*(3), 305–308.

J.M. Cullen. (2010). Histologic patterns of Hepatotoxic Injury. In *Comprehensive Toxicology (Second Edition)* (pp. 141–173).

Jacquemond, V. (1997). Indo-1 fluorescence signals elicited by membrane depolarization in enzymatically isolated mouse skeletal muscle fibers. *Biophysical Journal*, *73*(2), 920.

Jay, M. (1982). On the heredity of retinitis pigmentosa. *British Journal of Ophthalmology*, *66*(7), 405–416.

Jensen, T. P., Buckby, L. E., & Empson, R. M. (2004). Expression of plasma membrane Ca2+ ATPase family members and associated synaptic proteins in acute and cultured organotypic hippocampal slices from rat. *Developmental Brain Research*, *152*(2), 129–136.

Kanamori, T., Kanai, M. I., Dairyo, Y., Yasunaga, K., Morikawa, R. K., & Emoto, K. (2013). Compartmentalized Calcium Transients Trigger Dendrite Pruning in Drosophila Sensory Neurons. *Science*, *340*(6139), 1475 LP-1478. Retrieved from http://science.sciencemag.org/content/340/6139/1475.abstract

Kanow, M. A., Giarmarco, M. M., Jankowski, C. S. R., Tsantilas, K., Engel, A. L., Du, J., … Rountree, A. (2017). Biochemical adaptations of the retina and retinal pigment epithelium support a metabolic ecosystem in the vertebrate eye. *Elife*, *6*, e28899.

Kaplan, J., Bonneau, D., Frézal, J., Munnich, A., & Dufier, J.-L. (1990). Clinical and genetic heterogeneity in retinitis pigmentosa. *Human Genetics*, *85*(6), 635–642.

Kaupp, U. B., & Seifert, R. (2002). Cyclic nucleotide-gated ion channels. *Physiological Reviews*, *82*(3), 769–824.

Kefalov, V. J. (2010). Phototransduction: phototransduction in cones.

Kennedy, B., & Malicki, J. (2009). What drives cell morphogenesis: a look inside the vertebrate photoreceptor. *Developmental Dynamics: An Official Publication of the American Association of Anatomists*, *238*(9), 2115–2138.

Kerr, J. F. R., Wyllie, A. H., & Currie, A. R. (1972). Apoptosis: a basic biological phenomenon with wideranging implications in tissue kinetics. *British Journal of Cancer*, *26*(4), 239.

Koch, K.-W., & Kaupp, U. B. (1985). Cyclic GMP directly regulates a cation conductance in membranes of bovine rods by a cooperative mechanism. *Journal of Biological Chemistry*, *260*(11), 6788–6800.

Kraupp, B. G., Ruttkay-Nedecky, B., Koudelka, H., Bukowska, K., Bursch, W., & Schulte-Hermann, R. (1995). In situ detection of fragmented DNA (TUNEL assay) fails to discriminate among apoptosis, necrosis, and autolytic cell death: a cautionary note. *Hepatology*, *21*(5), 1465–1468.

Krizaj, D., & Copenhagen, D. R. (1998). Compartmentalization of calcium extrusion mechanisms in the outer and inner segments of photoreceptors. *Neuron*, *21*(1), 249–256.

Krizaj, D., & Copenhagen, D. R. (2002). Calcium regulation in photoreceptors. *Frontiers in Bioscience: A Journal and*

Virtual Library, *7*, d2023.

Kuboki, M., Ishii, H., & Kazama, M. (1990). Characterization of calpain I-binding proteins in human erythrocyte plasma membrane. *The Journal of Biochemistry*, *107*(5), 776–780.

Kulkarni, M., Schubert, T., Baden, T., Wissinger, B., Euler, T., & Paquet-Durand, F. (2015). Imaging Ca2+ dynamics in cone photoreceptor axon terminals of the mouse retina. *Journal of Visualized Experiments : JoVE*, (99), e52588. https://doi.org/10.3791/52588

Kulkarni, M., Trifunović, D., Schubert, T., Euler, T., & Paquet-Durand, F. (2016). Calcium dynamics change in degenerating cone photoreceptors. *Human Molecular Genetics*, *25*(17), 3729–3740.

Kurosaka, K., Takahashi, M., Watanabe, N., & Kobayashi, Y. (2003). Silent cleanup of very early apoptotic cells by macrophages. *The Journal of Immunology*, *171*(9), 4672–4679.

Lee, K. S., & Tsien, R. W. (1983). Mechanism of calcium channel blockade by verapamil, D600, diltiazem and nitrendipine in single dialysed heart cells. *Nature*, *302*(5911), 790.

Leist, M., Single, B., Castoldi, A. F., Kühnle, S., & Nicotera, P. (1997). Intracellular adenosine triphosphate (ATP) concentration: a switch in the decision between apoptosis and

necrosis. *Journal of Experimental Medicine*, *185*(8), 1481–1486.

Lieberthal, W., Menza, S. A., & Levine, J. S. (1998). Graded ATP depletion can cause necrosis or apoptosis of cultured mouse proximal tubular cells. *American Journal of Physiology-Renal Physiology*, *274*(2), F315–F327.

Lindley, D. V. (1956). On a Measure of the Information Provided by an Experiment. *The Annals of Mathematical Statistics*, *27*(4), 986–1005. Retrieved from http://www.jstor.org/stable/2237191

Liu, X., & Schnellmann, R. G. (2003). Calpain mediates progressive plasma membrane permeability and proteolysis of cytoskeleton-associated paxillin, talin, and vinculin during renal cell death. *Journal of Pharmacology and Experimental Therapeutics*, *304*(1), 63–70.

Liu, X., Van Vleet, T., & Schnellmann, R. G. (2004). The role of calpain in oncotic cell death. *Annu. Rev. Pharmacol. Toxicol.*, *44*, 349–370.

Lloyd-Evans, E., Morgan, A. J., He, X., Smith, D. A., Elliot-Smith, E., Sillence, D. J., … Platt, F. M. (2008). Niemann-Pick disease type C1 is a sphingosine storage disease that causes deregulation of lysosomal calcium. *Nature Medicine*, *14*(11), 1247.

Lolley, R. N., Farber, D. B., Rayborn, M. E., & Hollyfield, J. G. (1977). Cyclic GMP accumulation causes degeneration of photoreceptor cells: simulation of an inherited disease. *Science*, *196*(4290), 664–666.

Majno, G., & Joris, I. (1995). Apoptosis, oncosis, and necrosis. An overview of cell death. *The American Journal of Pathology*, *146*(1), 3.

Mank, M., Reiff, D. F., Heim, N., Friedrich, M. W., Borst, A., & Griesbeck, O. (2006). A FRET-based calcium biosensor with fast signal kinetics and high fluorescence change. *Biophysical Journal*, *90*(5), 1790–1796.

Maravall, áM, Mainen, Z. F., Sabatini, B. L., & Svoboda, K. (2000). Estimating intracellular calcium concentrations and buffering without wavelength ratioing. *Biophysical Journal*, *78*(5), 2655–2667.

Marszalek, J. R., Liu, X., Roberts, E. A., Chui, D., Marth, J. D., Williams, D. S., & Goldstein, L. S. B. (2000). Genetic evidence for selective transport of opsin and arrestin by kinesin-II in mammalian photoreceptors. *Cell*, *102*(2), 175–187.

McCormack, J. G., & Denton, R. M. (1994). Signal transduction by intramitochondrial Ca2+ in mammalian energy metabolism. *Physiology*, *9*(2), 71–76.

McCORMACK, J. G., Halestrap, A. P., & Denton, R. M. (1990). Role of calcium ions in regulation of mammalian intramitochondrial metabolism. *Physiological Reviews*, *70*(2), 391–425.

McLaughlin, M. E., Ehrhart, T. L., Berson, E. L., & Dryja, T. P. (1995). Mutation spectrum of the gene encoding the beta subunit of rod phosphodiesterase among patients with autosomal recessive retinitis pigmentosa. *Proceedings of the National Academy of Sciences*, *92*(8), 3249–3253.

McLaughlin, M. E., Sandberg, M. A., Berson, E. L., & Dryja, T. P. (1993). Recessive mutations in the gene encoding the β–subunit of rod phosphodiesterase in patients with retinitis pigmentosa. *Nature Genetics*, *4*(2), 130.

McRory, J. E., Hamid, J., Doering, C. J., Garcia, E., Parker, R., Hamming, K., … Feldcamp, L. (2004). The CACNA1F gene encodes an L-type calcium channel with unique biophysical properties and tissue distribution. *Journal of Neuroscience*, *24*(7), 1707–1718.

Moldoveanu, T., Hosfield, C. M., Lim, D., Elce, J. S., Jia, Z., & Davies, P. L. (2002). A Ca2+ switch aligns the active site of calpain. *Cell*, *108*(5), 649–660.

Morgans, C. W., Bayley, P. R., Oesch, N. W., Ren, G., Akileswaran, L., & Taylor, W. R. (2005). Photoreceptor calcium channels: insight from night blindness. *Visual Neuroscience*, *22*(5),

561–568.

Nakagawa, T., & Yuan, J. (2000). Cross-talk between two cysteine protease families: activation of caspase-12 by calpain in apoptosis. *The Journal of Cell Biology*, *150*(4), 887–894.

Nakajima, E., Hammond, K. B., Hirata, M., Shearer, T. R., & Azuma, M. (2017). Contribution of Calpain and Caspases to Cell Death in Cultured Monkey RPE Cells. *Investigative Ophthalmology & Visual Science*, *58*(12), 5412–5420.

Nakajima, E., Hammond, K. B., Shearer, T. R., & Azuma, M. (2014). Activation of the mitochondrial caspase pathway and subsequent calpain activation in monkey RPE cells cultured under zinc depletion. *Eye*, *28*(1), 85.

Nemova, N. N., Lysenko, L. A., & Kantserova, N. P. (2010). Proteases of the calpain family: Structure and functions. *Russian Journal of Developmental Biology*, *41*(5), 318–325. https://doi.org/10.1134/S1062360410050073

Noell, W. K. (1958). Studies on visual cell viability and differentiation. *Annals of the New York Academy of Sciences*, *74*(1), 337–361.

Novak-Lauš, K., Kukulj, S., Zoric-Geber, M., & Bastaic, O. (2002). Primary tapetoretinal dystrophies as the cause of blindness and impaired vision in the republic of Croatia. *Acta Clin Croat*, *41*(1), 23–27.

Orho-Melander, M., Klannemark, M., Svensson, M. K., Ridderstråle, M., Lindgren, C. M., & Groop, L. (2002). Variants in the calpain-10 gene predispose to insulin resistance and elevated free fatty acid levels. *Diabetes*, *51*(8), 2658–2664.

Orrenius, S., Zhihotovsky, B., & Nicotera, P. (2003). Regulation of cell death: the calcium-apoptosis link. Nature Rev Cell Biol 2003; 4: 552-65.

Paquet-Durand, F., Beck, S., Michalakis, S., Goldmann, T., Huber, G., Mühlfriedel, R., … Duetsch, G. (2010). A key role for cyclic nucleotide gated (CNG) channels in cGMP-related retinitis pigmentosa. *Human Molecular Genetics*, *20*(5), 941–947.

Paquet-Durand, F., Azadi, S., Hauck, S. M., Ueffing, M., van Veen, T., & Ekström, P. (2006). Calpain is activated in degenerating photoreceptors in the rd1 mouse. *Journal of Neurochemistry*, *96*(3), 802–814.

Paquet-Durand, F., Johnson, L., & Ekström, P. (2007). Calpain activity in retinal degeneration. *Journal of Neuroscience Research*, *85*(4), 693–702.

Patel, S., & Cai, X. (2015). Evolution of acidic Ca2+ stores and their resident Ca2+-permeable channels. *Cell Calcium*, *57*(3), 222–230.

Pawlyk, B. S., Li, T., Scimeca, M. S., Sandberg, M. A., & Berson, E. L. (2002). Absence of photoreceptor rescue with D-cis-diltiazem in the rd mouse. *Investigative Ophthalmology & Visual Science*, *43*(6), 1912–1915.

Pearce-Kelling, S. E., Aleman, T. S., Nickle, A., Laties, A. M., Aguirre, G. D., Jacobson, S. G., & Acland, G. M. (2001). Calcium channel blocker D-cis-diltiazem does not slow retinal degeneration in the PDE6B mutant rcd1 canine model of retinitis pigmentosa. *Molecular Vision*, *7*, 42.

Phillips, M. J., & Voeltz, G. K. (2016). Structure and function of ER membrane contact sites with other organelles. *Nature Reviews Molecular Cell Biology*, *17*(2), 69.

Pinton, P., Giorgi, C., Siviero, R., Zecchini, E., & Rizzuto, R. (2008). Calcium and apoptosis: ER-mitochondria Ca 2+ transfer in the control of apoptosis. *Oncogene*, *27*(50), 6407.

Pizzo, P., Lissandron, V., Capitanio, P., & Pozzan, T. (2011). Ca2+ signalling in the Golgi apparatus. *Cell Calcium*, *50*(2), 184–192.

Pörn-Ares, M. I., Samali, A., & Orrenius, S. (1998). Cleavage of the calpain inhibitor, calpastatin, during apoptosis. *Cell Death and Differentiation*, *5*(12), 1028.

Pozzan, T., Rizzuto, R., Volpe, P., & Meldolesi, J. (1994). Molecular and cellular physiology of intracellular calcium

stores. *Physiological Reviews*, *74*(3), 595–636.

Prakriya, M., & Lewis, R. S. (2015). Store-operated calcium channels. *Physiological Reviews*, *95*(4), 1383–1436.

Raffaello, A., Mammucari, C., Gherardi, G., & Rizzuto, R. (2016). Calcium at the center of cell signaling: interplay between endoplasmic reticulum, mitochondria, and lysosomes. *Trends in Biochemical Sciences*, *41*(12), 1035–1049.

Reverter, D., Sorimachi, H., & Bode, W. (2001). The structure of calcium-free human m-calpain: implications for calcium activation and function. *Trends in Cardiovascular Medicine*, *11*(6), 222–229.

Rizzuto, R., De Stefani, D., Raffaello, A., & Mammucari, C. (2012). Mitochondria as sensors and regulators of calcium signalling. *Nature Reviews Molecular Cell Biology*, *13*(9), 566.

Rizzuto, R., Pinton, P., Ferrari, D., Chami, M., Szabadkai, G., Magalhaes, P. J., … Pozzan, T. (2003). Calcium and apoptosis: facts and hypotheses. *Oncogene*, *22*(53), 8619.

Saido, T. C., Mizuno, K., & Suzuki, K. (1991). Proteolysis of protein kinase C by calpain: effect of acidic phospholipids. *Biomedica Biochimica Acta*, *50*(4–6), 485–489.

Saido, T. C., Shibata, M., Takenawa, T., Murofushi, H., & Suzuki, K. (1992). Positive regulation of mu-calpain action by polyphosphoinositides. *Journal of Biological Chemistry*,

267(34), 24585–24590.

Saido, T. C., Sorimachi, H., & Suzuki, K. (1994). Calpain: new perspectives in molecular diversity and physiological-pathological involvement. *The FASEB Journal*, *8*(11), 814–822.

Sancho-Pelluz, J., Arango-Gonzalez, B., Kustermann, S., Romero, F. J., van Veen, T., Zrenner, E., … Paquet-Durand, F. (2008). Photoreceptor cell death mechanisms in inherited retinal degeneration. *Molecular Neurobiology*, *38*(3), 253–269.

Savill, J., & Fadok, V. (2000). Corpse clearance defines the meaning of cell death. *Nature*, *407*(6805), 784.

Schaefer, K., Mahajan, M., Gore, A., Tsang, S. H., Bassuk, A. G., & Mahajan, V. B. (2017). Calpain-5 gene expression in the mouse eye and brain. *BMC Research Notes*, *10*(1), 602.

Shang, L., Huang, J.-F., Ding, W., Chen, S., Xue, L.-X., Ma, R.-F., & Xiong, K. (2014). Calpain: a molecule to induce AIF-mediated necroptosis in RGC-5 following elevated hydrostatic pressure. *BMC Neuroscience*, *15*(1), 63.

Shuart, N. G., Haitin, Y., Camp, S. S., Black, K. D., & Zagotta, W. N. (2011). Molecular mechanism for 3: 1 subunit stoichiometry of rod cyclic nucleotide-gated ion channels. *Nature Communications*, *2*, 457.

SIDMAN, R. L., & GREEN, M. C. (1965). Retinal degeneration in

the mouse. *Journal of Heredity*, *56*(1), 23–29.

Smalheiser, N. R., & Lugli, G. (2009). microRNA regulation of synaptic plasticity. *Neuromolecular Medicine*, *11*(3), 133–140.

Sorimachi, H., Ishiura, S., & Suzuki, K. (1997). Structure and physiological function of calpains. *Biochemical Journal*, *328*(3), 721–732.

Sperandio, S., de Belle, I., & Bredesen, D. E. (2000). An alternative, nonapoptotic form of programmed cell death. *Proceedings of the National Academy of Sciences*, *97*(26), 14376–14381.

Strobl, S., Fernandez-Catalan, C., Braun, M., Huber, R., Masumoto, H., Nakagawa, K., … Bartunik, H. (2000). The crystal structure of calcium-free human m-calpain suggests an electrostatic switch mechanism for activation by calcium. *Proceedings of the National Academy of Sciences*, *97*(2), 588–592.

Suzuki, K. (1990). The structure of calpains and the calpain gene. *Intracellular Calcium-Dependent Proteolysis*, 25–35.

Suzuki, K., Hata, S., Kawabata, Y., & Sorimachi, H. (2004). Structure, activation, and biology of calpain. *Diabetes*, *53*(suppl 1), S12–S18.

Tompa, P., Emori, Y., Sorimachi, H., Suzuki, K., & Friedrich, P. (2001). Domain III of calpain is a Ca2+-regulated

phospholipid-binding domain. *Biochemical and Biophysical Research Communications*, *280*(5), 1333–1339.

Trump, B. E., Berezesky, I. K., Chang, S. H., & Phelps, P. C. (1997). The pathways of cell death: oncosis, apoptosis, and necrosis. *Toxicologic Pathology*, *25*(1), 82–88.

Tsujimoto, Y. (1997). Apoptosis and necrosis: intracellular ATP level as a determinant for cell death modes. *Cell Death and Differentiation*, *4*(6), 429.

Twomey, C., & McCarthy, J. V. (2005). Pathways of apoptosis and importance in developement. *Journal of Cellular and Molecular Medicine*, *9*(2), 345–359.

Wang, K. K. W., Posmantur, R., Nadimpalli, R., Nath, R., Mohan, P., Nixon, R. A., … Allen, H. (1998). Caspase-mediated fragmentation of calpain inhibitor protein calpastatin during apoptosis. *Archives of Biochemistry and Biophysics*, *356*(2), 187–196.

Wang, S., Liao, L., Wang, M., Zhou, H., Huang, Y., Wang, Z., … Wang, Y. (2018). Pin1 promotes regulated necrosis induced by glutamate in rat retinal neurons via CAST/Calpain2 pathway. *Frontiers in Cellular Neuroscience*, *11*, 425.

Weerasinghe, P., & Buja, L. M. (2012). Oncosis: an important non-apoptotic mode of cell death. *Experimental and Molecular Pathology*, *93*(3), 302–308.

Wei, T., Schubert, T., Paquet-Durand, F., Tanimoto, N., Chang, L., Koeppen, K., … Euler, T. (2012). Light-driven calcium signals in mouse cone photoreceptors. *Journal of Neuroscience*, *32*(20), 6981–6994.

Werblin, F. S. (1978). Transmission along and between rods in the tiger salamander retina. *The Journal of Physiology*, *280*(1), 449–470.

Williams, C. K., & Rasmussen, C. E. (2006). Gaussian processes for machine learning. *The MIT Press*, *2*(3), 4.

Wood, D. E., & Newcomb, E. W. (1999). Caspase-dependent activation of calpain during drug-induced apoptosis. *Journal of Biological Chemistry*, *274*(12), 8309–8315.

Xu, H., Martinoia, E., & Szabo, I. (2015). Organellar channels and transporters. *Cell Calcium*, *58*(1), 1–10.

Yau, K.-W. (1994). Cyclic nucleotide-gated channels: an expanding new family of ion channels. *Proceedings of the National Academy of Sciences*, *91*(9), 3481–3483.

Zimmerman, U. J., & Schlaepfer, W. W. (1991). Two-stage autolysis of the catalytic subunit initiates activation of calpain I. *Biochimica et Biophysica Acta*, *1078*(2), 192–198.